

Unclassified

SECURITY CLASSIFICATION OF THIS REPORT

2

REPORT DOCUMENTATION PAGE

AD-A206 331

2b. DECLASSIFICATION/DOWNGRADING SCHEDULE		1d. RESTRICTIVE MARKINGS	
4. PERFORMING ORGANIZATION REPORT NUMBER(S) TR-342		3. DISTRIBUTION/AVAILABILITY OF REPORT Approved for Public Release; Distribution Unlimited	
6a. NAME OF PERFORMING ORGANIZATION Flow Research Company/ Flow Industries, Inc.		5. MONITORING ORGANIZATION REPORT NUMBER(S) APOSR TR- 89-0303	
6b. OFFICE SYMBOL (If applicable)		7a. NAME OF MONITORING ORGANIZATION Aerospace Sciences Directorate Air Force Office of Scientific Research	
6c. ADDRESS (City, State and ZIP Code) 21414 68th Avenue South Kent, WA 98032		7b. ADDRESS (City, State and ZIP Code) Bolling Air Force Base Washington, D.C. 20332	
8a. NAME OF FUNDING/SPONSORING ORGANIZATION Air Force Office of Scientific Research		9. PROCUREMENT INSTRUMENT IDENTIFICATION NUMBER Contract No. F49620-85-C-0028	
8b. OFFICE SYMBOL (If applicable)		10. SOURCE OF FUNDING NOS.	
8c. ADDRESS (City, State and ZIP Code) Bolling Air Force Base Washington, D.C. 20332		PROGRAM ELEMENT NO. 61102F	PROJECT NO. 2307
11. TITLE (Include Security Classification) Unsteady Flows Around Three-Dimensional Lifting Surfaces		TASK NO. A1	WORK UNIT NO.
12. PERSONAL AUTHOR(S) Gad-el-Hak, Mohamed			
13a. TYPE OF REPORT Final Technical Report		13b. TIME COVERED FROM 83/5/1 TO 85/9/30	14. DATE OF REPORT (Yr., Mo., Day) 85/11/1
15. PAGE COUNT 122			
16. SUPPLEMENTARY NOTATION			
17. COSATI CODES		18. SUBJECT TERMS (Continue on reverse if necessary and identify by block number)	
FIELD	GROUP	-Unsteady Separated Flows; Lifting Surfaces; Three-Dimensional Wings; Body of Revolution; Supermaneuverability	
19. ABSTRACT (Continue on reverse if necessary and identify by block number) The time-dependent flows around wings and slender bodies of revolution undergoing large-amplitude harmonic motions were investigated using unique flow visualization techniques. The lifting surfaces were towed in an 18-meter water channel at Reynolds numbers up to $7.5 \times 10^5$ . The effects of planform, leading edge contour, reduced frequency and Reynolds number were investigated. The unsteady separation phenomenon was found to be significantly different from the separation on a lifting surface in steady flight. The role of the separation vortices was elaborated and a model of the flow field is proposed.			
20. DISTRIBUTION/AVAILABILITY OF ABSTRACT UNCLASSIFIED/UNLIMITED <input checked="" type="checkbox"/> SAME AS RPT <input checked="" type="checkbox"/> DTIC USERS <input type="checkbox"/>		21. ABSTRACT SECURITY CLASSIFICATION Unclassified <b>E</b>	
22a. NAME OF RESPONSIBLE INDIVIDUAL Dr. <b>LEONIDAS SAKELL</b>		22b. TELEPHONE NUMBER (Include Area Code) (202) 767-4935	22c. OFFICE SYMBOL NH

DTIC ELECTE S 13 MAR 1989 9

**AFOSR-TR. 89-0305**

Flow Research Report No. 342

Unsteady Flows Around Three-Dimensional  
Lifting Surfaces  
(Final Technical Report)

by

Mohamed Gad-el-Hak

Supported Under AFOSR Contract F49620-85-C-0028

November 1985

Flow Research Company  
A Division of Flow Industries, Inc.  
21414-60th Avenue South  
Kent, Washington 98032  
(206) 872-8500

Approved for Public Release; Distribution Unlimited

83  
83  
83  
83  
83  
83

Table of Contents

	Page
FOREWORD	ii
1. Introduction	1
2. Summary of Progress To-Date	4
3. List of Publications and Films	11
References	13
Appendix I: Three-Dimensional Effects on a Pitching Lifting Surface	17
Appendix II: The Discrete Vortices from a Delta Wing	26
Appendix III: The Pitching Delta Wing	29
Appendix IV: Unsteady Vortical Flow Around Three-Dimensional Lifting Surfaces	58
Appendix V: Unsteady Flow Around an Ogive-Cylinder	89

<b>Accession For</b>	
NTIS GRA&I	<input checked="" type="checkbox"/>
DTIC TAB	<input type="checkbox"/>
Unannounced	<input type="checkbox"/>
Justification	
By _____	
Distribution/	
Availability Codes	
Dist	Avail and/or Special
A-1	



FOREWORD

On 1 May 1983, Flow Research Company was awarded an eighteen month contract, later extended to thirty months, from the Air Force Office of Scientific Research to investigate unsteady flows around three-dimensional wings and slender bodies of revolution. The contract monitor at AFOSR was Dr. James D. Wilson, and the principal investigator at FLOW was Dr. Mohamed Gad-el-Hak.

The investigation included flow visualization experiments to reveal the complex nature of the flow around seven wings and a slender body of revolution undergoing large-amplitude harmonic motions. The unsteady separation phenomenon was studied for different reduced frequencies and different Reynolds numbers, and was found to be significantly different from the separation on a lifting surface in steady flight. A simple model is proposed to explain the effects of planform, leading edge contour, reduced frequency and Reynolds number.

At the end of first phase, 1 May 1983 to 30 September 1984, Flow Research Report No. 305 was submitted to AFOSR to summarize the results of this phase including the study of seven different wings. During the second phase, 1 October 1984 to 30 September 1985, further visualization experiments were conducted to investigate the role of three-dimensionality on the unsteady separation phenomenon. Only two lifting surfaces were investigated during the second phase; a low-aspect-ratio rectangular wing and an ogive-cylinder. Two separation vortex pairs were identified as the slender body of revolution underwent a complete pitching cycle. We term these the "Frontward and Rearward Separation Vortices." The size, circulation and degree of symmetry of the leeward vortices change dramatically with subtle changes in the pitching parameters.

## 1. Introduction

With the recent advances in short-range infrared guided missiles, a significant change in close air combat characteristics emphasizing very fast maneuverability becomes highly desirable. This has led to a growing interest in the so called "supermaneuverability" of fighter aircraft where previously unattained regions of the maneuver envelope are attempted, such as post-stall flight maneuver and side slipping (Herbst, 1983a; 1983b). Current research in support of supermaneuverability involves studies to understand the dynamic stall on two- and three-dimensional lifting surfaces and the behavior of attached and separated unsteady shear layers affected by time-dependent boundary conditions, as well as attempts to exploit the unsteady flow characteristics to improve aerodynamic efficiency and enhance performance.

Aerodynamic research for time-dependent viscous flows at high incidence has, to date, centered primarily on the flow over two-dimensional airfoils (McCroskey et al., 1976; McCroskey, 1982; McCroskey & Pucci, 1982; Robinson & Luttges, 1983; Helin & Walker, 1985; Walker & Helin, 1985). The data from these studies have shed considerable light on the exceedingly complex viscous-inviscid interactions associated with time-varying flow separation. The data, furthermore, provide a meaningful base to assess numerical procedures and to develop alternative approaches as required (Baldwin & Lomax, 1978).

Two-dimensional data can play an essential role in high-aspect-ratio applications (e.g., helicopter blades and commercial aircraft) where the local flow behaves, in a sense, two-dimensionally. The classic lifting-line theory for an unswept wing in steady flow, for example, provides a local induced incidence correction to account for finite-aspect-ratio effects. This theory has been extended to include wings with sweep (Cheng, 1979). The lifting-line concept, however, is of little value for the low-aspect-ratio wings of fighter/attack aircraft because the local airfoil section, particularly for the higher incidence angles, cannot be divorced from the wing as an entirety. Therefore, two-dimensional data play a less significant role in the design of low-aspect-ratio wings.

Considerable experimental/theoretical research has been focused on studying the flow over delta and swept wings for steady flow and time-independent boundary conditions (Hoeijmakers et al., 1982). Sophisticated inviscid numerical/analytical models have been developed for design purposes to describe

the flow field at high angles of attack by "modeling" the vorticity shed from the wing edges. The sharpness of the leading edge invariably fixes the location of the shed vortices feeding the leeward "conical-like" vortical motion-- a factor embedded in theoretical modeling for delta wings (Legendre, 1952; Brown & Michael, 1954; Smith, 1968).

Recently this inviscid approach has been extended to time-dependent flows by a very efficient numerical method (Nayfeh et al., 1979; Konstadinopoulos et al., 1981; 1983). The unsteadiness is an important parameter to be considered for flight maneuverability. Studies of unsteady, two-dimensional airfoils have indicated that the lift and drag experience hysteresis loops during an oscillation cycle. Corresponding information for unsteady, three-dimensional wings is very scarce (Adler et al., 1983; Adler & Luttses, 1985). For three-dimensional lifting surfaces, it is quite likely that inviscid techniques coupled with empiricism will be the primary short-term "engineering" tool for predicting the time-dependent flow. The long-term goal would be a Navier-Stokes solution with appropriate turbulence modeling.

The performance of a highly-maneuverable aircraft is critically dependent upon the accurate prediction of the flow around the wings, body and other parts of the vehicle. While the wings are of the utmost importance aerodynamically, the unsteady flow around the body must play a role in the maneuverability of the airplane. At high angles of attack, the symmetric or asymmetric leeward-side separation on an axisymmetric body is exceedingly complex, and progress in forming the basis for describing and modeling how vorticity is shed from the body to the leeward wake has depended crucially upon experiment (Nielsen, 1979). While much remains to be investigated, a reasonable overall understanding of the steady flow about an axisymmetric body is evolving. Unfortunately, little is known about the influence of time-dependent motions (e.g., pitching oscillations) on the time-evolution of the leeward vortex structure or the flow field in general. Nielsen (1979), in his broad survey of missile aerodynamics, does not even discuss time-dependent motions.

Since 1 May 1983, Flow Industries has been under contract with the Air Force Office of Scientific Research to study the time-dependent flow around two generic classes of wings, the delta wing and the swept wing (including zero sweep), and around a slender body of revolution. Because of the pioneering nature of this work, our initial efforts have involved flow visualization techniques to study the unsteady flow fields and to establish a

qualitative overall picture of the flow around the lifting surfaces before embarking on a more detailed study. We have broadly delineated and qualitatively located the important salient features of the flow field associated with seven wings and an ogive-cylinder undergoing a harmonic pitching motion (Gad-el-Hak, 1985a; Gad-el-Hak et al., 1983; Gad-el-Hak & Ho, 1985a; 1985b; 1985c; 1985d; 1986).

Although the principal aim of the above research was to study the unsteady flow around lifting surfaces of current interest, a major and unique finding was that, in the case of steady flow around a delta wing, the classical vortices over its low-pressure side originate as a series of smaller vortices that are shed from the leading edge at a well-defined frequency (Gad-el-Hak & Blackwelder, 1985). This discovery, together with existing knowledge on modulating vortex shedding and pairing in free shear flows, has resulted in the development of a vortex control device that is capable of manipulating the lift of a delta wing in steady flight (Patent Serial No. 06/603,097).

In this report, we very briefly highlight the results of the present investigation in Section 2. Section 3 lists the publications and ciné films resulting from our research. Some of these documents are included in here as Appendices I through V.

## 2. Summary of Progress To-Date

Since 1 May 1983, Flow Industries has been under contract with AFOSR to study the time-dependent flow around two generic classes of wings, the delta wing and the swept wing (including zero sweep), and around a slender body of revolution. Because of the pioneering nature of this work, flow visualization techniques have been used to study the unsteady flow fields and to establish a qualitative overall picture of the flow around the lifting surfaces before embarking on a more detailed study. We have broadly delineated and qualitatively located the important salient features of the flow field associated with seven wings and an ogive-cylinder undergoing a harmonic pitching motion. The wing and body planforms are as follows:

1. A rectangular wing having a NACA 0012 cross section, a chord length of 12.5 cm and an aspect ratio of 4.
2. Same as (1) but with a sharp leading edge.
3. A 25° swept wing with an aspect ratio of 4 and a taper ratio of 0.5.
4. Same as (3) but the wing is swept forward.
5. A 60° delta wing with a sharp leading edge, a chord length of 25 cm and an aspect ratio of 2.3.
6. A 45° delta wing with a sharp leading edge and an aspect ratio of 4.
7. Same as (6) but the wing has a NACA 0012 profile at each spanwise location.
8. An ogive-cylinder having a diameter of 4 cm and a fineness ratio of 10.

To generate the unsteady motion with minimum disturbance to the flow around the lifting surface, a unique, four-bar mechanism was used to sting-mount and to pitch the different models around the desired position along the chord. The wings and body of revolution were pitched harmonically around the quarter-chord

and half-chord points with typical oscillations:  $\alpha(t)^\circ = 15^\circ + 15^\circ \sin(2\pi ft)$ , and with a reduced frequency in the range of 0.03 to 3.0. The wings and body were towed in Flow Industries' 18-meter water tank at a constant speed in the range of 5 to 300 cm/sec ( $2.0 \times 10^3 \leq Re \leq 7.5 \times 10^5$ ).

Several dye visualization techniques were used in the present investigation. Food color or fluorescent dyes were illuminated with flood lights or sheets of laser, respectively. To introduce the dye into the flow field, three methods were employed: direct injection from a system of slots and holes on the suction side of the lifting surface, uniform injection from the entire porous surface of a body, or by laying several thin, horizontal sheets of dye prior to towing the model. The dye layers remained thin due to the inhibition of vertical motion caused by introducing a weak saline stratification in the tank (Gad-el-Hak et al., 1981; Gad-el-Hak, 1985a).

## 2.1 Steady Flow Around Delta Wings

Although the principal aim of the ongoing research investigation has been to study the unsteady flow around three-dimensional lifting surfaces, a major and unique finding was the discovery of a new phenomenon related to the leading edge vortices that characterize the flow on a delta wing in steady flight. We start by briefly summarizing the classical view of such a flow field.

The flow over delta wings at constant angles of attack is dominated by two large bound vortices that result from the flow separation at the leading edge (Elle, 1958; Werlé, 1973; Hoerner & Borst, 1975). With a sharp leading edge at an angle of attack  $\alpha$ , the flow is separated along the entire leading edge forming a strong shear layer. The shear layer is wrapped up in a spiral fashion resulting in a large bound vortex on each side of the wing. The two vortices appear on the suction surface of the wing in the form of an expanding helix when viewed from the apex of the wing. The low pressure associated with the vortices produces additional lift on the wing, often called nonlinear or vortex lift, which is particularly important at large angles of attack.

During the present investigation, the flow around a delta wing in steady flight was visualized using fluorescent dye techniques. The flow visualization experiments clearly showed that the shear layer flow near the leading edge of a delta wing rolls up into discrete vortices. The trajectory of these vortices follows the general outline of the large bound vortex. As they

follow this course, two vortices begin to roll around each other and merge to form a single larger vortex, much the same as observed in a free shear layer originating at a splitter plate between two streams of differing velocity (Winant & Browand, 1974; Brown & Roshko, 1974).

For angles of attack below  $5^\circ$ , the pairing process seems to be inhibited by the proximity of the vortices to the wing surface. The discrete vortices were observed on delta wings with sharp leading edges, with blunt leading edges and with different sweep angles and with a Reynolds number varying over at least one order of magnitude. The shedding frequency of the discrete vortices depends on the mean velocity of the wing and the parameters affecting the thickness of the shear layer. This frequency can be modulated by a pitching motion of the wing (Gad-el-Hak et al., 1983).

The discrete vortices rotate around each other and pair to form larger vortices while simultaneously moving downstream. The vortices typically pair about three times before reaching the trailing edge of the wing. The number of vortices shed per unit time tends to increase as the Reynolds number increases ( $f_{\text{oc}}/U_\infty = 1625/R_c$ ;  $6.25 \times 10^3 \leq R_c \leq 3.50 \times 10^5$ ) and to decrease slightly as the angle of attack increases (Gad-el-Hak & Blackwelder, 1985).

It should be noted that the shedding of discrete vortices in a free shear layer has been observed to occur resonantly at all Reynolds numbers investigated in different laboratories around the world (Ho & Huerre, 1984), including Reynolds numbers well in excess of the critical one. We believe that the analogous phenomenon of shedding from a delta wing is also occurring at all Reynolds numbers and, hence, our observations have universal validity. The shedding of discrete vortices from a free shear layer or from the leading edge of a delta wing is to be contrasted to the shedding from a bluff body. In the latter case, the shedding occurs resonantly at subcritical Reynolds numbers but occurs more randomly at higher Reynolds numbers.

During the above-mentioned research program, attempts were made to modulate the shedding and pairing of the discrete vortices from a delta wing at constant angles of attack. This was inspired by the recent attempts to control the growth rate of a free shear layer by perturbing the flow at the end of the splitter plate (Ho & Huerre, 1984). The flow at the leading edge of the delta wing was perturbed by impulsively injecting a secondary fluid from a slot along that edge. The frequency of perturbation was varied over a wide range, and it was found that maximum changes in the flow field occurred when this frequency

was a subharmonic of the natural shedding frequency of the unperturbed wing. The size of the bound vortices increased by as much as 35 percent by using "weak" perturbation. This offers the potential for a new vortex control device that could conceivably be used to maneuver a delta wing at very high rates. Flow Industries has applied for a patent for a vortex control device that utilizes the principles outlined above (Patent Serial No. 06/603,097).

## 2.2 Unsteady Flow Around Rectangular, Swept and Delta Wings

The time-dependent flow around two generic classes of wings, the delta wing and the swept wing (including zero sweep), was investigated using flow visualization techniques (Gad-el-Hak et al., 1983; Gad-el-Hak & Ho, 1985a; 1985b; 1985c). Recent publications resulting from our research are given in Appendices I through V. Here, we briefly summarize our major findings.

The unsteady separated flow around three-dimensional wings is dominated by large-scale vortices, about a chord length in size. Several features observed at different operating parameter ranges can be understood through the mutual induction among the leading edge separation vortex and the vortices shed as a result of the vertical motion of the trailing edge.

The effect of the mutual induction between the leading edge separation vortex and the trailing edge shedding vortex is very obvious in the high reduced frequency range,  $1 \leq K \leq \pi$ , where the two types of vortices are separated in space. At a low reduced frequency, e.g.,  $K = 0.2$ , the trailing edge is located inside the separation zone originating from the leading edge and the situation is less clear. However, the general concept about the mutual induction should still hold.

The wake pattern of the rectangular wing varies significantly with the reduced frequency and is determined by the phase angle of the leading edge vortex's arrival at the trailing edge. At  $K = 1.0$ , the wake consists of a vortex pair above the chord line and a single clockwise vortex below the chord line. The clockwise vortex induces an upward motion that results in a thick separation zone on the chord. At  $K = 3.0$ , the wake has a vortex pair below the chord line. The induction of the counterclockwise trailing edge vortex suppresses the upward motion of the leading edge vortex; hence, the separation zone on the chord is much thinner than that at  $K = 1.0$ .

A secondary counter-rotating vortex is clearly identified on the sharp leading edge rectangular wing. The mutual induction between the vortex pair lifts the vortices from the wall and results in a large intrusion into the inviscid region. The separation zone is about twice as thick as that on the blunt leading edge wing. The fact that changing the shape of the leading edge leads to changes in the flow field implies that the aerodynamic properties of a wing could be changed with the proper passive control device. This may have important consequences on the ability to achieve supermaneuverability. We speculate that the counter-rotating vortex could have an important role in the generation of unsteady lift.

On the rectangular wing, the leading edge separation vortex convects downstream, while it is stationary during part of the cycle on the swept wing. Near the leading edge separation vortex, a counter-rotating vortex can be seen on the forward swept wing but not on the backward swept wing at the same visualization station. This is not surprising since the separation patterns along the span are known to be very different on backward and forward swept wings having finite aspect ratios. On the delta wing, the leading edge vortex does not convect, rather it experiences a growth-decay cycle.

Additional end and side views of the sharp leading edge rectangular wing revealed the existence of three distinct regions similar to those observed by Adler & Luttgies (1985) on a NACA 0015 wing: the tip vortex, which undergoes a growth-decay cycle; the leading edge separation vortex, which convects downstream and seems to be triggered by the upstream-propagating separation near the wing tip; and the intermediate zone, where the tip vortex and the leading edge vortex interact. The strong three-dimensional effects demonstrated in the present results make it clear that any attempt to model the unsteady flow around finite-aspect-ratio wings using a two-dimensional approximation is bound to fail.

### 2.3 Unsteady Flow Around Slender Bodies of Revolution

The performance of a highly-maneuverable aircraft is critically dependent upon the accurate prediction of the flow around the wings, body and other parts of the vehicle. While the wings are of the utmost importance aerodynamically, the unsteady flow around the body must play a role in the maneuverability of the airplane. During the second phase of the present research, an experimental

program to study the flow about a pitching body of revolution was conducted. The flow visualization results obtained during this study provided crucial data to describe the flow, including quantitative information on the time evolution of the vortex structure, and demonstrated the viability of the approach for more detailed force and/or pressure measurements.

The flow over an ogive-cylinder undergoing a time-dependent pitching motion about the 0.5 station for a mean angle of attack in the range of  $10^\circ$  to  $20^\circ$  was studied. The body is 4 cm in diameter and has a fineness ratio of 10. It was sting-mounted to the existing dynamic support system. We have examined the effects of both a high and a low reduced frequency on the flow field structure for a forward speed in the range of 5 to 140 cm/sec. Longitudinal and transverse planes of the flow field were visualized to provide better detail and to locate more precisely the separation vortex position. Vertical laser light sheets were projected either parallel to or perpendicular to the axis of symmetry of the body. Fluorescent dyes were either placed in the tank as horizontal layers prior to a run, or released continuously from the porous body surface. Our results are summarized in Appendix V. Here we briefly present the main conclusions.

It is found that the unsteady separation phenomenon is significantly different from the separation around a body in steady flight. Two separation vortex pairs were identified as the slender body underwent a complete pitching cycle. We term these the "Frontward and Rearward Separation Vortices". During the upstroke, the unsteady separation starts near the tail of the body and propagates upstream as the angle of attack increases. During the downstroke, the separated zone moves downstream and a secondary separation is triggered by the primary one near the nose of the body. Both separation regions are in the form of counter-rotating vortex pairs that undergo a growth-decay cycle.

The size, circulation and degree of symmetry of the leeward vortices change dramatically with subtle changes in the pitching parameters. On the other hand, at moderate to large reduced frequencies, the Reynolds number effects are negligible. The unsteady effects dominate viscous effects and are mainly responsible for the variations of the aerodynamic properties.

The present investigation provided a first look at the unsteady motion around a body of revolution undergoing a pitching motion. Other modes of unsteadiness should also be studied, for example plunging or time-dependent

ambient velocity. Recent research indicates that the mode of the unsteady motion can significantly affect the hysteresis loops and the aerodynamic properties of a lifting surface. The results of the visualization experiments should be used to design fast-response probe experiments to measure the velocity field and to correlate the visualization events with the unsteady forces and moments experienced by the slender body.

3. List of Publications and Films

The results to-date of the investigation on unsteady flow around wings and bodies of revolution are summarized in the following films and publications:

1. Gad-el-Hak, M. (1983) "The Pitching Delta Wing," Flow Research Film No. 55.
2. Gad-el-Hak, M. (1984) "Three-Dimensional Wing Configurations in a Pitching Motion, Part I: Low Reduced Frequency," Flow Research Film No. 57.
3. Gad-el-Hak, M. (1984) "Three-Dimensional Wing Configurations in a Pitching Motion, Part II: Moderate-to-High Reduced Frequency," Flow Research Film No. 58.
4. Gad-el-Hak, M. (1984) "Vortex Control Device for a Delta Wing," Flow Research Film No. 59.
5. Gad-el-Hak, M. (1985) "Unsteady Flow Around a Slender Body of Revolution," Flow Research Film No. 60, Parts 1-4.
6. Gad-el-Hak, M., Ho, C.-M., and Blackwelder, R. F. (1983) "A Visual Study of a Delta Wing in Steady and Unsteady Motion," in Unsteady Separated Flows, eds. M. S. Francis & M. W. Luttges, Univ. Colorado, p. 45.
7. Gad-el-Hak, M., Blackwelder, R. F., and Ho, C.-M. (1983) "Coherent Structures in Steady and Unsteady Motions of a Delta Wing," Bul. Am. Phys. Soc. 28, p. 1397.
8. Gad-el-Hak, M., and Ho, C.-M. (1984) "Vortex Interaction on Pitching, Three-Dimensional Lifting Surfaces," Bul. Am. Phys. Soc. 29, p. 1574.
9. Gad-el-Hak, M., and Ho, C.-M. (1985) "Three-Dimensional Effects on a Pitching Lifting Surface," AIAA Paper No. 85-0041.

10. Gad-el-Hak, M., and Blackwelder, R. F. (1985) "The Discrete Vortices from a Delta Wing," AIAA J. 23, p. 961.
11. Gad-el-Hak, M., and Ho, C.-M. (1985) "The Pitching Delta Wing," AIAA J., in Press.
12. Gad-el-Hak, M. (1985) "The Use of the Dye-Layer Technique for Unsteady Flow Visualization," J. Fluids Eng., in press.
13. Gad-el-Hak, M., and Ho, C.-M. (1985) "Unsteady Vortical Flow Around Three-Dimensional Lifting Surfaces," AIAA J. in press.
14. Gad-el-Hak, M., and Ho, C.-M. (1985) "Unsteady Flow Around a Slender Body of Revolution," Bul. Am. Phys. Soc. 30.
15. Gad-el-Hak, M., (1985) "Unsteady Flow Around an Ogive-Cylinder", submitted to J. Aircraft.
16. Gad-el-Hak, M., and Ho, C.-M. (1986) "Aerodynamics of a Missile in Unsteady Flight," AIAA Paper No. 86-0572.

Copies of these films and papers have been given to the contract monitor at AFOSR, Dr. James D. Wilson. Papers No. 9, 10, 11, 13 and 15 above are included in this report as Appendices I through V. We have also applied for a patent entitled "Method and Apparatus for Controlling Bound Vortices in the Vicinity of Lift- ing Surfaces." The idea for this vortex control device was inspired by the present research results. The principal investigator, Dr. Mohamed Gad-el-Hak, has been invited by numerous universities and research institutes to speak about unsteady aerodynamics and supermaneuverability.

REFERENCES

- Adler, J. N., and Luttgies, M. W. (1985) "Three-Dimensionality in Unsteady Flow About a Wing," AIAA Paper No. 85-0132.
- Adler, J. N., Robinson, M. C., Luttgies, M. W., and Kennedy, D. A. (1983) "Visualizing Unsteady Separated Flows," in Flow Visualization 3, ed. W. J. Yang, Hemisphere, p. 342.
- Baldwin, B. S., and Lomax, H. (1978) "Thin Layer Approximation and Algebraic Model for Separated Turbulent Flows," AIAA Paper No. 78-257.
- Brown, C. E., and Michael, W. H. (1954) "Effect of Leading-Edge Separation on the Lift of a Delta Wing," J. Aero. Sci. 21, p. 690.
- Brown, G. L., and Roshko, A. (1974) "On Density Effects and Large Structure in Turbulent Mixing Layers," J. Fluid Mech. 64, p. 775.
- Cheng, H. K. (1977) "Lifting-Line Theory for Oblique Wings," AIAA J. 16, p. 1211.
- Elle, B. J. (1958) "An Investigation at Low Speed of the Flow Near the Apex of Thin Delta Wings with Sharp Leading Edges," ARC Tech. Rep. R&M No. 3176.
- Gad-el-Hak, M. (1985a) "The Use of the Dye-Layer Technique for Unsteady Flow Visualization," J. Fluids Eng., in press
- Gad-el-Hak, M., and Blackwelder, R. F. (1985) "The Discrete Vortices from a Delta Wing," AIAA J. 23, p. 161.
- Gad-el-Hak, M., Blackwelder, R. F., and Riley, J. J. (1981) "On the Growth of Turbulent Regions in Laminar Boundary Layers," J. Fluid Mech. 110, p. 73.
- Gad-el-Hak, M., and Ho, C.-M. (1985a) "Three-Dimensional Effects on a Pitching Lifting Surface," AIAA Paper No. 85-0041.

Gad-el-Hak, M., and Ho, C.-M. (1985b) "The Pitching Delta Wing," AIAA J., in press.

Gad-el-Hak, M., and Ho, C.-M. (1985c) "Unsteady Vortical Flow Around Three-Dimensional Lifting Surfaces," AIAA J., in press.

Gad-el-Hak, M., and Ho, C.-M. (1985d) "Unsteady Flow Around an Ogive-Cylinder," submitted to J. Aircraft.

Gad-el-Hak, M., and Ho, C.-M. (1986) "Aerodynamics of a Missile in Unsteady Flight," AIAA Paper No. 86-0572.

Gad-el-Hak, M., Ho, C.-M., and Blackwelder, R. F. (1983) "A Visual Study of a Delta Wing in Steady and Unsteady Motion," in Unsteady Separated Flows, eds. M. S. Francis & M. W. Luttges, Univ. Colorado, p. 45.

Herbst, W. B. (1983a) "Dynamics of Air Combat," J. Aircraft 20, p. 594.

Herbst, W. B. (1983b) "Supermaneuverability," in Unsteady Separated Flows, eds. M. S. Francis & M. W. Luttges, Univ. Colorado, p. 1.

Helin, H. E., and Walker, J. M. (1985) "Interrelated Effects of Pitch Rate and Pivot on Airfoil Dynamic Stall," AIAA Paper No. 85-0130.

Ho, C.-M., and Huerre (1984) "Perturbed Free Shear Layers," Ann. Review Fluid Mech. 16, p. 365.

Hoeijmakers, H. W. M., Vaatstra, W., and Verhaagen, N. G. (1982) "On the Vortex Flow Over Delta and Double-Delta Wings," AIAA Paper No. 82-0949.

Hoerner, S. F., and Borst, H. V. (1975) Fluid Dynamic Lift, L. A. Hoerner publisher, Brick Town, NJ.

Konstadinopoulos, P., Mook, D. T., and Nayfeh, A. H. (1981) "A Numerical Method for General Unsteady Aerodynamics," AIAA Paper No. 81-1877.

- Konstadinopoulos, P., Mook, D. T. and Nayfeh, A. H. (1983) "Numerical Simulation of the Subsonic Wing-Rock Phenomenon," AIAA Paper No. 83-2115.
- Legendre, R. (1952) "Ecoulement au Voisinage de la Pointe Avant D'une Aile a Forte Fleche aux Incidences Moyennes," La Rech. Aéro. 30, p. 3.
- McCroskey, W. J. (1982) "Unsteady Airfoils," Ann. Rev. Fluid Mech. 14, p. 285.
- McCroskey, W. J., Carr, L. W., and McAlister, K. W. (1976) "Dynamic Stall Experiments on Oscillating Airfoils," AIAA J. 14, p. 57.
- McCroskey, W. J., and Pucci, S. L. (1982) "Viscous-Inviscid Interaction on Oscillating Airfoils in Subsonic Flow," AIAA J. 20, p. 167.
- Nayfeh, A. H., Mook, D. T., and Yen, A. (1979) "The Aerodynamics of Small Harmonic Oscillations Around Large Angles of Attack," AIAA Paper No. 79-1520.
- Nielsen, J. N. (1979) "Missile Aerodynamics-Past, Present, Future," AIAA Paper No. 79-1819.
- Robinson, M. C., and Luttgies, M. W. (1983) "Unsteady Flow Separation and Attachment Induced by Pitching Airfoils," AIAA Paper No. 83-0131.
- Smith, J. H. B. (1968) "Improved Calculations of Leading-Edge Separation from Slender, Thin, Delta Wings," Proc. Roy. Soc. A 306, p. 69.
- Walker, J. M., and Helin, H. E. (1985) "An Experimental Investigation of an Airfoil Undergoing Large Amplitude Pitching Motions," AIAA Paper No. 85-0039.
- Werlé, H. (1973) "Hydrodynamic Flow Visualization," Ann. Review Fluid Mech. 5, p. 361.

Winant, C. D., and Browand, F. K. (1974) "Vortex Pairing: the Mechanism of Turbulent Mixing-Layer Growth at Moderate Reynolds Number," J. Fluid Mech. 63, p. 237.

Appendix I: Three-Dimensional Effects on a Pitching  
Lifting Surface

# AIAA'85

**AIAA-85-0041**

**Three-Dimensional Effects on a  
Pitching Lifting Surface**

M. Gad-el-Hak and Chih-Ming Ho,  
Flow Research Co., Kent, WA

**AIAA 23rd Aerospace Sciences Meeting**

January 14-17, 1985/Reno, Nevada

For permission to copy or republish, contact the American Institute of Aeronautics and Astronautics  
1633 Broadway, New York, NY 10019

# THREE-DIMENSIONAL EFFECTS ON A PITCHING LIFTING SURFACE

Mohamed Gad-el-Hak\*  
and  
Chih-Ming Ho\*\*

Flow Research Company  
Kent, WA 98032

## Abstract

The low Reynolds number, time-dependent flow around two generic classes of wings is studied in a water towing tank. Delta and swept (including zero sweep) wings were sting-mounted to a four-bar mechanism which generated a large amplitude, harmonic pitching motion around the 1/4-chord location, at a reduced frequency that varied in the range of 0.2 to 3. Fluorescent dye-layers were placed in the weakly-stratified water channel prior to towing the wing. The horizontal dye sheets were excited using a vertical sheet of laser light. The dye marked the flow in the separation region around the wing, the wake region, and the potential flow away from the lifting surface. The complex, time-dependent flow field around the different wings can be mostly explained from the mutual induction between the leading edge separation vortex and the trailing edge shedding vortex. The reduced frequency, the shape of the leading edge, and the wing's planform play important roles in determining the flow patterns.

## Nomenclature

AR	aspect ratio
c	root chord
f	pitching frequency
K	reduced frequency, $\pi fc/U_\infty$
$R_c$	chord Reynolds number, $U_\infty c/\nu$
r	rotation arm along the chord
s	wing semispan
t	time (sec)
$U_\infty$	towing speed
V	vertical velocity
$V_w$	vertical velocity at the wing surface
x,y,z	Cartesian coordinates fixed with the wing
$\alpha(t)$	angle of attack
$\nu$	kinematic viscosity

## I. Introduction

With the recent advances in short range infrared guided missiles, a significant change in close air combat characteristics emphasizing very fast maneuverability becomes highly desirable. This has led to a growing interest in the so called "supermaneuverability" of fighter aircraft, where previously unattained regions of the maneuver envelope are attempted. For example, post-stall flight maneuver and side slipping.<sup>1,2</sup> Current research in support of supermaneuverability involves studies of dynamic stall on two- and three-dimensional lifting surfaces, understanding the behavior of attached and

separated unsteady shear layers affected by time-dependent boundary conditions, and productively exploiting the unsteady flow characteristics to improve aerodynamic efficiency and enhance performance.

Aerodynamic research for time-dependent viscous flows at high incidence has, to date, centered primarily on the flow over two-dimensional airfoils.<sup>3,4</sup> The data from these studies have shed considerable light on the exceedingly complex viscous-inviscid interactions associated with time-varying flow separation. The data, furthermore, provide a meaningful base to assess numerical procedures and to develop alternative approaches as required.<sup>5</sup>

Two dimensional data can play an essential role in high aspect ratio applications (e.g., helicopter blades and commercial aircraft) where the local flow behaves, in a sense, two-dimensionally. The classic lifting line theory for an unswept wing in steady flow, for example, provides a local induced incidence correction to account for finite aspect ratio effects. This theory has been extended to include wings with sweep.<sup>6</sup> The lifting line concept, however, is of little value for the low aspect ratio wings of fighter/attack aircraft because the local airfoil section, particularly for the higher incidence angles, cannot be divorced from the wing as an entirety. In other words, the three dimensionality of the lifting surface is a non-negligible factor in determining its aerodynamic properties.

Considerable experimental/theoretical research has been focused on studying the flow over delta and swept wings for steady flow and time-independent boundary conditions.<sup>7</sup> Sophisticated inviscid numerical/analytical models have been developed for design purposes to describe the flow field at high angles of attack by "modeling" the vorticity shed from the wing edges. The sharpness of the leading edge invariably fixes the location of the shed vorticity feeding the leeward "conical-like" vortices -- a factor embedded in theoretical modeling for delta wings.<sup>8-10</sup>

Very recently A. H. Nayfeh (private communication) has extended this inviscid approach to time-dependent flows by a very efficient numerical method. During maneuvering, the unsteadiness is an important parameter to be considered. The studies about the unsteady, two-dimensional airfoils have indicated that the lift and drag experience hysteresis loops during an oscillation cycle. Corresponding information for unsteady, three-dimensional wings are very scarce. For three-dimensional lifting surface, it is quite likely that inviscid techniques coupled with empiricism will be the primary short term "engineering" tool for predicting the time-dependent flow. The long term goal would be a Navier-Stokes solution with appropriate turbulence modeling.

\*Senior Research Scientist.

\*\*Consultant. Permanent Address: Department of Aerospace Engineering, University of Southern California. Member AIAA.

### III. Results and Discussion

The seven lifting surfaces were pitched around the 1/4 chord position at a reduced frequency,  $K$ , that varied in the range of 0.2 to 3.0. The wings were towed in the water channel at a root-chord Reynolds number that varied in the range of  $6.25 \times 10^3$  to  $3.50 \times 10^5$ . The dye-layers technique was used to visualize the unsteady flow in the separation region around the wing, the potential flow region away from the wing and the wake of the lifting surface.

Figure 1 is a sequence of photographs taken from the ciné film depicting a left to right ambient flow and the NACA 0012 rectangular wing ( $c = 12.5$  cm,  $AR = 4$ ) undergoing the pitching motion  $\alpha(t)^\circ = 15^\circ + 15^\circ \sin(1.57t)$ , where  $\alpha(t)$  is the time-dependent angle of attack, and  $t$  is time in seconds. The wing was towed at a speed of  $U_\infty = 10$  cm/sec ( $Re_c = 1.25 \times 10^4$ ), and the reduced frequency was  $K = 1.0$ . The photographs in Figure 1 show a typical oscillation cycle\* ( $0^\circ$  to  $30^\circ$  to  $0^\circ$ ) of the unsteady flow field in a vertical plane, parallel to the flow direction and located at  $z = 10$  cm (40% of the semispan,  $s$ ). Both the upward and downward motions of the wing are shown side by side for  $\alpha = 0^\circ, 5^\circ, 10^\circ, 15^\circ, 20^\circ, 25^\circ$  and  $30^\circ$ .

The complex, unsteady flow field associated with the pitching wing can be mostly explained from the mutual induction between the leading edge separation vortex and the trailing edge shedding vortex. At large angle of attack, the flow separates at the leading edge and a clockwise vortex is formed and is convected downstream. This vortex is eventually shed from the trailing edge. When the wing is in the upstroke, the trailing edge moves downward and a shear layer is created at the upper surface. The shear layer rolls up into a counter-clockwise vortex that is also shed from the trailing edge. Conversely, a clockwise vortex is formed during the downstroke. These vortices enter the wake at different phase of the cycle and result in a particular wake pattern for a given reduced frequency. For the rectangular wing pitching at the reduced frequency of  $K = 1$ , the clockwise separation vortex from the leading edge convects downstream and is shed from the trailing edge just before the wing starts the upstroke of the new cycle. During this upstroke, a counter-clockwise vortex is generated at the trailing edge and forms a vortex pair with the leading edge vortex. This vortex pair tends to convect downstream and upward, so that the induced flow above the chord is more or less cancelled. During the downstroke, a clockwise vortex is generated at the trailing edge and its induced velocity tends to thicken the separation zone above the wing.

#### Effects of Leading Edge Shape

Two rectangular wings having the same chord ( $c = 12.5$  cm) and aspect ratio ( $AR = 4$ ) were tested to determine the effects of the leading edge shape. The first wing has a NACA 0012 cross-section, while the second wing has a flat surface and a sharp leading edge. The two wings were towed at a speed of  $U_\infty = 10$  cm/sec ( $Re_c = 1.25 \times 10^4$ ) and were harmonically pitched around the 1/4 chord point such

\* The first oscillation cycle is different from the second or subsequent cycles, hence the first cycle is not used in any of the figures presented here.

that  $\alpha(t)^\circ = 15^\circ + 15^\circ \sin(1.6t)$ ;  $K = 1.0$ . A typical oscillation cycle of the unsteady flow field in a vertical plane, parallel to the flow direction and located at  $z = 10$  cm is shown in Figures 1 and 2 for the blunt and the sharp leading edge wings, respectively.

The distinct characteristics of the sharp leading edge wing is the existence of a counter-rotating vortex upstream of the leading edge separation vortex. The mutual induction of the vortex pair lifts itself away from the wall and results in a large intrusion into the inviscid region. The counter-rotating vortex is not observed on the blunt leading edge wing. In this case, the leading edge separation vortex rolls along the chord. The separated region is much thinner than that on the sharp leading edge wing.

The counter-rotating vortex may have important implication in controlling the unsteady flow. In the boundary layer produced by an impinging jet, a counter-rotating vortex occurs as a result of the unsteady separation produced by the shear layer vortex in the jet.<sup>13</sup> Large suction is generated on the impinging plate by the counter-rotating vortex. It has been speculated<sup>14</sup> that the high level, unsteady lift of pitching wings are caused by a corresponding large suction associated with a counter-rotating vortex. Such a vortex has been clearly identified on the sharp leading edge rectangular wing depicted on Figure 2. The large suction associated with the counter-rotating vortex implies that the aerodynamic characteristics could be significantly altered by modifying the evolution of this vortex, offering the potential for enhancing the performance of a given lifting surface.

#### Effects of Reduced Frequency

To investigate the effects of the reduced frequency on the flow field, the sharp leading edge rectangular wing was pitched at the reduced frequencies  $K = 0.2, 1.0$  and  $3.0$ . The root chord Reynolds number for all three runs was approximately  $Re_c = 10^4$ , and the angle of attack was  $\alpha(t)^\circ = 15^\circ + 15^\circ$ . Figures 2, 3 and 4 show the sequence of photographs during a typical cycle at the three reduced frequencies 1.0, 0.2 and 3.0, respectively. The vertical laser light was parallel to the flow and was at a distance of 10 cm off the wing centerline, in all three cases.

At the lowest reduced frequency,  $K = 0.2$ , the oscillation period is relatively long and the flow has more time to adjust to angle of attack variations. As shown in Figure 3, the trailing edge vortices are located inside the separated zone originating from the leading edge. The mutual induction between the two vortical zones is less clear compared to higher reduced frequency runs. However, the general concept should still hold.

For  $K = 1.0$  and  $3.0$ , the effect of the mutual induction between the leading edge separation vortex and the trailing edge shedding vortex is more apparent, since the two types of vortices are separated in space. The difference between the  $K = 1.0$  case and the  $K = 3.0$  case is due to the vortex pattern in the wake. For  $K = 1.0$  (Figure 2), the clockwise leading edge separation vortex convects downstream at about 45% of the towing speed, and is shed from the trailing edge just before the wing starts the upstroke of the new cycle. During this

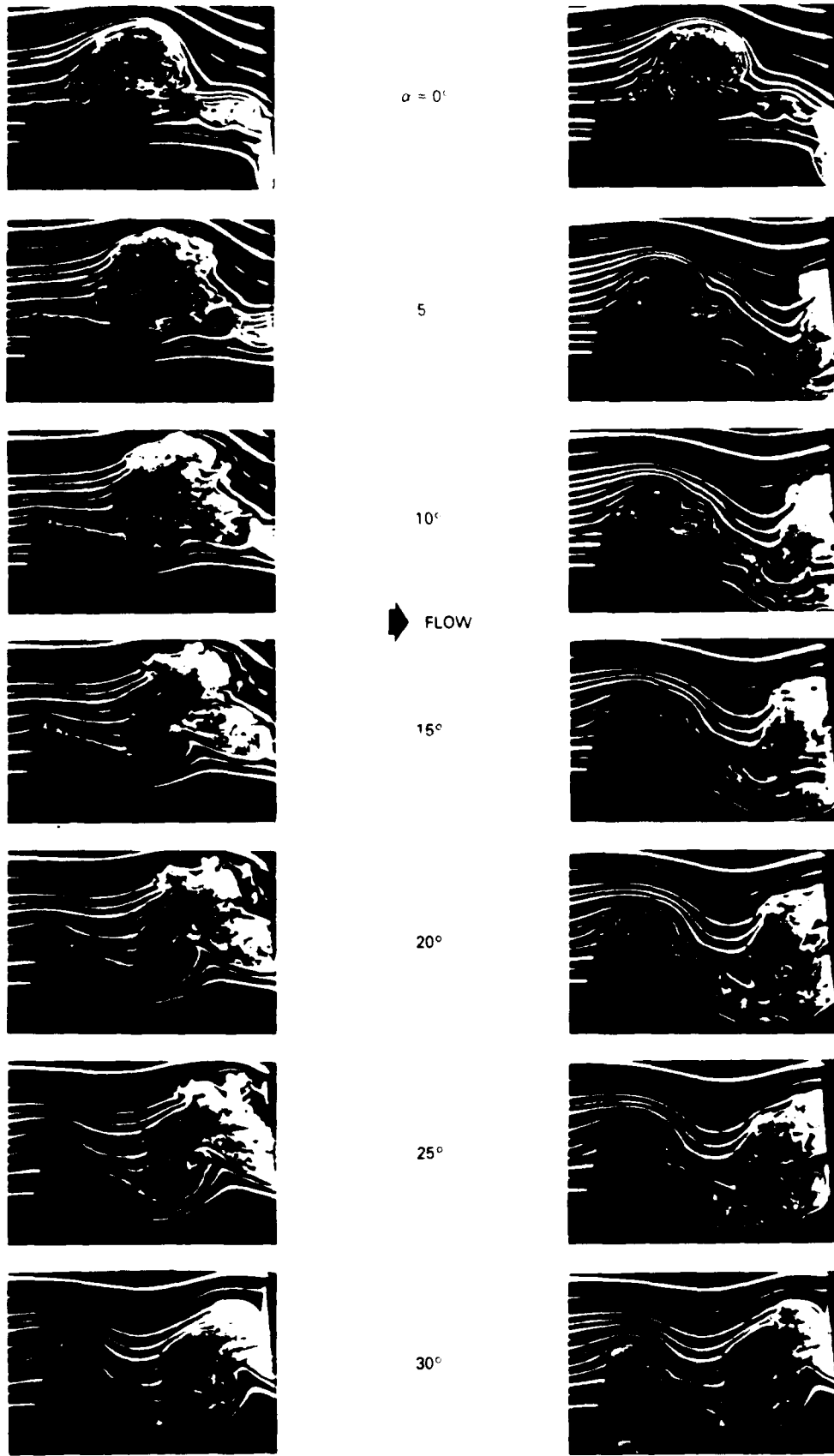


Figure 2. Side View of Sharp Leading Edge Rectangular Wing.

$AR = 4; R_c = 1.25 \times 10^4; K = 1.0; \alpha(t)^\circ = 15^\circ + 15^\circ \sin(1.63t).$

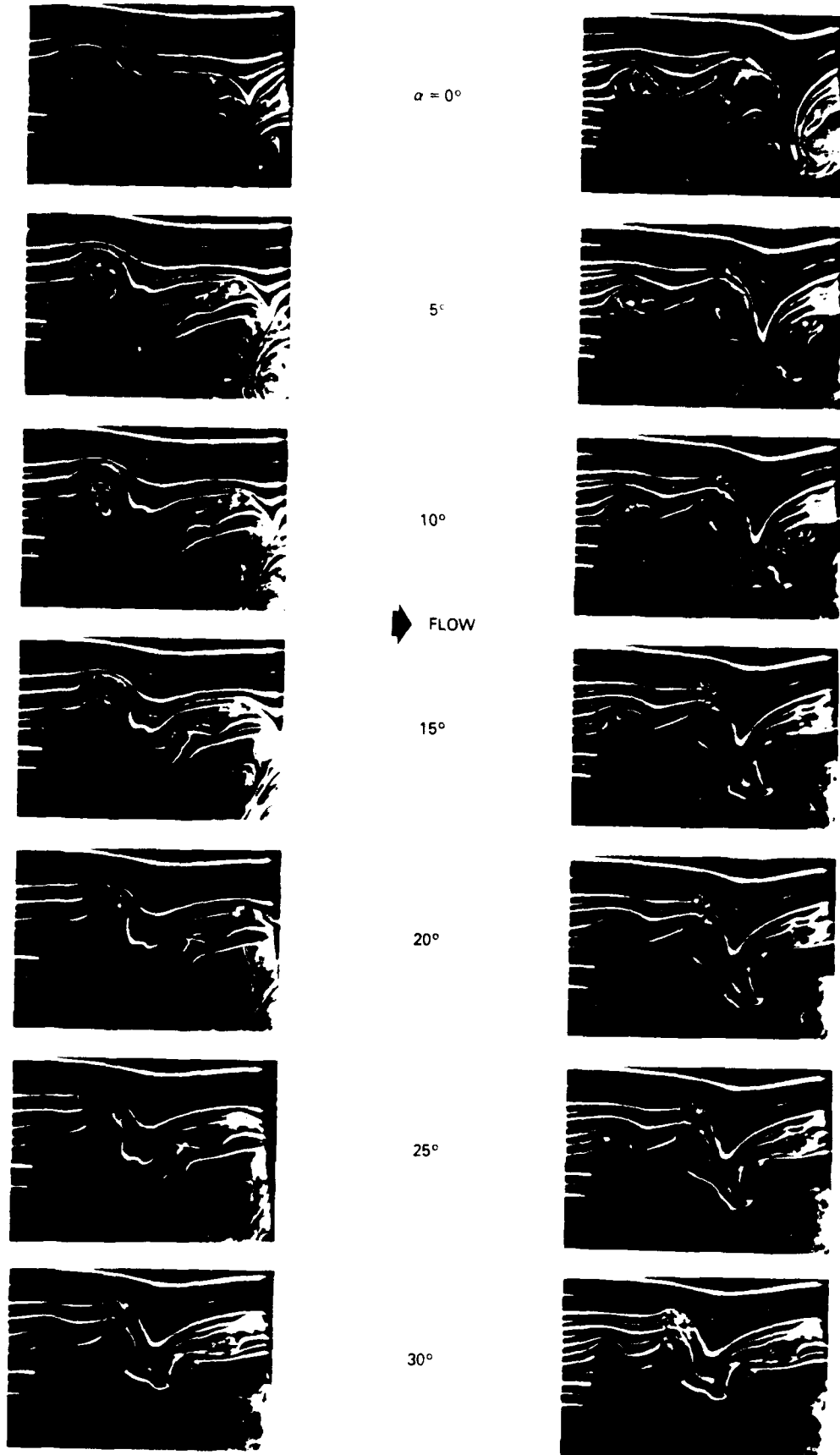


Figure 4. Side View of Sharp Leading Edge Rectangular Wing.

$AR = 4; R_c = 8.63 \times 10^3; K = 3.0; \alpha(t) = 15^\circ + 15^\circ \sin(3.33t).$

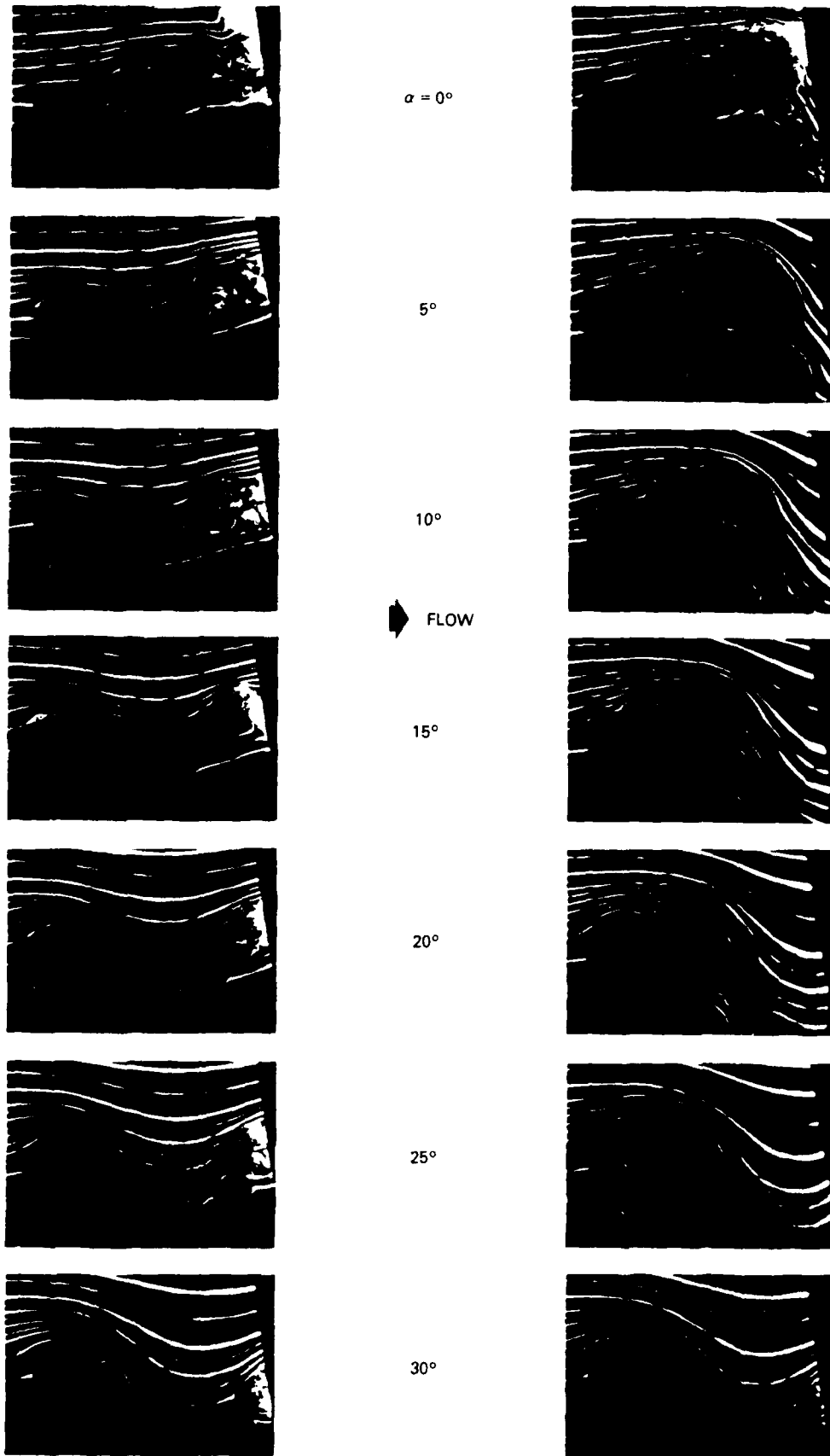


Figure 7. Side View of Sharp Leading Edge Swept Wing.  
 $AR = 4; R_c = 1.65 \times 10^4; K = 1.0; \alpha(t) = 15^\circ + 15^\circ \sin(1.19t)$ .

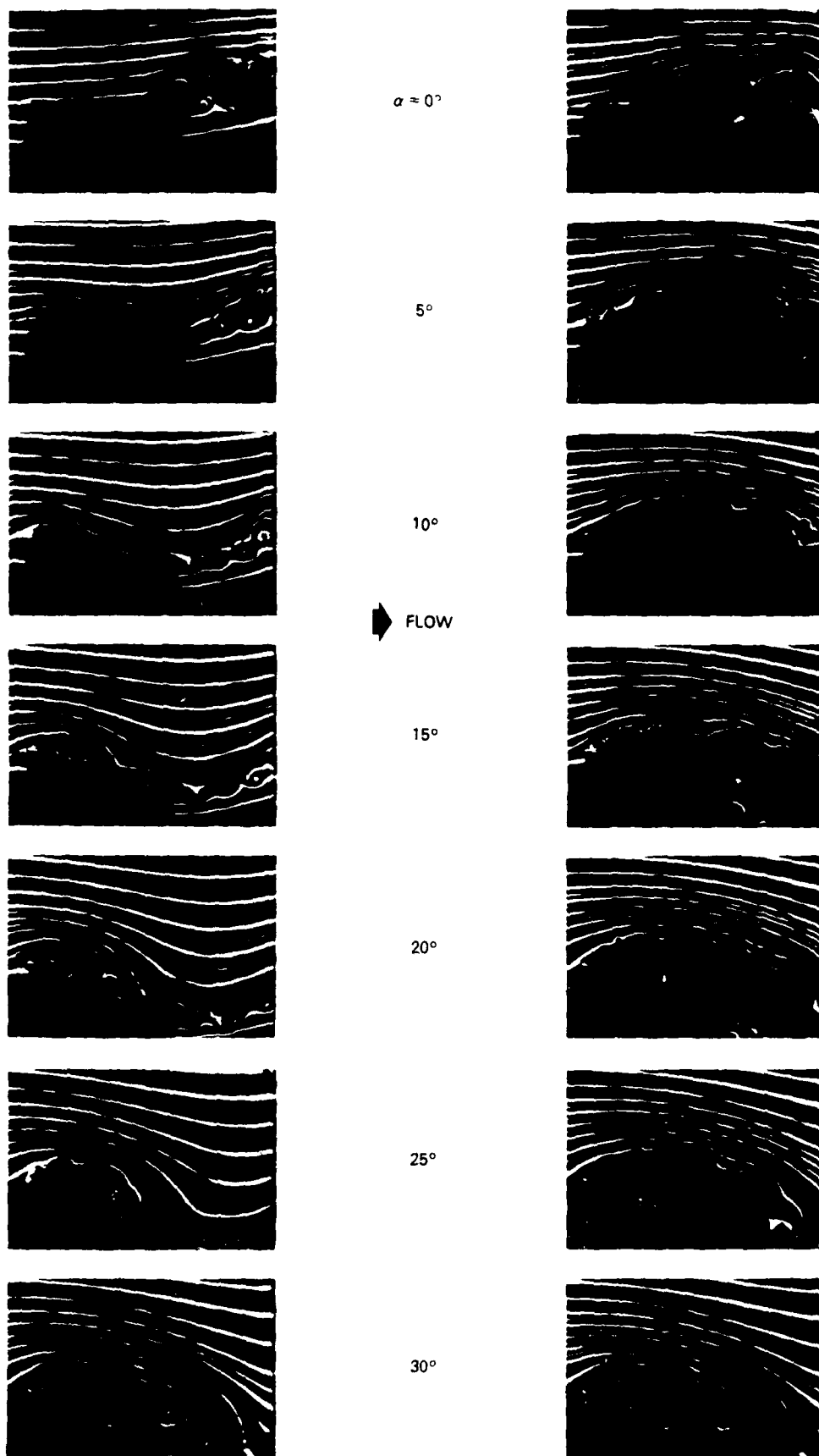


Figure 9. Side View of 45° Sweep, Sharp Leading Edge, Delta Wing.

$$AR = 4; R_c = 2.5 \times 10^4; K = 1.0; \alpha(t) = 15^\circ + 15^\circ \sin(0.82t).$$

-- NOTES --

Appendix II: The Discrete Vortices from a Delta Wing

# **The Discrete Vortices from a Delta Wing**

M. Gad-el-Hak and R. F. Blackwelder



Reprinted from

**AIAA Journal**

Volume 23, Number 6, June 1985, Page 961

AMERICAN INSTITUTE OF AERONAUTICS AND ASTRONAUTICS • 1633 BROADWAY • NEW YORK, N. Y. 10019

Appendix III: The Pitching Delta Wing

Revised Manuscript Submitted to

the AIAA Journal

Log Number: J14936

The Pitching Delta Wing

Mohamed Gad-el-Hak\*  
Chi-Ming Ho\*\*

Flow Research Company  
Kent, Washington 98032

\*Senior Research Scientist.

\*\*Consultant. Permanent address: Department of Aerospace Engineering,  
University of Southern California, Los Angeles, California 90007.  
Member AIAA.

## The Pitching Delta Wing

Mohamed Gad-el-Hak\*  
Chih-Ming Ho\*\*

Flow Research Company  
Kent, WA 98032

### ABSTRACT

Delta wings in steady flow can provide high lift at large angles of attack and are therefore used on many high performance aircrafts. However, the unsteady aerodynamic properties of a delta wing are practically unknown, though they are vital information for operating and designing airplanes for post-stall and other maneuvering. In this study, the flow fields around two pitching delta wings with apex angles of  $90^\circ$  and  $60^\circ$  were visualized in a towing tank at chord Reynolds numbers up to  $3.5 \times 10^5$ . The reduced frequency was varied in the range of 0.05 to 3. The leading edge separation vortex went through a growth-decay cycle with hysteresis during a pitching period. A distinct change of the separated flow was observed at a reduced frequency around  $\pi$ .

---

\*Senior Research Scientist.

\*\*Consultant. Permanent address: Department of Aerospace Engineering,  
University of Southern California, Los Angeles, California 90007.  
Member AIAA.

## NOMENCLATURE

AR	aspect ratio
c	root chord
f	pitching frequency
H	height of the dyed region in a y-z plane
K	reduced frequency, $\pi fc/U_\infty$
N	Brunt-Väisälä frequency
$R_c$	chord Reynolds number, $U_\infty c/\nu$
s	wing semispan
t	time (sec)
$U_\infty$	towing speed
V	vertical velocity
$V_w$	vertical velocity at the wing surface
x,y,z	Cartesian coordinates fixed with the wing
$\alpha(t)$	angle of attack
$\alpha_0$	mean angle of attack
$\beta$	apex angle
$\gamma$	angle between vortex cores
$\lambda$	perturbation wavelength
$\nu$	kinematic viscosity

## 1. INTRODUCTION

In a steady flow, the lift of a two-dimensional airfoil is mainly contributed by the leading edge suction peak. The lift increases with increasing angle of attack until the stall angle is reached. The separation on the upper surface will then reduce the leading edge suction peak causing the lift to drop. The static stall angle for a two-dimensional airfoil is about  $12^\circ$ . The lift-producing mechanism of a delta wing is somewhat different. The leading edge suction peaks predicted by potential theory do not exist.<sup>1</sup> Instead, two smooth suction peaks inward of the leading edges are detected. These peaks are produced by a pair of stationary leading edge vortices that are formed by separated flow on the low-pressure side of the wing. Therefore, the lift on a delta wing is created by the separated vortical structures rather than by the attached flow over a convex surface. The lift keeps increasing with  $\alpha$  until the leading edge vortex breaks down at an angle of attack of  $30^\circ$  or more. Hence, a delta wing is a good means to obtain high lift at large angles of attack. The aspect ratio of a delta wing is relatively small, which results in a low lift-to-drag ratio at subsonic speeds. Accordingly, delta wings are primarily designed for supersonic speeds.

Fairly extensive studies about the steady flow around delta wings have been reported by various researchers. The flow field is essentially determined by the sweep angle of the leading edge, the cross-section shape and the angle of attack. Elle examined the core positions of the separation vortex as a function of the angle of attack.<sup>2</sup> He visualized the vortices by using air bubbles in a water channel. The angle between the two cores,  $\gamma$ , does not change significantly at different angles of attack. The ratio between  $\gamma$  and the apex angle,  $\beta$ , stays around 0.6, but the vortex cores lift away from the wing

surface with increasing  $\alpha$ . Fink and Taylor investigated the pressure distribution on a wing with  $\beta = 20^\circ$ .<sup>3</sup> The suction peaks of the spanwise pressure distribution at several chordwise locations always occurred at about 60% of the semispan from the center for all tested angles of attack,  $5^\circ \leq \alpha \leq 30^\circ$ . In other words, the suction peaks were located under the vortex cores.

Under practical conditions, fast maneuvering is always required for high performance airplanes. The unsteady aerodynamic properties can be significantly different from those in steady flow. The operation of the aircraft can either benefit or be hampered by the special features in the unsteady flow. For example, the maximum lift of a pitching two-dimensional airfoil is much higher than the static maximum lift.<sup>4,5</sup> However, the dynamic stall is much more abrupt than the static stall. In the case of a delta wing, the pressing problem is that the unsteady aerodynamic properties are practically unknown,<sup>5,6</sup> although the delta wing is the main type of airfoil used on high-performance airplanes.

In the present investigation, the unsteady flow field around a delta wing was visualized by several dye techniques. The experimental approach is discussed in Section 2. The detailed development process of the leading edge separation vortex is first described in Section 3. Then, the hysteresis loop of the vortex, the effect of the reduced frequency, as well as the existence and possible importance of a counter-rotating vortex are discussed.

## 2. EXPERIMENTAL APPROACH

### 2.1 Model and Test Conditions

Two delta wings with leading edge sweeps of  $45^\circ$  and  $60^\circ$  were used in the present investigation. The root chord of both wings was 25 cm, and the chord Reynolds number varied in the range of  $2.5 \times 10^4$  to  $3.5 \times 10^5$ . Figure 1 is a sketch of the  $45^\circ$  delta wing, which had a NACA 0012 profile at each spanwise section. The wing was made of two aluminum pieces with grooves on the inner surface of each for dye passage and storage. The  $60^\circ$  delta wing had a flat surface and a sharp leading edge and was made of Plexiglas.

A four-bar mechanism was used to sting-mount and to pitch the delta wing around the desired position along the chord. In the experiments reported herein, the wing was pitched around the quarter-chord position. The mean angle of attack could be set from  $0^\circ$  to  $45^\circ$ . A Boston Ratiotrol motor drove the four-bar linkages to produce approximately sinusoidal oscillations of amplitude  $\pm 5^\circ$ ,  $\pm 10^\circ$  and  $\pm 15^\circ$  about a given mean angle of attack. The reduced frequency,  $K \equiv \pi fc/U_\infty$ , was varied in the range of 0.05 to 3.\* A digital readout displayed the instantaneous angle of attack of the wing.

### 2.2 Towing Tank System

The wing used in the present investigation was towed at speeds in the range of 10 to 140 cm/sec through the water channel described by Gad-el-Hak et al.<sup>7</sup> The towing tank is 18 m long, 1.2 m wide, and 0.9 m deep. The pitching

---

\*An aircraft will not, of course, maneuver at a reduced frequency of 3.

However, several important features of the complex flow field under investigation were more readily apparent in the high frequency range.

mechanism was rigidly mounted on a carriage that rides on two tracks mounted on top of the towing system. During towing, the carriage was supported by an oil film, which ensured a vibrationless tow. The equivalent freestream turbulence was checked using a hot-film probe, and was found to be about 0.1 percent of the mean towing speed.

### 2.3 Flow Visualization

Food color and fluorescent dyes were used in the present investigation. The food color dyes were illuminated with conventional flood lights. The fluorescent dyes were excited with sheets of laser light projected in the desired plane. To produce a sheet of light, a 5-Watt argon-ion laser (Spectra Physics, Model 164) was used with a mirror mounted on an optical scanner having a 720-Hz natural frequency (General Scanning, Model G124). A sine-wave signal generator, set at a frequency equal to the inverse of the camera shutter speed, drove the optical scanner to produce light sheets approximately 1 mm thick.

Side views of the flow field were obtained using a vertical sheet of laser light in the x-y plane at  $z = 10$  cm (40% of the semispan of the  $45^\circ$  sweep wing) and a camera towed with the wing but located outside the tank, as shown in Figure 1. End views were obtained using a vertical sheet of laser light in the y-z plane at  $x = 20$  cm (80% of the root chord) and an underwater camera towed behind the wing using the same carriage.

Dye sheets or dye lines were seeped into the boundary layer through a system of slots and holes on the suction side of the wing. The slots were 0.2 mm wide and were milled at a  $45^\circ$  angle to minimize the flow disturbance. The holes were 0.4 mm in diameter and were spaced at 1 cm center to center.

Dye was also placed in the flow field by laying several thin, horizontal sheets prior to towing the wing. The dye layers remained thin, about 1 mm in thickness, due to the inhibition of vertical motion caused by introducing a weak saline stratification in the tank. The dye layers remained quiescent until disturbed by the flow field on and around the wing. Thus, the boundary layer flow as well as the potential flow could be observed since the dye layers existed in both flow regions. Ciné films of the runs presented in this paper are available upon request (Flow Research Films No. 55 through 59).

For the dye-layer runs, the density gradient in the tank was about  $10^{-4}$  gm/cm<sup>4</sup>, which yields a Brunt-Väisälä frequency of  $N = 0.05$  Hz. The time scale associated with this weak stratification is large compared to a typical convection time scale; hence, the stratification should have little effect on the dynamics of the flow. This was verified experimentally by conducting two runs using the dye injection method, in the presence and in the absence of stratification in the tank. The visualization patterns in the two runs were indistinguishable.

### 3. EXPERIMENTAL RESULTS

The main feature of the delta wing flow is the leading edge separation vortex, which produces the lift. The flow visualization results in the steady case are reported elsewhere.<sup>8,9</sup> In the unsteady case, the flow alternates between attached and separated phases during one cycle. Obviously, the complicated phenomenon of unsteady separation plays the main role in changing the aerodynamic properties.<sup>10,11</sup> The precise determination of the onset of the unsteady separation needs detailed surveys of the velocity and the pressure field.<sup>12</sup> In the present experiment, the data are obtained from visualization results, and only the first-order effect is considered here. The phase angle and the location of the separation are based upon the abrupt thickening of the dyed boundary layer.

#### 3.1 The Overall Unsteady Flow Pattern

The complicated three-dimensional separated flow pattern of the pitching delta wing can be best observed from an overall view, which will first be discussed. Food color dyes were seeped from the slots on the suction side of the 45° sweep delta wing. The flow field was illuminated with a bank of flood lights. The angle of attack was varied in the range of 0 to 30°, at a reduced frequency of  $K = 1.0$ . During the upstroke, the separation first started across the whole trailing edge at  $\alpha = 2^\circ$  (Flow Research Film No. 55). As the angle of attack increased, the separation vortices started to develop at the two corners of the trailing edge. The unsteady separation process looked as if a vortex sheet first peeled off from the corner of the wing and then rolled up into the separation vortex. The separation propagated from the corner toward the apex. The upstream propagation speed along the leading edge was approximately equal

to the freestream speed. At  $\alpha = 30^\circ$ , the separation front reached the apex, and the separation vortices were fully developed.

During the downstroke, the flow started to reattach. Both the top view using the food-color dye technique, and the end view using the dye-layer technique were used to clarify the reattachment process. As the angle of attack decreased from  $30^\circ$ , the flow near the whole leading edge (from the apex to the corners of the trailing edge) became reattached. Unlike the flow during the upstroke, there was no propagation phenomenon along the leading edge. While the angle of attack decreased, the attached area increased from the leading edge toward the center-span. Near  $\alpha = 5^\circ$ , the flow was completely attached. Either during the separation phase or the reattachment phase, small discrete vortices can be observed at the thin shear layer between the large separation vortex and the external potential flow.<sup>8</sup> This flow configuration was due to the coexistence of high frequency instability waves and a low frequency artificial perturbation. This phenomenon is similar to the collective interaction in an impinging jet as described by Ho and Nosseir.<sup>13</sup>

The dye-layer technique was used to visualize the flow near the wall as well as the external flow around the wing. When the wing passed through the quiescent dye layers, the originally flat layers were deformed. The local motion could be inferred from the moving dye layers as depicted in the movie frames. The flow was caused by the motion of the wing and the induced flow of the separation vortices. A typical case is examined here in more detail, and selected movie frames are shown in Figure 2. The sharp-leading-edge,  $60^\circ$  delta wing underwent the pitching motion  $\alpha = 15^\circ + 15^\circ \sin(2.4t)$  at a chord Reynolds number of  $R_c = 2.5 \times 10^5$  and a reduced frequency of  $K = 3.0$ . The vertical sheet of laser light was perpendicular to the flow direction and

located at a chordwise location of  $0.8c$ . Both the upward and downward motions are shown in Figure 2, for the attack angles of  $0^\circ$ ,  $5^\circ$ ,  $10^\circ$ ,  $15^\circ$ ,  $20^\circ$ ,  $25^\circ$  and  $30^\circ$ . The spanwise variations of the vertical velocity (in the laboratory frame) at  $0.13c$  above the wing and at an attack angle of  $\alpha = 0^\circ$  are shown in Figure 3. During the upstroke (the trailing edge moving downward), the velocity near the center-span was almost uniform and equaled about one-half of the vertical wing speed at this station. The same magnitude and a narrower region of uniform velocity were also observed during the downstroke as shown in the same figure. This result suggests that the vertical velocity near the center-span is mainly caused by the up-down motion of the wing. The tapering of the velocity near the leading edge is due to the separation vortices.

The vertical velocities at the center-span, along different positions above the wing, are plotted in Figure 4 for different phase angles in a cycle. The curves were approximately symmetric for corresponding phase angles during the downstroke and the upstroke. The data in Figure 4 further substantiate the aforementioned observation. Another interesting point is that the velocity decays exponentially away from the wing as shown in the semi-log plot in Figure 4b. In an incompressible flow, a large vertical gradient of the horizontal motion (streamwise or spanwise) must exist. However, measurements of the horizontal velocities were not performed in the present investigation.

### 3.2 The Hysteresis Loop

During one pitching cycle, the leading edge separation vortices executed a growth-decay cycle. Figure 5 is a side view of the flow on the suction side of the  $45^\circ$  sweep wing undergoing the pitching motion  $\alpha(t)^\circ = 15^\circ + 5^\circ \sin(0.4t)$  at a chord Reynolds number of  $R_c = 2.5 \times 10^4$  and a reduced frequency of

Appendix IV: Unsteady Vortical Flow Around  
Three-Dimensional Lifting Surfaces

Revised Manuscript Accepted for Publication in the AIAA Journal

Log Number: J15305

UNSTEADY VORTICAL FLOW AROUND THREE-DIMENSIONAL  
LIFTING SURFACES

Mohamed Gad-el-Hak<sup>\*</sup>

and

Chih-Ming Ho<sup>\*\*</sup>

August 1985

Flow Research Company

21414-68th Avenue South

Kent, WA 98032

---

Presented as Paper 85-0041 at the AIAA 23rd Aerospace Sciences Meeting, Reno, Nevada, January 14-17, 1985.

\*Senior Research Scientist. Member AIAA.

\*\*Consultant. Permanent address: Department of Aerospace Engineering, University of Southern California, Los Angeles, CA 90089. Member AIAA.

UNSTEADY VORTICAL FLOW AROUND THREE-DIMENSIONAL  
LIFTING SURFACES

Mohamed Gad-el-Hak

and

Chih-Ming Ho

Flow Research Company

Kent, WA 98032

ABSTRACT

Flow visualization experiments were conducted in a low Reynolds number towing tank to study the time-dependent flow around two generic classes of wings. Delta and swept (including zero sweep) wings were sting-mounted to a four-bar mechanism, which generated a large-amplitude, harmonic pitching motion around the  $1/4$ -chord location at a reduced frequency that varied in the range of 0.2 to 3.0. Fluorescent dye layers were placed in the weakly stratified water channel prior to towing the wing. The horizontal dye sheets were excited using a vertical sheet of laser light parallel to or perpendicular to the flow direction. The dye marked the flow in the separation region around the wing, the flow in the wake region, and the potential flow away from the lifting surface. The complex, time-dependent flow field around the different wings can be mostly explained from the mutual induction between the leading edge separation vortex and the trailing edge shedding vortex. The reduced frequency, the shape of the leading edge, and the wing's planform play important roles in determining the flow patterns. The effects of the finite aspect ratio on the flow around the wing are explored.

NOMENCLATURE

AR	aspect ratio
c	root chord
f	pitching frequency
K	reduced frequency, $\pi fc/U_\infty$
$R_c$	chord Reynolds number, $U_\infty c/\nu$
s	wing semispan
t	time (sec)
$U_\infty$	towing speed
V	vertical velocity
$V_w$	vertical velocity at the wing surface
x,y,z	Cartesian coordinates fixed with the wing
$\alpha(t)$	time-dependent angle of attack
$\nu$	kinematic viscosity

1. INTRODUCTION

With the recent advances in short-range infrared guided missiles, a significant change in close air combat characteristics emphasizing very fast maneuverability becomes highly desirable. This has led to a growing interest in the so called "supermaneuverability" of fighter aircraft where previously unattained regions of the maneuver envelope are attempted, such as post-stall flight maneuver and side slipping.<sup>1,2</sup> Current research in support of supermaneuverability involves studies to understand the dynamic stall on two- and three-dimensional lifting surfaces and the behavior of attached and separated unsteady shear layers affected by time-dependent boundary conditions, as well

as attempts to exploit the unsteady flow characteristics to improve aerodynamic efficiency and enhance performance.

Aerodynamic research for time-dependent viscous flows at high incidence has, to date, centered primarily on the flow over two-dimensional airfoils.<sup>3-8</sup> The data from these studies have shed considerable light on the exceedingly complex viscous-inviscid interactions associated with time-varying flow separation. The data, furthermore, provide a meaningful base to assess numerical procedures and to develop alternative approaches as required.<sup>9</sup>

Two-dimensional data can play an essential role in high-aspect-ratio applications (e.g., helicopter blades and commercial aircraft) where the local flow behaves, in a sense, two-dimensionally. The classic lifting-line theory for an unswept wing in steady flow, for example, provides a local induced incidence correction to account for finite-aspect-ratio effects. This theory has been extended to include wings with sweep.<sup>10</sup> The lifting-line concept, however, is of little value for the low-aspect-ratio wings of fighter/attack aircraft because the local airfoil section, particularly for the higher incidence angles, cannot be divorced from the wing as an entirety. Therefore, two-dimensional data play a less significant role in the design of low-aspect-ratio wings.

Considerable experimental/theoretical research has been focused on studying the flow over delta and swept wings for steady flow and time-independent boundary conditions.<sup>11,12</sup> Sophisticated inviscid numerical/analytical models have been developed for design purposes to describe the flow field at high angles of attack by "modeling" the vorticity shed from the wing edges. The sharpness of the leading edge invariably fixes the location of the shed

vortices feeding the leeward "conical-like" vortical motion--a factor embedded in theoretical modeling for delta wings.<sup>13-15</sup>

Recently this inviscid approach has been extended to time-dependent flows by a very efficient numerical method.<sup>16-18</sup> The unsteadiness is an important parameter to be considered for flight maneuverability. Studies of unsteady, two-dimensional airfoils have indicated that the lift and drag experience hysteresis loops during an oscillation cycle. Corresponding information for unsteady, three-dimensional wings is very scarce.<sup>19,20</sup> For three-dimensional lifting surfaces, it is quite likely that inviscid techniques coupled with empiricism will be the primary short-term "engineering" tool for predicting the time-dependent flow. The long-term goal would be a Navier-Stokes solution with appropriate turbulence modeling.

The essential purpose of the present investigation was to study the time-dependent flow over three-dimensional lifting surfaces at high incidence and to provide data necessary to bridge the gap from our understanding of the unsteady, two-dimensional flow about airfoils to the flow about three-dimensional wing configurations of current interest. The need to establish a detailed understanding of the physics of three-dimensional time-dependent flows coupled with the need to establish a data base to assess and to improve prediction methods provides the motivation for the present experiments. Two generic classes of wings were studied: the delta wing and the swept wing (including zero sweep). The lifting surfaces were pitched harmonically and towed in an 18-m water channel. Flow visualization techniques that utilize fluorescent dyes and sheets of laser light were used to clarify the nature of the complex flow field around the oscillating wings. The apparatus and the visualization method are described in the next section. In Section 3, the effects of the operating

parameters on the separation vortices are categorized and elaborated. Concluding remarks are presented in the last section.

## 2. EXPERIMENTAL APPROACH

Seven lifting surfaces undergoing a harmonic pitching motion were studied. The three-dimensional surfaces were: (1) a NACA 0012 rectangular wing having a chord length of  $c = 12.5$  cm and an aspect ratio of  $AR = 4$ ; (2) a similar rectangular wing but having a flat surface and a sharp leading edge; (3) a  $25^\circ$  swept wing with a sharp leading edge, a root chord of  $c = 16.5$  cm and  $AR = 4$ ; (4) a similar but swept forward wing; (5) a  $60^\circ$  delta wing with a sharp leading edge,  $c = 25$  cm and  $AR = 2.3$ ; (6) a  $45^\circ$  delta wing with a sharp leading edge,  $c = 25$  cm and  $AR = 4$ ; and (7) a similar  $45^\circ$  delta wing but having a NACA 0012 profile at each spanwise location.

The wings were towed in the water channel described by Gad-el-Hak et al.<sup>21</sup> This towing tank is 18 m long, 1.2 m wide and 0.9 m deep, and the towing speed was varied in the range of 5 to 140 cm/sec. A four-bar mechanism was used to sting-mount and to pitch the wings around the desired position along the chord. In the experiments reported herein, the wings were pitched around the 1/4-chord position. The mean angle of attack could be set from  $0^\circ$  to  $45^\circ$ . A Boston Ratiotrol motor drove the four-bar linkages to produce approximately sinusoidal oscillations of amplitude  $\pm 5^\circ$ ,  $\pm 10^\circ$  or  $\pm 15^\circ$  about a given mean angle of attack. The reduced frequency,  $K \equiv \pi fc/U_\infty$ , where  $f$  is the pitching frequency and  $U_\infty$  is the towing speed, was varied in the range of 0.2 to 3.0, and a digital readout displayed the instantaneous angle between the chord line and the towing direction,  $\alpha(t)$ .

The complex, unsteady, separated flows around the three-dimensional lifting surfaces were visualized using the dye-layer technique described by Gad-el-Hak.<sup>22</sup>

Fluorescent dye layers were placed in the weakly stratified water channel prior to towing the wing and excited using a vertical sheet of laser light parallel to or perpendicular to the flow direction. The dye marked the flow in the separation region around the wing, the flow in the wake region, and the potential flow away from the lifting surface. The visualization results were recorded using 35-mm photographs and 16-mm ciné films (movie films are available upon request).

### 3. RESULTS AND DISCUSSION

The seven lifting surfaces were pitched around the 1/4-chord position at a reduced frequency,  $K$ , that varied in the range of 0.2 to 3.0. The wings were towed in the water channel at a root chord Reynolds number that varied in the range of  $6.25 \times 10^3$  to  $3.50 \times 10^5$ . The dye-layer technique was used to visualize the unsteady, three-dimensional flow field around the low-pressure side of each wing.

Figure 1 is a sequence of photographs taken from the ciné film depicting a left-to-right ambient flow and the NACA 0012 rectangular wing ( $c = 12.5$  cm,  $AR = 4$ ) undergoing the pitching motion  $\alpha(t)^\circ = 15^\circ + 15^\circ \sin(1.57t)$ , where  $\alpha(t)$  is the time-dependent (geometric) angle of attack, and  $t$  is time in seconds. The wing was towed at a speed of  $U_\infty = 10$  cm/sec ( $R_c = 1.25 \times 10^4$ ), and the reduced frequency was  $K = 1.0$ . The photographs in Figure 1 show a typical oscillation cycle\* ( $0^\circ$  to  $30^\circ$  to  $0^\circ$ ) of the unsteady flow field in a vertical plane, parallel to the flow direction and located at  $z = 10$  cm (40 percent of the semispan,  $s$ ). The sheet of laser light is projected from the

---

\*The first oscillation cycle is different from the second or subsequent cycles, hence the first cycle is not used in any of the figures presented here.

top of the tank and the dark area below the wing is the shadow of the lifting surface. Both the upward and downward motions of the wing are shown side by side for  $\alpha = 0^\circ, 5^\circ, 10^\circ, 15^\circ, 20^\circ, 25^\circ$  and  $30^\circ$ .

The complex, unsteady flow field associated with the pitching wing can be mostly explained from the mutual induction between the leading edge separation vortex and the trailing edge shedding vortex. At large angles of attack, the flow separates at the leading edge, and a clockwise vortex is formed and is convected downstream. This vortex is eventually shed from the trailing edge. When the wing is in the upstroke, the trailing edge moves downward and a shear layer is created at the upper surface. The shear layer rolls up into a counterclockwise vortex that is also shed from the trailing edge. Conversely, a clockwise vortex is formed during the downstroke. These vortices enter the wake at different phases of the cycle and result in a particular wake pattern for a given reduced frequency. For the rectangular wing pitching at the reduced frequency of  $K = 1.0$ , the clockwise separation vortex from the leading edge convects downstream and is shed from the trailing edge just before the wing starts the upstroke of the new cycle. During this upstroke, a counterclockwise vortex is generated at the trailing edge and forms a vortex pair with the leading edge vortex. This vortex pair tends to convect downstream and upward, so that the induced flow above the chord is more or less cancelled. During the downstroke, a clockwise vortex is generated at the trailing edge, and its induced velocity tends to thicken the separation zone above the wing.

### 3.1 Effects of Leading Edge Shape

Two rectangular wings having the same chord ( $c = 12.5$  cm) and aspect ratio ( $AR = 4$ ) were tested to determine the effects of the leading edge shape. The first wing had a NACA 0012 cross-section, while the second wing had a flat

surface and a sharp leading edge. The two wings were towed at a speed of  $U_\infty = 10$  cm/sec ( $R_c = 1.25 \times 10^4$ ) and were harmonically pitched around the 1/4-chord point such that  $\alpha(t)^\circ = 15^\circ + 15^\circ \sin(1.6t)$ , and  $K = 1.0$ . Typical oscillation cycles of the unsteady flow field in a vertical plane, parallel to the flow direction and located at  $z = 10$  cm, are shown in Figures 1 and 2 for the blunt and the sharp leading edge wings, respectively.

The distinct characteristic of the sharp leading edge wing is the existence of a counter-rotating vortex upstream of the leading edge separation vortex. Although this is more clearly indicated in the ciné film from which Figure 2 was drawn, the outer boundaries of the counter-rotating vortex are outlined by the white circle in the still frame taken at  $\alpha = 5^\circ$  during the downstroke. The mutual induction of the vortex pair lifts itself away from the wall and results in a large intrusion into the inviscid region. The counter-rotating vortex is not observed on the blunt leading edge wing. In this case, the leading edge separation vortex rolls along the chord. The separation region is much thinner than that on the sharp leading edge wing.

The counter-rotating vortex may have important implications in controlling the unsteady flow. In the boundary layer produced by an impinging jet, a counter-rotating vortex occurs as a result of the unsteady separation produced by the shear layer vortex in the jet.<sup>23</sup> Large suction is generated on the impinging plate by the counter-rotating vortex. It has been speculated that the high-level, unsteady lift of pitching wings is caused by a corresponding large suction associated with a counter-rotating vortex.<sup>24</sup> Such a vortex has been clearly identified on the sharp-leading-edge rectangular wing depicted on Figure 2. The large suction associated with the counter-rotating vortex implies that the aerodynamic characteristics could be significantly altered by modifying the evolution of this vortex, offering the potential for enhancing the performance of a given lifting surface.

### 3.2 Effects of Reduced Frequency

To investigate the effects of reduced frequency on the flow field, the sharp leading edge rectangular wing was pitched at a frequency that varied in the range of  $K = 0.2$  to  $3.0$ . The root chord Reynolds number for all runs was approximately  $R_c = 10^4$ , and the angle of attack was  $\alpha(t)^\circ = 15^\circ \pm 15^\circ$ . Figures 2 and 3 show a sequence of photographs during a typical cycle at the reduced frequencies  $K = 1.0$  and  $3.0$ , respectively. The vertical laser light was parallel to the flow and was at a distance of 10 cm off the wing centerline in both cases. The difference between the  $K = 1.0$  case and the  $K = 3.0$  case is due to the vortex pattern in the wake. For  $K = 1.0$  (Figure 2), the clockwise leading edge separation vortex convects downstream at about 45 percent of the towing speed and is shed from the trailing edge just before the wing starts the upstroke of the new cycle. During this upstroke, a counterclockwise vortex is generated at the trailing edge and forms a vortex pair with the leading edge vortex. This vortex pair tends to convect downstream and upward, so that the induced flow above the chord is more or less cancelled. During the downstroke, a clockwise vortex is generated at the trailing edge, and its induced velocity tends to thicken the separation zone above the wing.

The situation is different at  $K = 3.0$  (Figure 3). The vortex from the leading edge is convected at a slower rate relative to the oscillation period and is shed at the downstroke of the next cycle with the clockwise trailing edge vortex. The combined vortex forms a vortex pair with the counterclockwise vortex produced in the previous upstroke. During the new upstroke, another counterclockwise vortex forms at the trailing edge and has a net effect of suppressing the thickness of the separation zone above the wing.

The wake pattern for  $K = 1.0$  and  $K = 3.0$  is shown schematically in Figure 4. In this figure,  $TE_{up}$  refers to the counterclockwise vortex shed

from the trailing edge during the upstroke ( $0^\circ$  to  $30^\circ$ ),  $TE_{\text{down}}$  refers to the clockwise vortex shed from the trailing edge during the downstroke ( $30^\circ$  to  $0^\circ$ ), and LE refers to the leading edge separation vortex.

At the lowest reduced frequency,  $K = 0.2$ , the oscillation period is relatively long and the flow has more time to adjust to angle-of-attack variations. The trailing edge vortices are located inside the separation zone originating from the leading edge.<sup>22,25</sup> The mutual induction between the two vortical zones is less clear compared to higher reduced-frequency runs. However, the general concept should still hold.

### 3.3 Effects of Wing Planform

Four sharp leading edge wings having an aspect ratio of  $AR = 4$  were tested to determine the effects of wing planform. A rectangular wing, a  $25^\circ$  swept wing, a forward swept wing and a  $45^\circ$  sweep delta wing were pitched at an angle of attack of  $\alpha^\circ = 15^\circ \pm 15^\circ$  and a reduced frequency of  $K = 1.0$ . A typical oscillation cycle of the unsteady flow field in a vertical plane, parallel to the flow direction and located at  $z = 10$  cm, is shown in Figures 2, 5, 6 and 7 for the rectangular, swept, forward swept and delta wings, respectively.

On the rectangular wing, the leading edge separation vortex convects downstream (Figure 2), while it is stationary during part of the cycle on the swept wing (Figure 5). In the ciné film from which the still photographs were drawn, a counter-rotating vortex can be seen near the leading edge separation vortex on the forward swept wing (Figure 6), but not on the (backward) swept wing at the present visualization station ( $z = 40$  percent of the semispan). This is not surprising since the separation patterns along the span are known to be very different on backward and forward swept wings in steady flight.

On the delta wing, the leading edge separation vortex does not convect, rather it experiences a growth-decay cycle (Figure 7). There exists a blob of dye that moves along the chord, while the leading edge vortex shrinks to minimum size. This blob of dye could be related to the possible separation bubble in the center part of the span.<sup>26,27</sup>

At one chordwise position on a delta wing (0.8c from the apex), Gad-el-Hak and Ho<sup>27</sup> found that the vertical velocity near the center span is mainly caused by the vertical motion of the wing. In the present investigation, we further confirmed this finding by measuring, from the visualization movies, the vertical velocity,  $V$ , about 1/4-chord above the 60°-sweep, sharp leading edge delta wing along several chordwise locations. The normalized values of the vertical displacement ( $V/V_w$ ) at different attack angles and at several locations along the chord were found to be constant within the experimental error.<sup>25</sup> This supports the hypothesis advanced by Gad-el-Hak and Ho<sup>27</sup> that the vertical velocity away from the wing is mainly produced by the normal motion of the wing (potential effect).

### 3.4 Effects of Finite Aspect Ratio

Due to the finite aspect ratio, a spanwise flow is necessary to accommodate the discontinuity at the wing tips. In the case of the pitching delta wing, a pair of vortices develops near the leading edge and experiences a growth-decay cycle with hysteresis during a pitching period.<sup>26,27</sup> For the rectangular wing, a streamwise vortex is formed at the tip while a spanwise, convective vortex is generated in the center portion of the span.<sup>19,20</sup>

The sharp leading edge rectangular wing was used to examine the nature of the three-dimensional flow. End views at different streamwise stations as well as side views at different spanwise locations were visualized using the dye-

layer technique. Figure 8 is a sequence of photographs of the pitching, sharp leading edge rectangular wing taken with an underwater movie camera. The vertical sheet of laser was perpendicular to the flow and located at  $x/c = 0.8$ . The wing was towed at a speed of  $U_\infty = 10$  cm/sec ( $R_c = 1.25 \times 10^4$ ), and underwent the pitching motion  $\alpha(t)^\circ = 15^\circ + 15^\circ \sin(1.6t)$  at the reduced frequency  $K = 1.0$ . The typical oscillation cycle ( $0^\circ$  to  $30^\circ$  to  $0^\circ$ ) shown in Figure 10 depicts the left side of the symmetric wing and a flow out of the plane of the photographs. Both the upward and downward motions of the wing are shown side by side for  $\alpha = 0^\circ, 5^\circ, 10^\circ, 15^\circ, 20^\circ, 25^\circ$  and  $30^\circ$ . The end views confirm the general model proposed by Adler and Luttges.<sup>20</sup> The flow could be divided into three distinct regions: the tip vortex, the leading edge vortex and an interaction zone.

The streamwise tip vortex undergoes a growth-decay cycle, much the same as the leading edge vortices on a pitching delta wing.<sup>27</sup> The tip vortices grow during the upstroke, presumably resulting in a corresponding lift increase. The maximum size of the tip vortex is about  $0.35c$  and is reached shortly after the end of the upstroke. When the angle of attack decreases, a pair of counter-rotating vortices is generated. The emergence of the coherent, reversed vortices leads to the decay of the unsteady tip vortex.

The spanwise leading edge vortex convects downstream, arriving at the observation station during the downstroke. It achieves its maximum height of about  $0.8c$  at the completion of the oscillation cycle ( $\alpha = 0^\circ$ ), and occupies about 65 percent of the wing's span. This leading edge vortex is a result of flow separation at high attack angles and is very similar to that observed on two-dimensional airfoils undergoing large-amplitude pitching motions.<sup>3-8</sup>

The interactive interface, identified by Adler and Luttges<sup>20</sup> on a pitching, finite aspect ratio wing having a NACA 0015 cross section, is located between

the tip vortex and the leading edge vortex and occupies a spanwise region of about 8 percent of the wing's span.

The unsteady separation process on the sharp leading edge rectangular wing can be reconstructed from side views at different spanwise locations. Figure 9 depicts events at two instances, one during the upstroke at  $\alpha = 15^\circ$  and the second at the same angle of attack during the downstroke. The stations shown in the figure are  $z/s = 0, 0.2, 0.4, 0.6, 0.8$  and  $1.0$ , where  $z$  is the spanwise coordinate measured from the wing's centerline and  $s$  is the semispan (25 cm). The run conditions are the same as those for the case shown in Figure 8. During the upstroke (Figure 9a) and away from the wing tip, a spanwise vortex is formed near the leading edge while the corresponding vortex from the preceding cycle has convected into the wake of the wing. The drastic change in size of the latter vortex as the observation station is moved from the root region toward the wing tip is a dramatic demonstration of the degree of three-dimensionality of the unsteady flow. It is clear that any attempt to model such flow using a two-dimensional approximation is bound to fail. Similar strong three-dimensional effects have been observed by Winkelmann and Barlow<sup>28</sup> in the case of a steady flow around a low-aspect-ratio rectangular wing beyond stall.

By observing the movie sequences from which Figure 9 was drawn, a more complete picture of the unsteady separation can be reconstructed. At the wing tip ( $z/s = 1.0$ ), the flow separates first at  $\alpha \approx 5^\circ$  during the upstroke. The separation rolls up in a tip vortex and propagates upstream, eventually reaching the leading edge at  $\alpha = 10^\circ$ . The tip vortex grows in size as the angle of attack increases, and its strength is reduced when the counter-rotating vortex is produced during the downstroke. Near the root of the wing, the flow separates at the leading edge at  $\alpha = 10^\circ$  during the upstroke. This separation seems to be evoked by the upstream-propagating separation at the wing tip. The

leading edge vortex grows in size, and its convection speed varies with the oscillation phase. When the leading edge vortex reaches the trailing edge of the wing, its vertical extent is about  $0.6c$  at  $z/s = 0$ , and about  $0.8c$  at  $z/s = 0.5$ . The separation vortex is not observed at the trailing edge in the interactive region ( $z/s = 0.65$  to  $0.82$ ). Since a vortex cannot end in free space, a three-dimensional vortical structure must exist in this region.

#### 4. CONCLUSIONS

The unsteady separated flow around three-dimensional lifting surfaces is dominated by large-scale vortices, about a chord length in size. Several features observed at different operating parameter ranges can be understood through the mutual induction among the leading edge separation vortex and the vortices shed as a result of the vertical motion of the trailing edge.

The wake pattern of the rectangular wing varies significantly with the reduced frequency and is determined by the phase angle of the leading edge vortex's arrival at the trailing edge. At  $K = 1.0$ , the wake consists of a vortex pair above the chord line and a single clockwise vortex below the chord line. The clockwise vortex induces an upward motion that results in a thick separation zone on the chord. At  $K = 3.0$ , the wake has a vortex pair below the chord line. The induction of the counterclockwise trailing edge vortex suppresses the upward motion of the leading edge vortex; hence, the separation zone on the chord is much thinner than that at  $K = 1.0$ .

A secondary counter-rotating vortex is clearly identified on the sharp leading edge rectangular wing. The mutual induction between the vortex pair lifts the vortices from the wall and results in a large intrusion into the inviscid region. The separation zone is about twice as thick as that on the

blunt leading edge wing. We speculate that the counter-rotating vortex could have an important role in the generation of unsteady lift.

On the rectangular wing, the leading edge separation vortex convects downstream, while it is stationary during part of the cycle on the swept wing. On the delta wing, the leading edge vortex does not convect, rather it experiences a growth-decay cycle.

Additional end and side views of the sharp leading edge rectangular wing revealed the existence of three distinct regions similar to those observed by Adler and Luttgens<sup>20</sup> on a NACA 0015 wing: the tip vortex, which undergoes a growth-decay cycle; the leading edge separation vortex, which convects downstream and seems to be triggered by the upstream-propagating separation near the wing tip; and the intermediate zone, where the tip vortex and the leading edge vortex interact. The strong three-dimensional effects demonstrated in the present results make it clear that any attempt to model the unsteady flow around finite-aspect-ratio wings using a two-dimensional approximation is bound to fail.

More visualization experiments are needed to further clarify the topology of the complex vortical structures on the different wing planforms used in the present investigation. The results should then be used to design fast-response probe experiments to measure the velocity field and to correlate the visualization events with the forces and moments experienced by the pitching wing.

#### ACKNOWLEDGEMENT

This work is supported by the U.S. Air Force Office of Scientific Research, under Contract No. F49620-82-C-0020, and monitored by Major M. S. Francis and Dr. J. D. Wilson. The authors would like to acknowledge the valuable help of Messrs. Morton Cooper and Randy Srnsky.

REFERENCES

1. Herbst, W. B., "Dynamics of Air Combat," J. Aircraft 20, pp. 594-598, 1983.
2. Herbst, W. B., "Supermaneuverability," in Unsteady Separated Flows, eds. M. S. Francis & M. W. Luttges, Univ. Colorado, pp. 1-9, 1983.
3. McCroskey, W. J., Carr, L. W., and McAlister, K. W., "Dynamic Stall Experiments on Oscillating Airfoils," AIAA J. 14, pp. 57-63, 1976.
4. McCroskey, W. J., "Unsteady Airfoils," Ann. Rev. Fluid Mech. 14, pp. 285-311, 1982.
5. McCroskey, W. J., and Pucci, S. L., "Viscous-Inviscid Interaction on Oscillating Airfoils in Subsonic Flow," AIAA J. 20, pp. 167-174, 1982.
6. Robinson, M. C., and Luttges, M. W., "Unsteady Flow Separation and Attachment Induced by Pitching Airfoils," AIAA Paper No. 83-0131, 1983.
7. Walker, J. M., and Helin, H. E., "An Experimental Investigation of an Airfoil Undergoing Large Amplitude Pitching Motions," AIAA Paper No. 85-0039, 1985.
8. Helin, H. E., and Walker, J. M., "Interrelated Effects of Pitch Rate and Pivot on Airfoil Dynamic Stall," AIAA Paper No. 85-0130, 1985.
9. Baldwin, B. S., and Lomax, H., "Thin Layer Approximation and Algebraic Model for Separated Turbulent Flows," AIAA Paper No. 78-257, 1978.
10. Cheng, H. K., "Lifting-Line Theory for Oblique Wings," AIAA J. 16, pp. 1211-1213, 1979.
11. Hoesijmakers, H. W. M., Vaatstra, W., and Verhaagen, N. G., "On the Vortex Flow Over Delta and Double-Delta Wings," AIAA Paper No. 82-0949, 1982.
12. Gad-el-Hak, M., and Blackwelder, R. F., "The Discrete Vortices from a Delta Wing," AIAA J. 23, pp. 961-962, 1985.

13. Legendre, R., "Ecoulement au Voisinage de la Pointe Avant D'une Aile a Forte Fleche aux Incidences Moyennes," La Rech. Aéro. 30, pp. 3-8, 1952.
14. Brown, C. E., and Michael, W. H., "Effect of Leading-Edge Separation on the Lift of a Delta Wing," J. Aero. Sci. 21, pp. 690-694, 1954.
15. Smith, J. H. B., "Improved Calculations of Leading-Edge Separation from Slender, Thin, Delta Wings," Proc. Roy. Soc. A 306, pp. 69-90, 1968.
16. Nayfeh, A. H., Mook, D. T., and Yen, A., "The Aerodynamics of Small Harmonic Oscillations Around Large Angles of Attack," AIAA Paper No. 79-1520, 1979.
17. Konstadinopoulos, P., Mook, D. T., and Nayfeh, A. H., "A Numerical Method for General Unsteady Aerodynamics," AIAA Paper No. 81-1877, 1981.
18. Konstadinopoulos, P., Mook, D. T. and Nayfeh, A. H., "Numerical Simulation of the Subsonic Wing-Rock Phenomenon," AIAA Paper No. 83-2115, 1983.
19. Adler, J. N., Robinson, M. C., Luttgies, M. W., and Kennedy, D. A., "Visualizing Unsteady Separated Flows," in Flow Visualization 3, ed. W. J. Yang, Hemisphere, pp. 342-347, 1983.
20. Adler, J. N., and Luttgies, M. W., "Three-Dimensionality in Unsteady Flow About a Wing," AIAA Paper No. 85-0132, 1985.
21. Gad-el-Hak, M., Blackwelder, R. F., and Riley, J. J., "On the Growth of Turbulent Regions in Laminar Boundary Layers," J. Fluid Mech. 110, pp. 73-95, 1981.
22. Gad-el-Hak, M., "The Use of the Dye-Layer Technique for Unsteady Flow Visualization," J. Fluid Eng., in press, 1985.
23. Didden, N., and Ho, C.-M., "Unsteady Separation in the Boundary Layer Produced by an Impinging Jet," J. Fluid Mech., in press, 1985.
24. Ho, C.-M., "An Alternative Look at the Unsteady Separation Phenomenon," in Recent Advances in Aerodynamics, eds. A. Krothapalli & C.A. Smith, Springer, pp. 165-178, 1985.

25. Gad-el-Hak, M., and Ho, C.-M., "Three-Dimensional Effects on a Pitching Lifting Surface," AIAA Paper No. 85-0041, 1985.
26. Gad-el-Hak, M., Ho, C.-M., and Blackwelder, R. F., "A Visual Study of a Delta Wing in Steady and Unsteady Motion," in Unsteady Separated Flows, eds. M. S. Francis & M. W. Luttges, Univ. Colorado, pp. 45-51, 1983.
27. Gad-el-Hak, M., and Ho, C.-M., "The Pitching Delta Wing," AIAA J., in press, 1985.
28. Winkelmann, A. E., and Barlow, J. B., "Flowfield Model for a Rectangular Planform Wing beyond Stall," AIAA J. 18, pp. 1006-1008, 1980.

FIGURE CAPTIONS

Figure 1. Side View of NACA 0012 Rectangular Wing Undergoing a Pitching Motion.  $AR = 4$ ;  $R_c = 1.25 \times 10^4$ ;  $K = 1.0$ ;  
 $\alpha(t)^\circ = 15^\circ + 15^\circ \sin(1.57t)$ ;  $z/s = 0.4$ .

Figure 2. Side View of Sharp Leading Edge Rectangular Wing.  $AR = 4$ ;  
 $R_c = 1.25 \times 10^4$ ;  $K = 1.0$ ;  $\alpha(t)^\circ = 15^\circ + 15^\circ \sin(1.63t)$ .

Figure 3. Side View of Sharp Leading Edge Rectangular Wing.  $AR = 4$ ;  
 $R_c = 8.63 \times 10^3$ ;  $K = 3.0$ ;  $\alpha(t)^\circ = 15^\circ + 15^\circ \sin(3.33t)$ .

Figure 4. Effects of Reduced Frequency on Wake Pattern Behind Pitching Wing.

Figure 5. Side View of Sharp Leading Edge Swept Wing.  $AR = 4$ ;  
 $R_c = 1.65 \times 10^4$ ;  $K = 1.0$ ;  $\alpha(t)^\circ = 15^\circ + 15^\circ \sin(1.19t)$ .

Figure 6. Side View of Forward Swept Wing.  $AR = 4$ ;  $R_c = 1.65 \times 10^4$ ;  
 $K = 1.0$ ;  $\alpha(t)^\circ = 15^\circ + 15^\circ \sin(1.19t)$ .

Figure 7. Side View of  $45^\circ$  Sweep, Sharp Leading Edge, Delta Wing.  $AR = 4$ ;  
 $R_c = 2.5 \times 10^4$ ;  $K = 1.0$ ;  $\alpha(t)^\circ = 15^\circ + 15^\circ \sin(0.82t)$ .

Figure 8. End View of Sharp Leading Edge Rectangular Wing at  $x/c = 0.8$ .  
 $AR = 4$ ;  $R_c = 1.25 \times 10^4$ ;  $K = 1.0$ ;  
 $\alpha(t)^\circ = 15^\circ + 15^\circ \sin(1.6t)$ . Flow Out of Plane of Paper.

Figure 9. Spanwise Variations of the Flow Around Sharp Leading Edge

Rectangular Wing.  $z/s = 0, 0.2, 0.4, 0.6, 0.8$  and  $1.0$ .  $K = 1.0$ ;

$$\alpha(t)^\circ = 15^\circ + 15^\circ \sin(1.6t).$$

a.  $\alpha = 15^\circ$  (Increasing).

b.  $\alpha = 15^\circ$  (Decreasing).

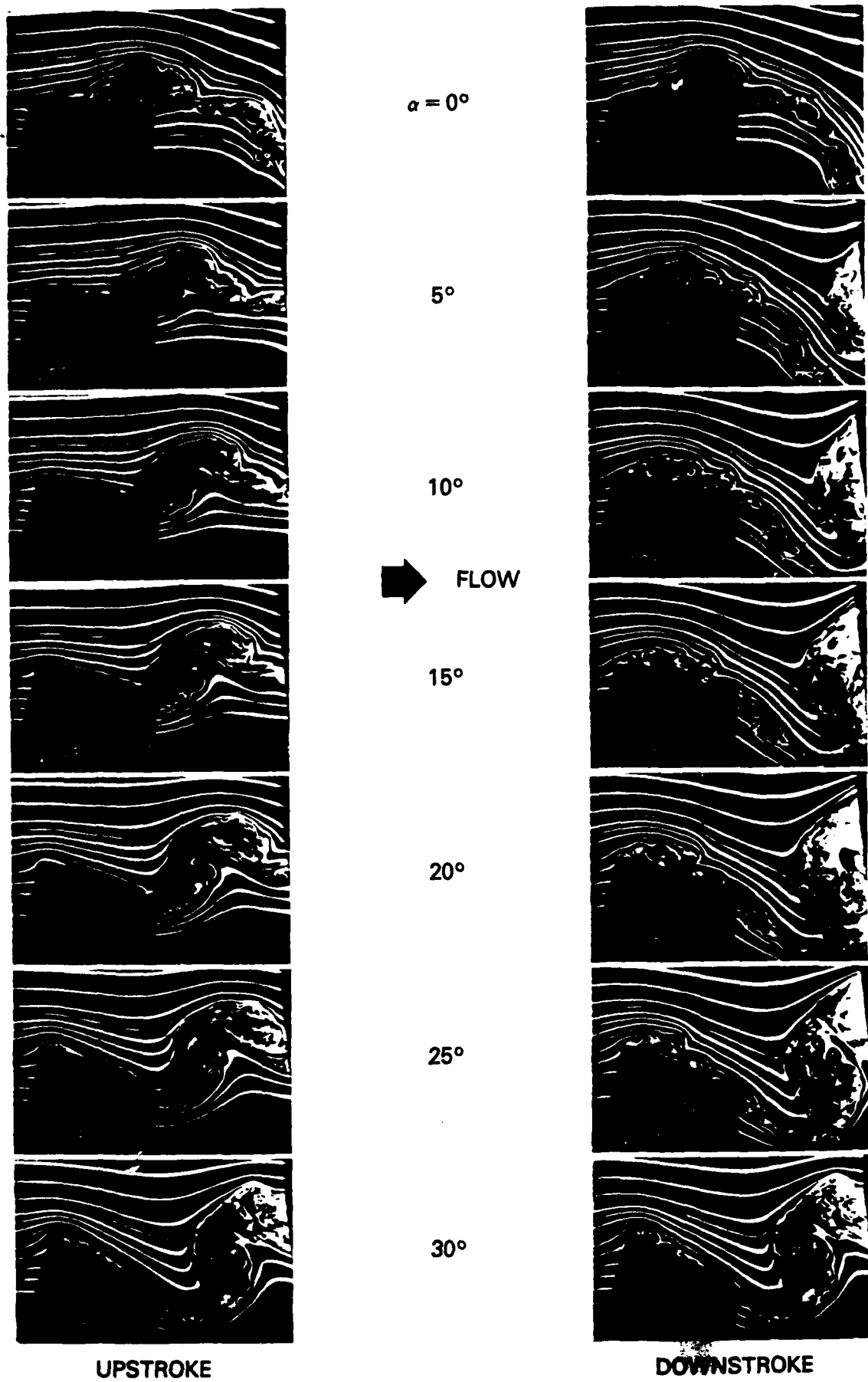


Figure 1. Side View of NACA 0012 Rectangular Wing Undergoing a Pitching Motion.  
 $AR = 4$ ;  $R_c = 1.25 \times 10^4$ ;  $K = 1.0$ ;  $\alpha(t)^\circ = 15^\circ + 15^\circ \sin(1.57t)$ ;  $z/s = 0.4$ .





UPSTROKE



FLOW



DOWNSTROKE

$\alpha = 0^\circ$

$5^\circ$

$10^\circ$

$15^\circ$

$20^\circ$

$25^\circ$

$30^\circ$

Figure 3. Side View of Sharp Leading Edge Rectangular Wing.  
 $AR = 4$ ;  $R_c = 8.63 \times 10^3$ ;  $K = 3.0$ ;  $\alpha(t)^\circ = 15^\circ + 15^\circ \sin(3.33t)$ .

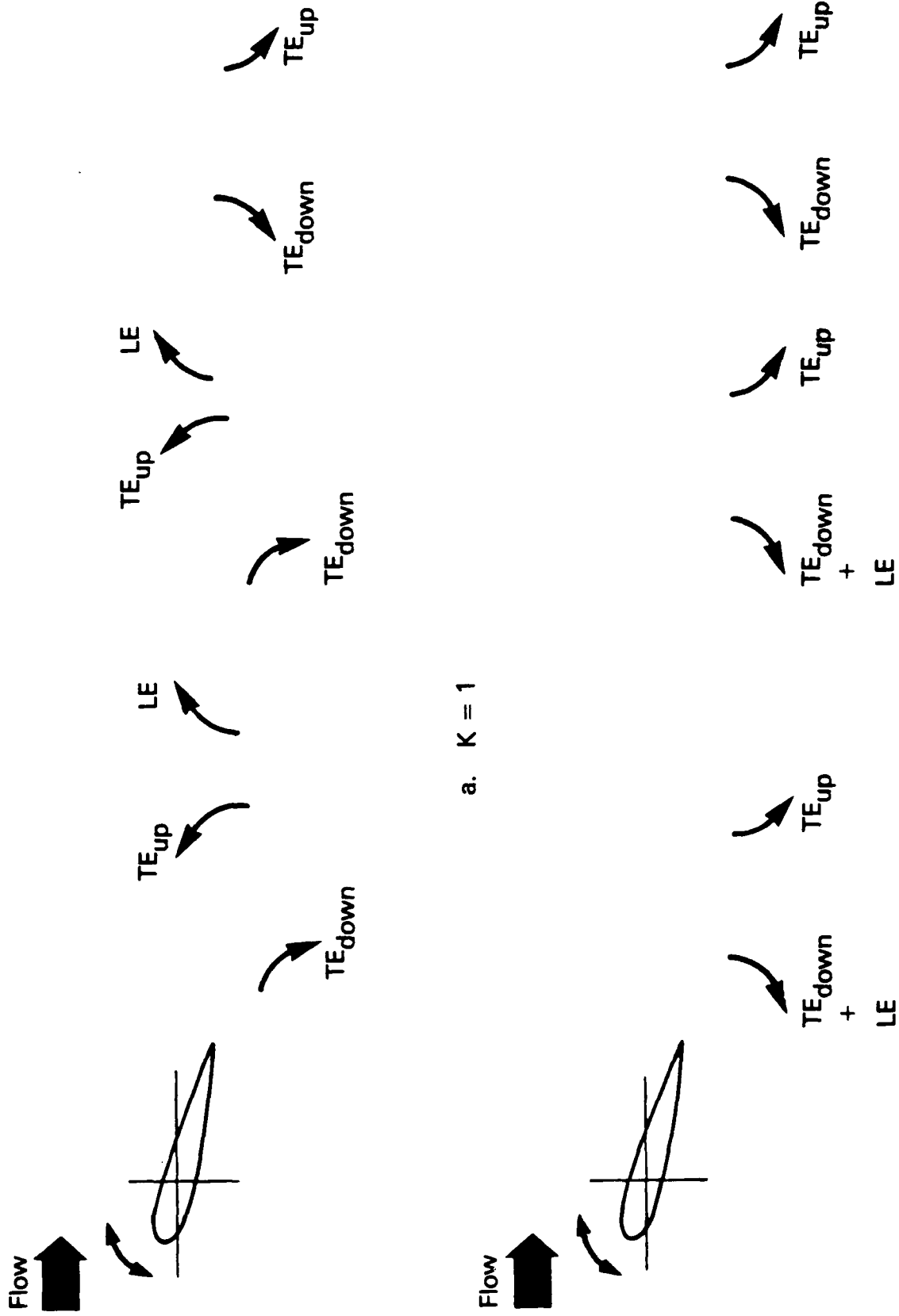
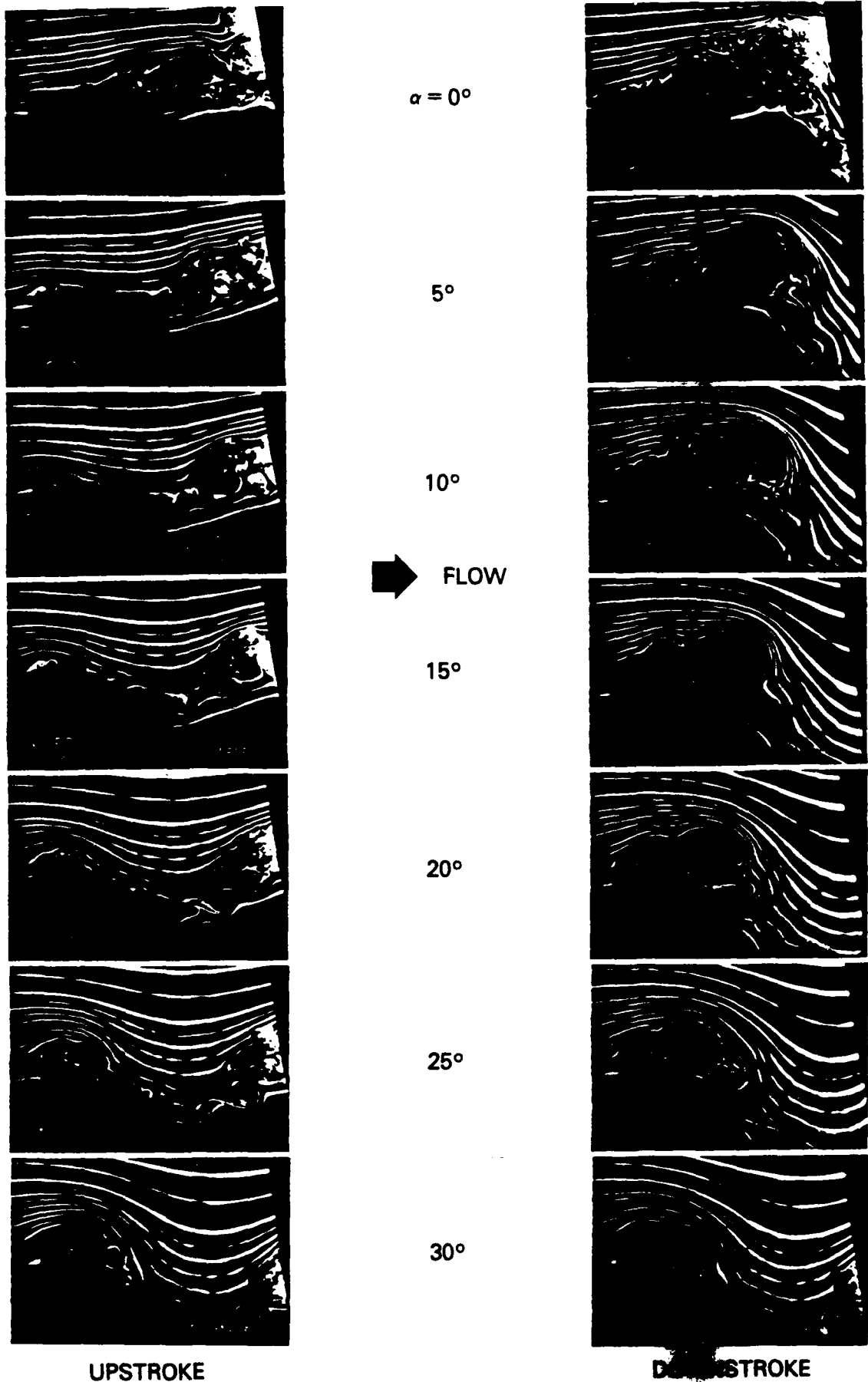
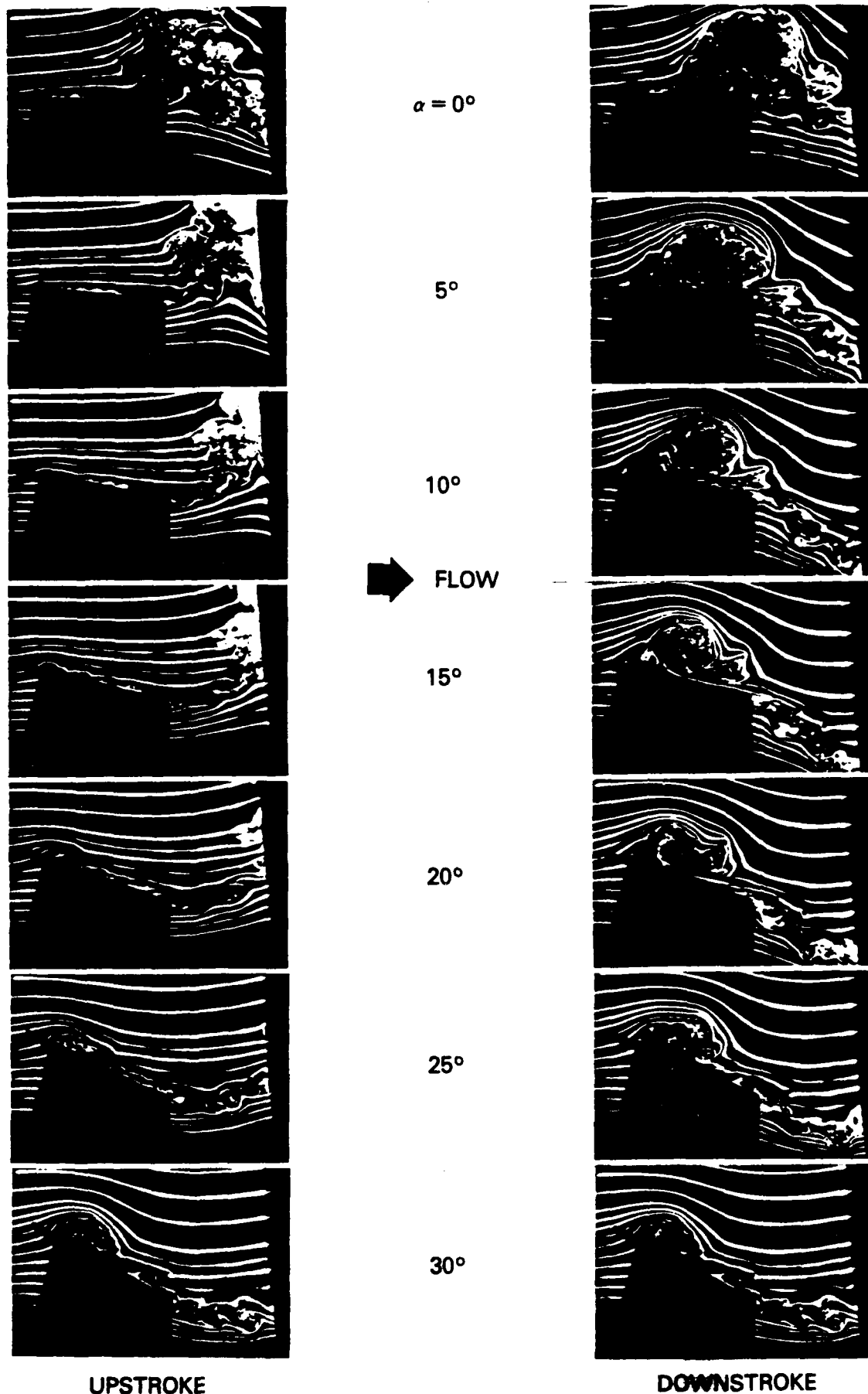


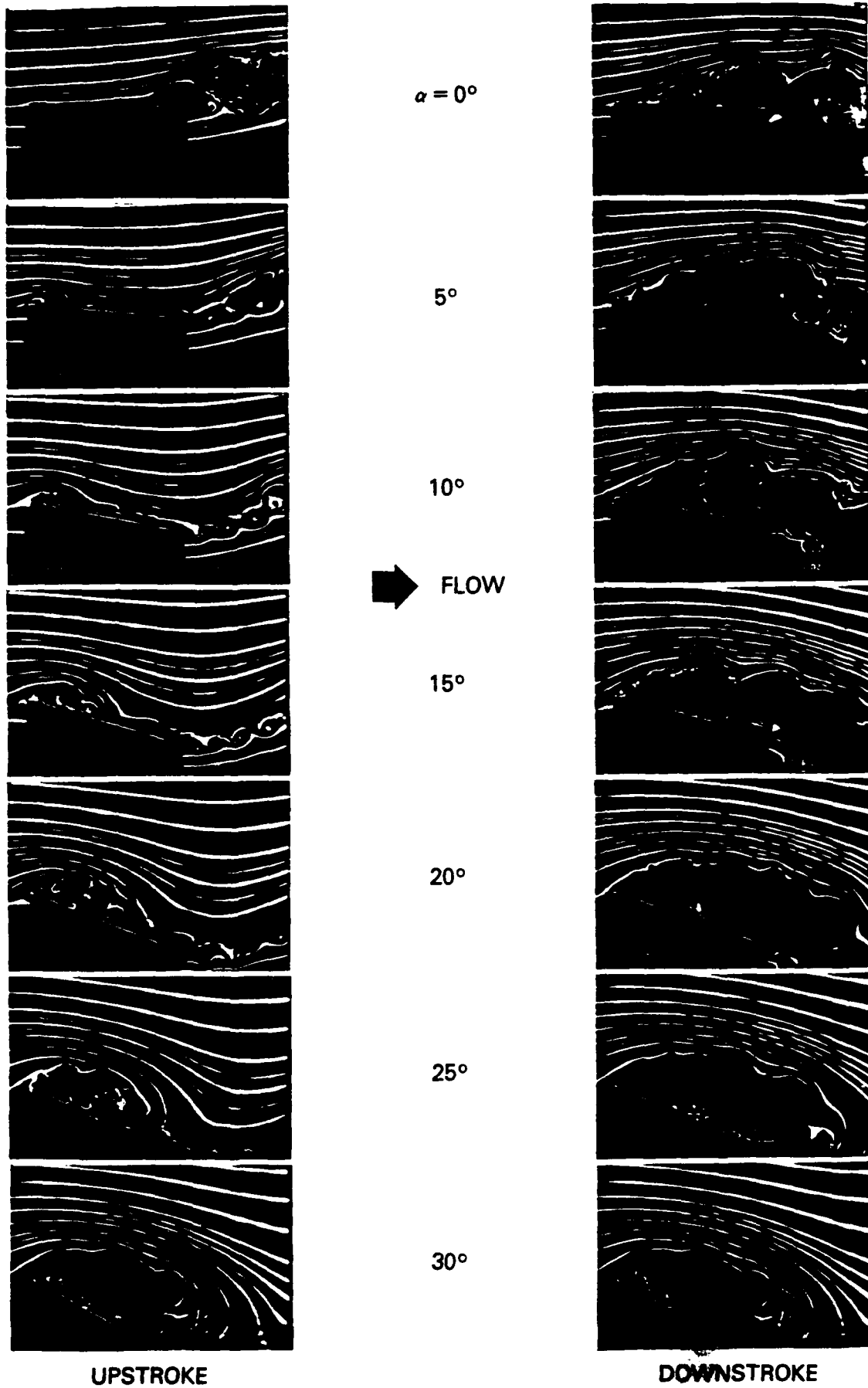
Figure 4. Effects of Reduced Frequency on Wake Pattern behind Pitching Wing



**Figure 5. Side View of Sharp Leading Edge Swept Wing.**  
 $AR = 4$ ;  $R_C = 1.65 \times 10^4$ ;  $K = 1.0$ ;  $\alpha(t)^\circ = 15^\circ + 15^\circ \sin(1.19t)$ .



**Figure 6. Side View of Forward Swept Wing.**  
 **$AR = 4; R_c = 1.65 \times 10^4; K = 1.0; \alpha(t)^\circ = 15^\circ + 15^\circ \sin(1.19t).$**



UPSTROKE

DOWNSTROKE

Figure 7. Side View of  $45^\circ$  Sweep, Sharp Leading Edge, Delta  
 $AR = 4$ ;  $R_c = 2.5 \times 10^4$ ;  $K = 1.0$ ;  $\alpha(t)^\circ = 15^\circ + 15^\circ \sin(0.82t)$ .

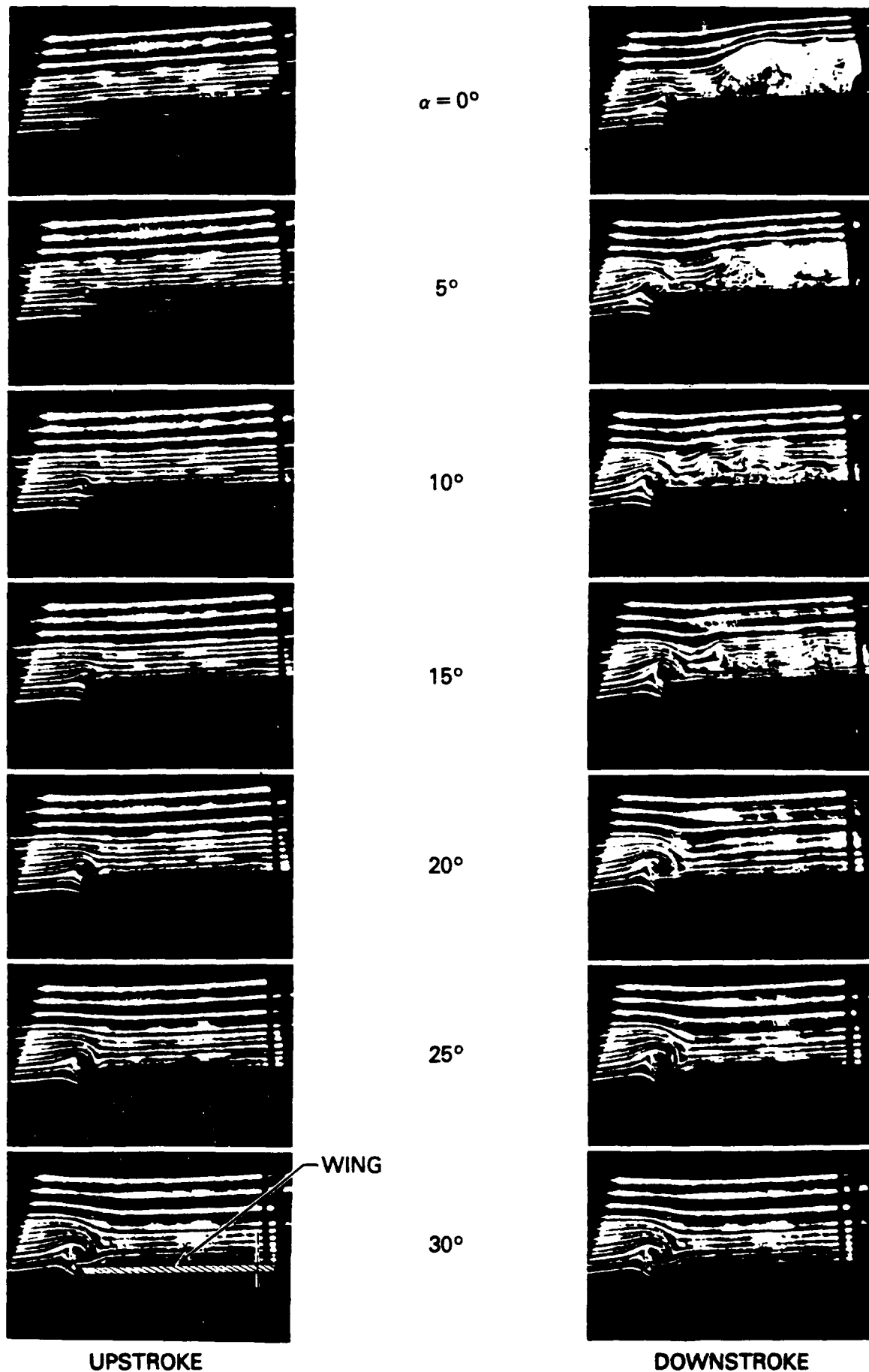
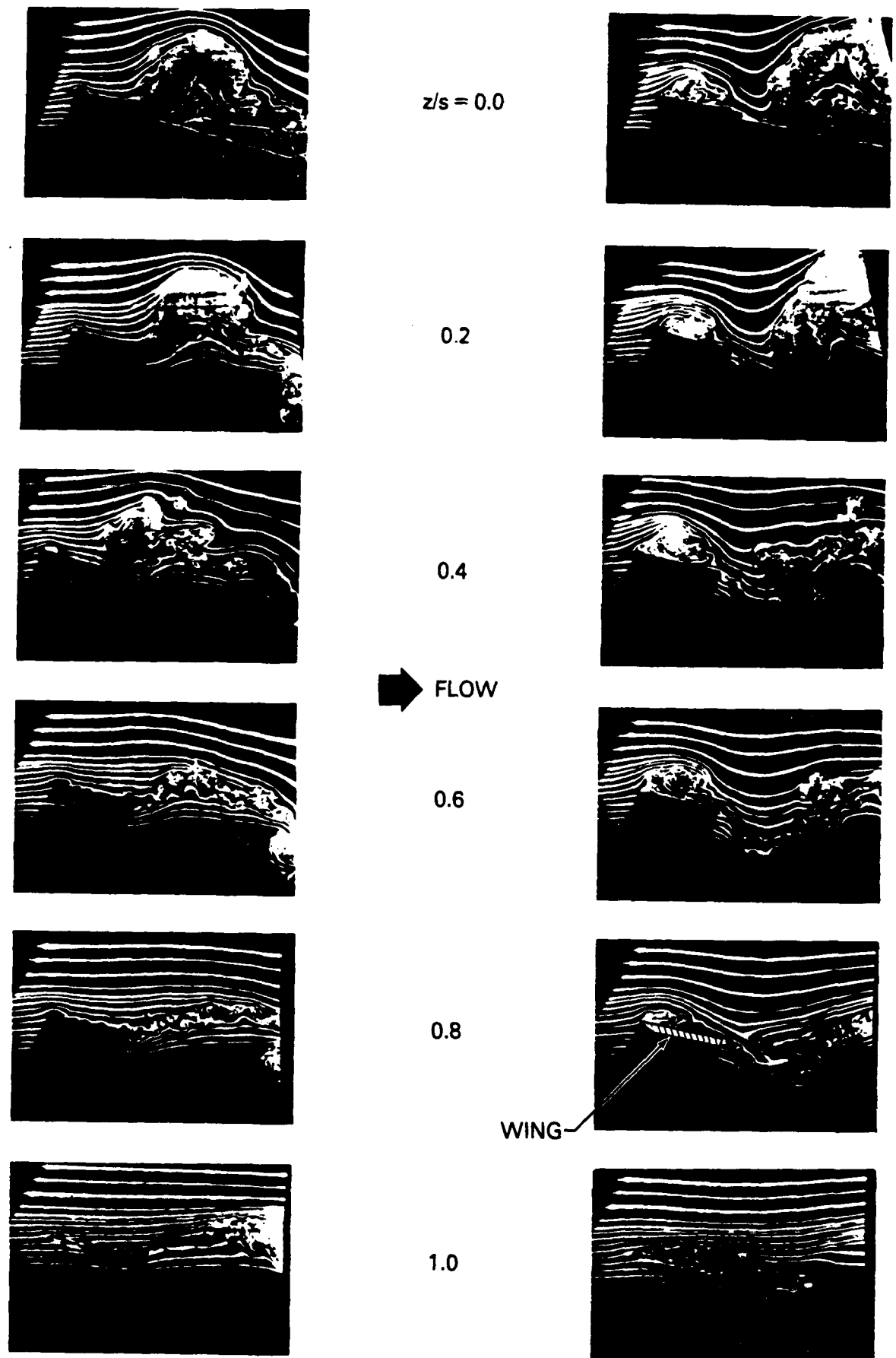


**Figure 8. End View of Sharp Leading Edge Rectangular Wing**  
**at  $x/c = 0.8$ .  $AR = 4$ ;  $R_c = 1.25 \times 10^4$ ;  $K = 1.0$ ;  $\alpha(t)^\circ = 15^\circ + 15^\circ \sin(1.6t)$ .**  
**Flow Out of Plane of Paper.**



a.  $\alpha = 15^\circ$  (Increasing).

b.  $\alpha = 15^\circ$  (Decreasing).

**Figure 9. Spanwise Variations of the Flow Around Sharp Leading Edge Rectangular Wing.  $K = 1.0$ ;  $\alpha(t)^\circ = 15^\circ + 15^\circ \sin(1.0t)$ .**

$K = 0.5$ . Both the upward and downward motions are shown side by side for the angles of attack of  $10^\circ$ ,  $12^\circ$ ,  $14^\circ$ ,  $16^\circ$ ,  $18^\circ$  and  $20^\circ$ . At any particular angle of attack, the flow patterns were very different during the upward and downward motions. The separation region at the downstroke was visually thicker than that at the upstroke, indicating the existence of a hysteresis loop. For a two-dimensional unsteady airfoil, the lift, drag and moment also experience hysteresis in one oscillation cycle,<sup>4,5</sup> but it is caused by a convecting separation vortex rather than by the stationary separation vortices encountered in the present investigation. When the reduced frequency is decreased to a very low value, the hysteresis should diminish, and the flow should reach a quasi-steady state. In the present study, the hysteresis could still be detected at  $K = 0.05$ . A quasi-steady state was thus not achieved.\*

The hysteresis loop was also observed from the end view of the pitching wing obtained using a vertical sheet of light in the  $y-z$  plane at  $x = 0.8c$ . The dye released from the slots on the suction side of the wing marked the leading edge separation vortex. The growth-decay of the vortex can be inferred from the size of the dye blob. The height of the dye blob,  $H$ , in several test conditions of the  $45^\circ$  sweep wing is plotted in Figure 6. The hysteresis loop is obvious in this diagram, and several other interesting features are also revealed here. In Figure 6a, three unsteady cases were performed at the same Reynolds number,  $R_c = 5.0 \times 10^4$ , but at different reduced frequencies,  $K = 0.25$ ,  $0.5$  and  $1.0$ . At an angle of attack less than  $15^\circ$ , the values of  $H$  are not a function of the reduced frequency, and the size of the vortex in the

---

\*Two-dimensional oscillating airfoil experiments indicate the presence of a hysteresis loop and the lack of quasi-steady behavior for reduced frequencies as low as  $0.001$ .<sup>14,15</sup>

steady case is about equal to the averaged values of  $H$  at the upstroke and the downstroke. The effect of the reduced frequency becomes obvious for  $\alpha > 15^\circ$ . At the lowest reduced frequency,  $K = 0.25$ , the hysteresis loop followed the trend of  $H$  in the steady case to fairly high angles of attack. At higher reduced frequencies, the deviation between the unsteady  $H$  and the static  $H$  became larger. The maximum value of  $H$  could be controlled by two time scales, the period of oscillation and a scale associated with the roll-up time of the separation vortex. At high reduced frequencies, the wing changed to a downstroke before the vortices reached the fully developed stage and, hence, the maximum  $H$  decreased with increasing  $K$ . This phenomenon is mainly due to an inertial effect, and viscosity should not play a role. This is demonstrated in Figure 6b for two unsteady cases performed at the same reduced frequency of  $K = 1$ , but at two different Reynolds numbers,  $R_c = 2.5 \times 10^4$  and  $3.4 \times 10^5$ . The Reynolds numbers in these two tests were more than one order of magnitude apart; however, there is no measurable difference in the measured values of  $H$ .

### 3.3 Effects of the Reduced Frequency

In general, the unsteadiness on a delta wing delayed stall and prompted hysteresis, which is similar to results obtained with unsteady two-dimensional airfoils. As the oscillation frequency increased, the formation of the separation region appeared further downstream. At  $K = 1$ , the streamlines remained parallel to the wing surface until high angles of attack were reached.

Significant changes occurred when the reduced frequency was about  $\pi$ . No thick separation zone was then observed on the wing; however, a strong vortex was shed at the trailing edge as  $\alpha$  passed through its maximum value. Figure 7 is a side view of the pitching wing visualized using the dye-layer technique.

The 45° sweep wing underwent the pitching motion  $\alpha(t)^\circ = 15^\circ + 15^\circ \sin(2.4t)$  at a chord Reynolds number of  $R_c = 2.5 \times 10^4$  and a reduced frequency of  $K = 3.0$ . The movie sequence in the figure shows the wing at attack angles of 0°, 5°, 10°, 15°, 20°, 25° and 30° during the upstroke and the downstroke. The dye layers in the outer flow region indicate that the potential flow is following the motion of the wing, and that the separation region is restricted to be very close to the wing surface.

A tentative explanation for the distinct change at  $K \approx \pi$  is as follows. The reduced frequency can be viewed as the ratio of the chord to a "perturbation" wavelength:  $K = \pi c / U_\infty = \pi c / \lambda$ . In other words, the perturbation wavelength is about equal to the chord length at  $K = \pi$ . As a matter of fact, the reattachment point can be seen near the trailing edge in Figure 7. After the flow is reattached, a thin shear layer with intense vortices formed, and a strong vortex counter-rotating with respect to the attached wing circulation was shed from the trailing edge. The induced velocity of this vortex kept the potential flow moving downward with the wing. If the perturbation wavelength was longer than the chord, i.e.,  $K < \pi$ , the wake remained thick. The diffused vortex could not enforce a thin separation region on the wing. Based on these arguments, it appears that the Strouhal number based on the chord length is more appropriate to describe the flow than the conventional reduced frequency.

### 3.4 The Counter-Rotating Vortices

With steady flow, a detailed visualization showed that there was a small counter-rotating vortex next to each primary separation vortex.<sup>16</sup> In the present investigation, a counter-rotating vortex was also observed in ciné films of the unsteady delta wing. Moreover, this counter-rotating vortex had a

hysteresis loop. A pair of such vortices commonly occurred in other unsteady separated flows.<sup>17,18</sup> In some flows, the counter-rotating vortices have a very strong dynamic influence. For example, in an impinging jet, the ring-shaped coherent structure in the shear layer induces a counter-rotating vortex while it approaches the wall. The suction generated on the wall by the induced vortex was found to be considerably higher than that generated by the coherent structure.<sup>12</sup> The large suction associated with the counter-rotating vortex implies that the aerodynamic characteristics of a given surface could be significantly altered by modifying the evolution of this vortex. This is easier than changing the flow structure far away from the wall, because an active device can be placed on the wall to alter the low-speed flow region. The importance of the counter-rotating vortex on the delta wing is not clear at present. It certainly deserves further investigation, especially the counter-rotating vortices located at about 60% of the semispan from the center, where the suction peaks occur.<sup>3</sup>

#### 4. CONCLUSIONS

Two delta wings with leading edge sweeps of  $45^\circ$  and  $60^\circ$  were studied in a towing tank at chord Reynolds numbers up to  $3.5 \times 10^5$ . The wings were pitched about the quarter-chord point with sinusoidal oscillations of amplitude  $\pm 5^\circ$ ,  $\pm 10^\circ$  and  $\pm 15^\circ$  about a given mean attack angle. Food color and fluorescent dyes were used to visualize the flow field on and around the wing. Sheets of laser light excited the fluorescent dye to yield detailed flow information in the desired plane.

The three-dimensional separation process of the leading edge vortex started from the trailing edge corners and propagated upstream and inward. The evolution of the separation vortex revealed a hysteresis loop that is a strong function of the reduced frequency. At low reduced frequencies, the separation region on the suction side was fairly thick. A distinct change of the flow pattern happened at  $K \approx \pi$ . The shedding vortex became strongly coherent in this range of reduced frequencies, and its induced velocity kept the separated region to a thin layer near the wing surface.

#### ACKNOWLEDGMENT

This work is supported by the U.S. Air Force Office of Scientific Research Contract number F49620-80-C-0020, and monitored by Major M. S. Francis and Dr. J. D. Wilson. The authors would like to acknowledge the valuable help of R. F. Blackwelder, M. Cooper and R. Srnsky.

## REFERENCES

1. Jones, R. T., and Cohen D., High Speed Wing Theory, Princeton University Press, Princeton, 1960.
2. Elle, B. J., "An Investigation at Low Speed of the Flow Near the Apex of Thin Delta Wings with Sharp Leading Edges," Aeronautical Research Council, R&M No. 3176, Jan. 1958.
3. Fink, P. T., and Taylor, J., "Some Early Experiments on Vortex Separation, Part II: Some Low Speed Experiments with 20 Degree Delta Wings," Aeronautical Research Council, R&M No. 3489, Sept. 1966.
4. McAlister, K. W., and Carr, L. W., "Water Tunnel Visualization of Dynamic Stall," J. Fluid Eng., Vol. 101, Sept. 1979, pp. 376-380.
5. McCroskey, W. J., "Unsteady Airfoils," Ann. Rev. Fluid Mech., Vol. 14, Jan. 1982, pp. 285-311.
6. Lambourne, N. C., Bryer, D. W., and Maybrey, J. F. M., "The Behaviour of the Leading-Edge Vortices Over a Delta Wing Following a Sudden Change of Incidence," Aeronautical Research Council, R&M No. 3645, March 1969.
7. Gad-el-Hak, M., Blackwelder, R. F., and Riley, J. J., "On the Growth of Turbulent Regions in Laminar Boundary Layers," J. Fluid Mech., Vol. 110, Sept. 1981, pp. 73-95.
8. Gad-el-Hak, M., Ho, C.-M., and Blackwelder, R. F., "A Visual Study of a Delta Wing in Steady and Unsteady Motion," in Unsteady Separated Flows, eds. M. S. Francis & M. W. Luttges, University of Colorado, Aug. 1983, pp. 45-51.
9. Gad-el-Hak, M., and Blackwelder, R. F., "On the Discrete Vortices from a Delta Wing," AIAA J., in press, 1985.

10. Williams, J. C. III, "Incompressible Boundary-Layer Separation," Ann. Rev. Fluid Mech., Vol. 9, Jan. 1977, pp. 113-144.
11. Telionis, P. P., Unsteady Viscous Flows, Springer, New York, 1981.
12. Didden, N., and Ho, C.-M., "Unsteady Separation in the Boundary Layer Produced by an Impinging Jet," J. Fluid Mech., in press, 1985.
13. Ho, C.-M., and Nasseir, N. S. M., "Dynamics of an Impinging Jet. Part 1: The Feedback Mechanism," J. Fluid Mech., Vol. 105, April 1981, pp. 119-142.
14. McAlister, K. W., Carr, L. W., and McCroskey, W. J., "Dynamic Stall Experiments on the NACA 0012 Airfoil," NASA Technical Paper 1100, Jan. 1978.
15. Francis, M. S., and Keesee, J. E., "Airfoil Dynamic Stall Performance with Large Amplitude Motions," submitted to AIAA J., 1985.
16. Fink, P. T., "Some Early Experiments on Vortex Separation, Part III: Further Experiments with 20 Degree Delta Wings," Aeronautical Research Council, R&M No. 3489, Sept. 1966.
17. Freymuth, P., Bank, W., and Palmer, M., "Visualization of Accelerating Flow Around an Airfoil at High Angles of Attack," Z. Flugwiss. Weltraumforsch., Vol. 7, July 1983, pp. 392-400.
18. Gad-el-Hak, M., and Ho, C.-M., "Three-Dimensional Effects on a Pitching Lifting Surface," AIAA Paper No. 85-0041, Jan. 1985.

FIGURE CAPTIONS

- Figure 1. Schematic of the Delta Wing and Definition Sketch.
- Figure 2. End View Using the Dye-Layer Technique.  $R_c = 2.5 \times 10^4$ ,  $K = 3.0$ ,  
 $\alpha^\circ = 15^\circ + 15^\circ \sin(2.4t)$ . Flow is Out of the Plane of the  
Photographs.
- Figure 3. Spanwise Variations of Vertical Velocity.  $R_c = 2.5 \times 10^4$ ,  $K = 3.0$ ,  
 $\alpha = 0^\circ$ ,  $y/c = 0.13$ .
- Figure 4. Variations of Vertical Velocity with Normal Coordinate.  $R_c = 2.5 \times 10^4$ ,  
 $K = 3.0$ ,  $\alpha^\circ = 15^\circ \pm 15^\circ$ ,  $z/c = 0$ .
- a. Linear Plot.
- b. Semi-Log Plot.
- Figure 5. Side View of the Pitching Wing.  $R_c = 2.5 \times 10^4$ ,  $K = 0.5$ ,  
 $\alpha(t)^\circ = 15^\circ + 5^\circ \sin(0.4t)$ .
- Figure 6. Hysteresis Loop.
- a. Effects of Reduced Frequency.  $R_c = 5.0 \times 10^4$ ,  $\alpha^\circ = 15^\circ \pm 10^\circ$ .
- b. Effects of Reynolds Number.  $K = 1.0$ ,  $\alpha^\circ = 15^\circ \pm 15^\circ$ .
- Figure 7. Side View Using the Dye-Layer Technique.  $R_c = 2.5 \times 10^4$ ,  $K = 3.0$ ,  
 $\alpha(t)^\circ = 15^\circ + 15^\circ \sin(2.4t)$ .

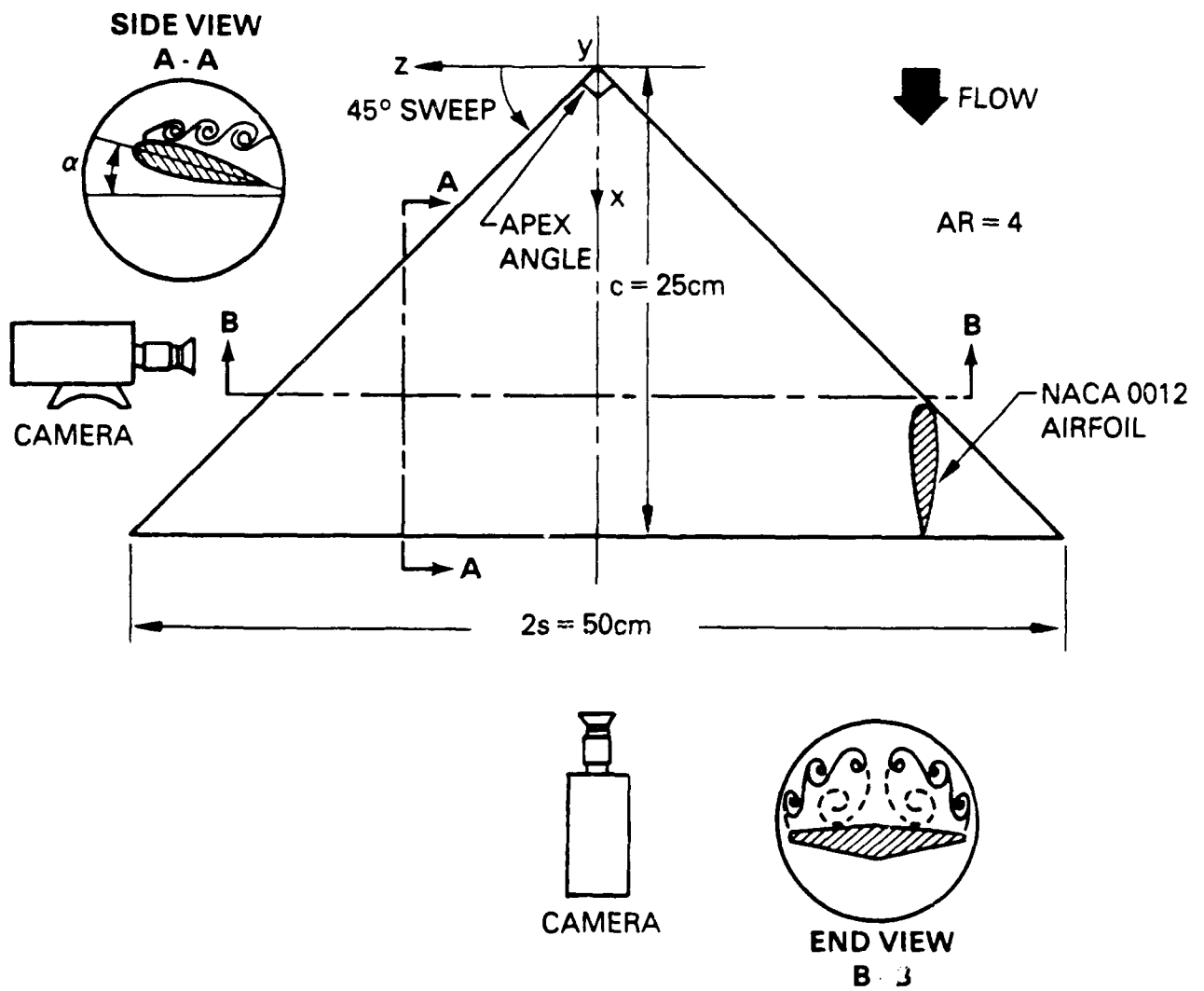


Figure 1. Schematic of the Delta Wing and Definition Sketch

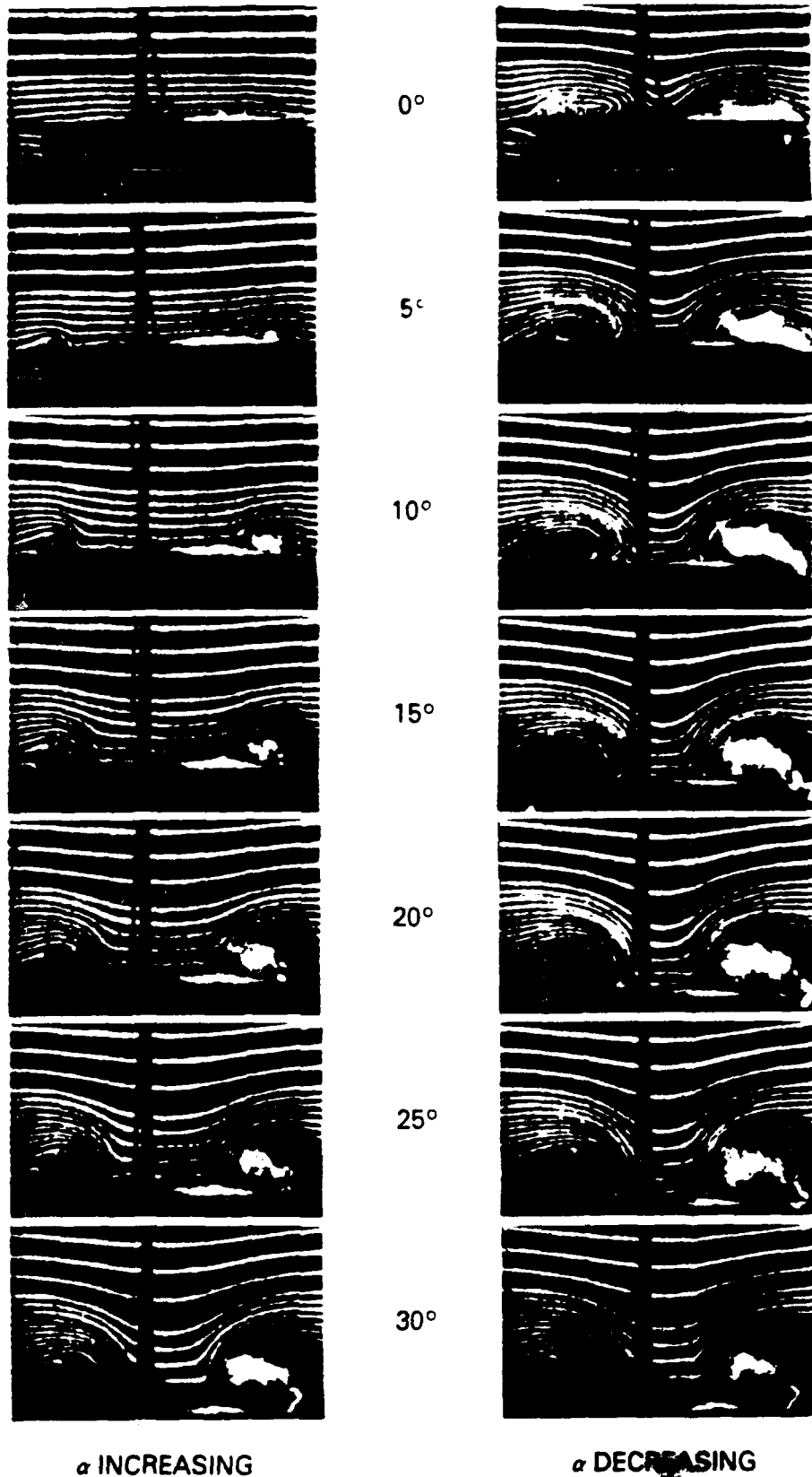


Figure 2. End View Using the Dye-Layer Technique.  $R_C = 2.5 \times 10^4$ ,  $K = 3.0$ ,  $\alpha^\circ = 15^\circ + 15^\circ \sin(2.4t)$ . Flow is out of the Plane of the Photographs

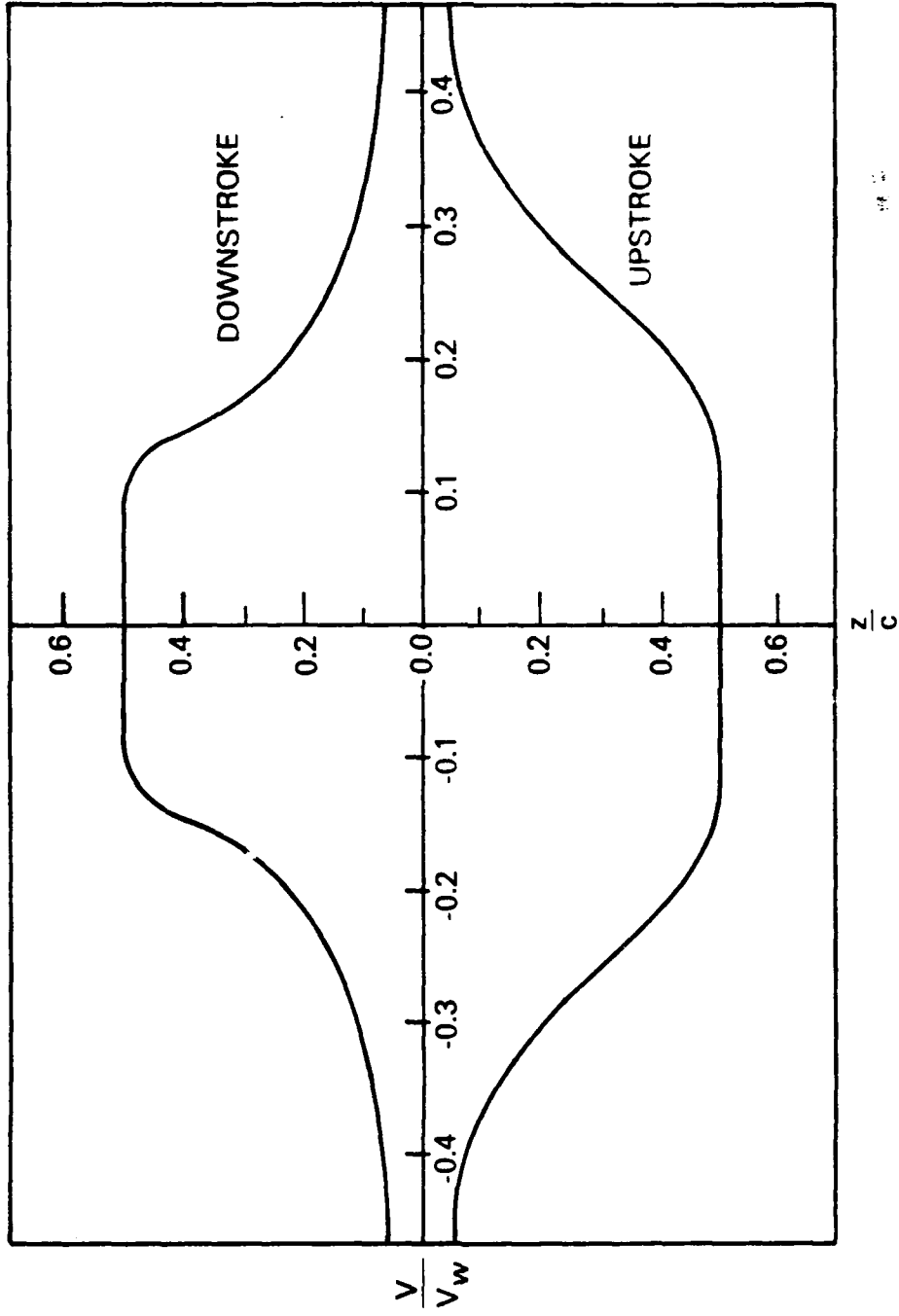
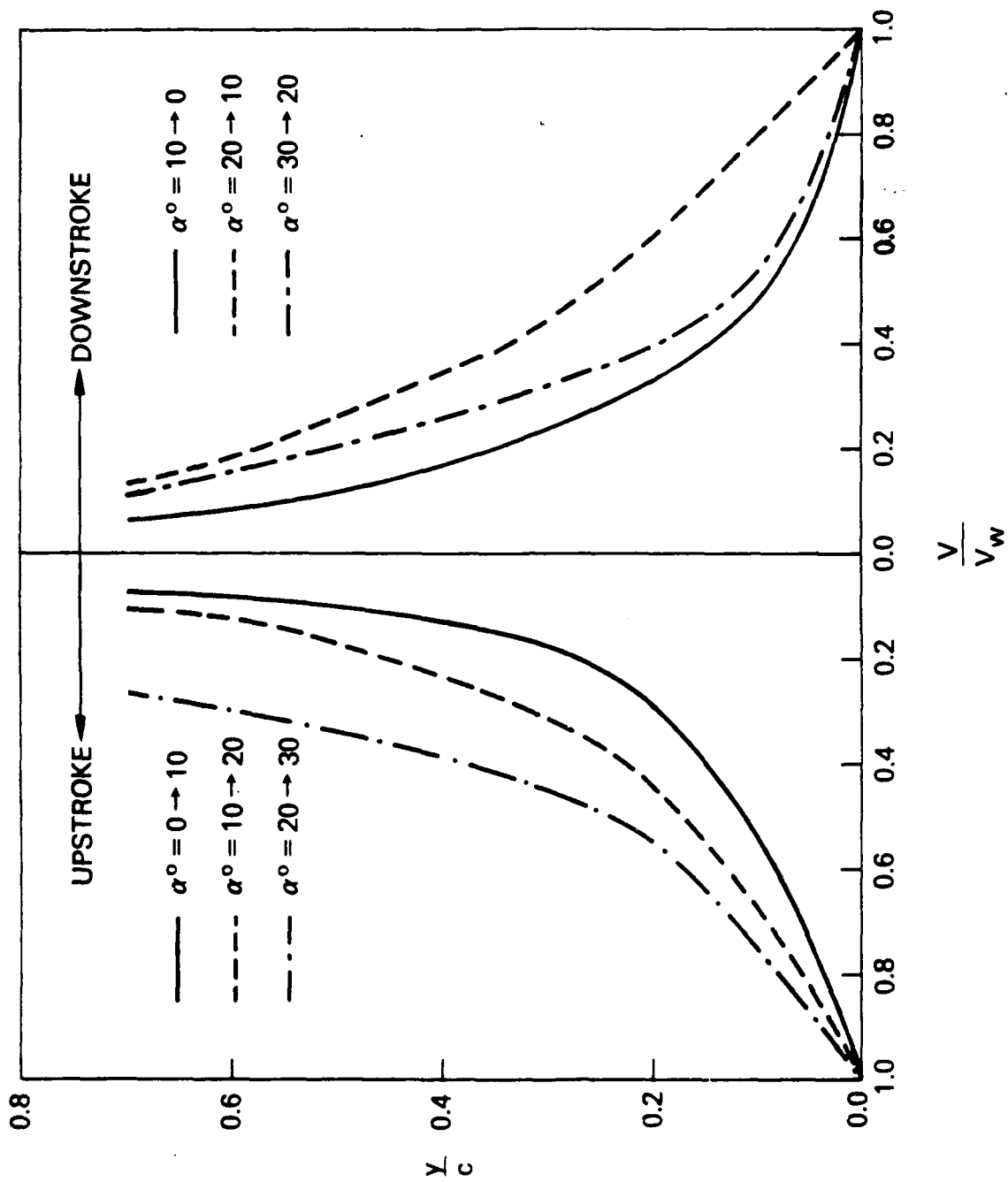
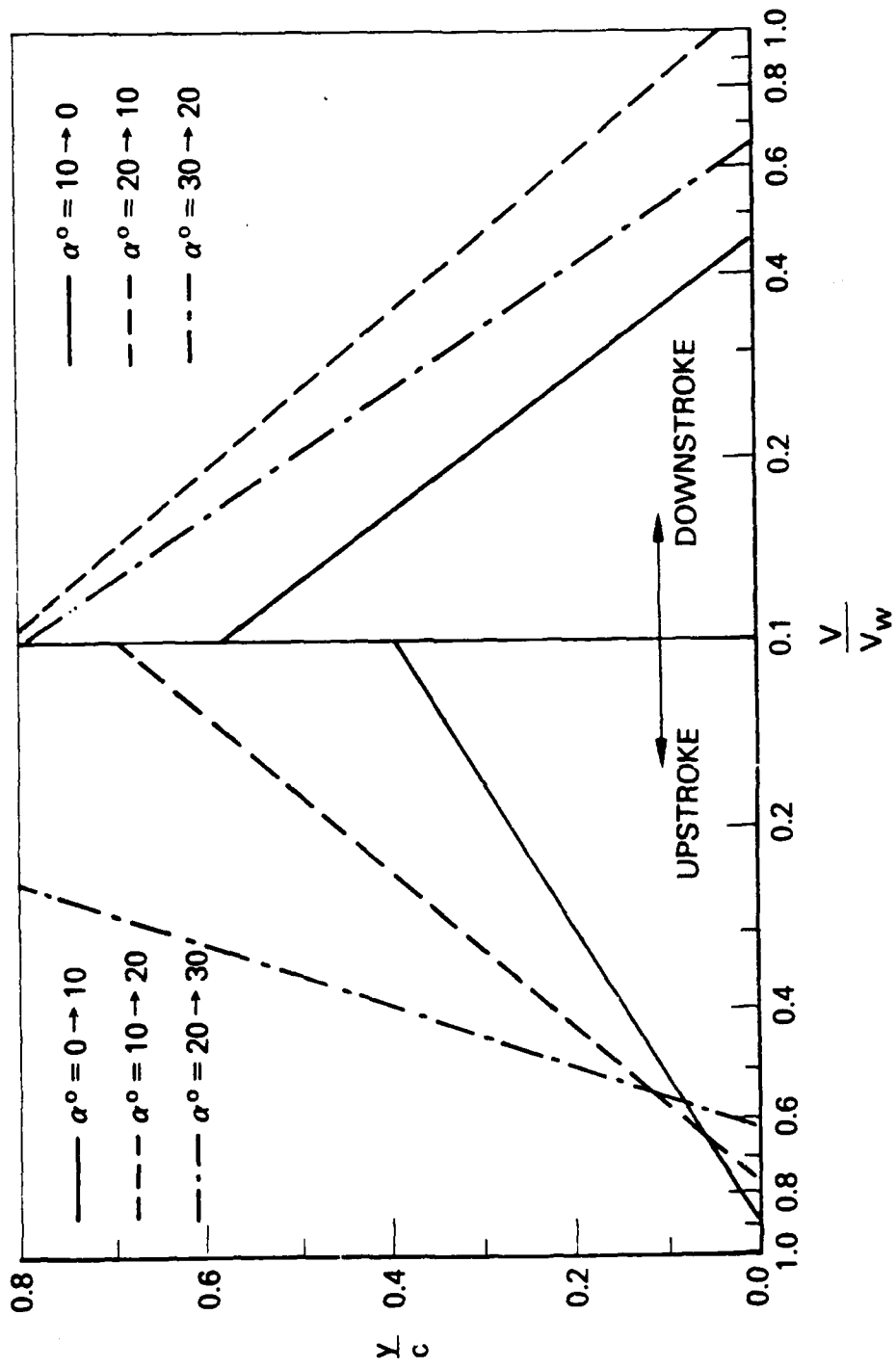


Figure 3. Spanwise Variations of Vertical Velocity.  
 $R_c = 2.5 \times 10^4$ ,  $K = 3.0$ ,  $\alpha = 0^\circ$ ,  $y/c = 0.13$ .



a. Linear Plot.

Figure 4. Variations of Vertical Velocity with Normal Coordinate.  
 $R_c = 2.5 \times 10^4$ ,  $K = 3.0$ ,  $\alpha^0 = 15^\circ \pm 15^\circ$ ,  $z/c = 0$ .



b. Semi-Log Plot.

Figure 4. Variations of Vertical Velocity with Normal Coordinate (Concluded).

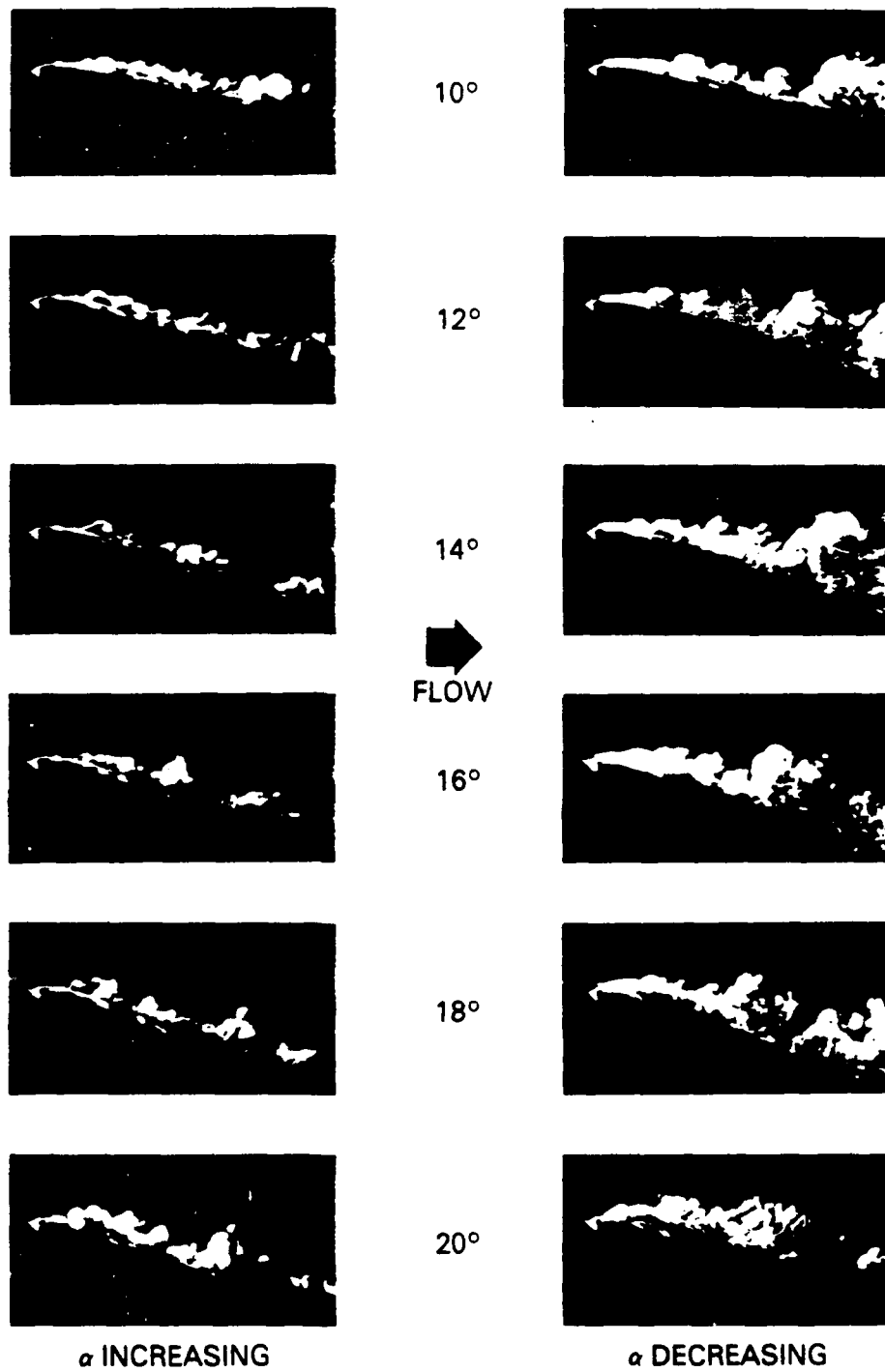
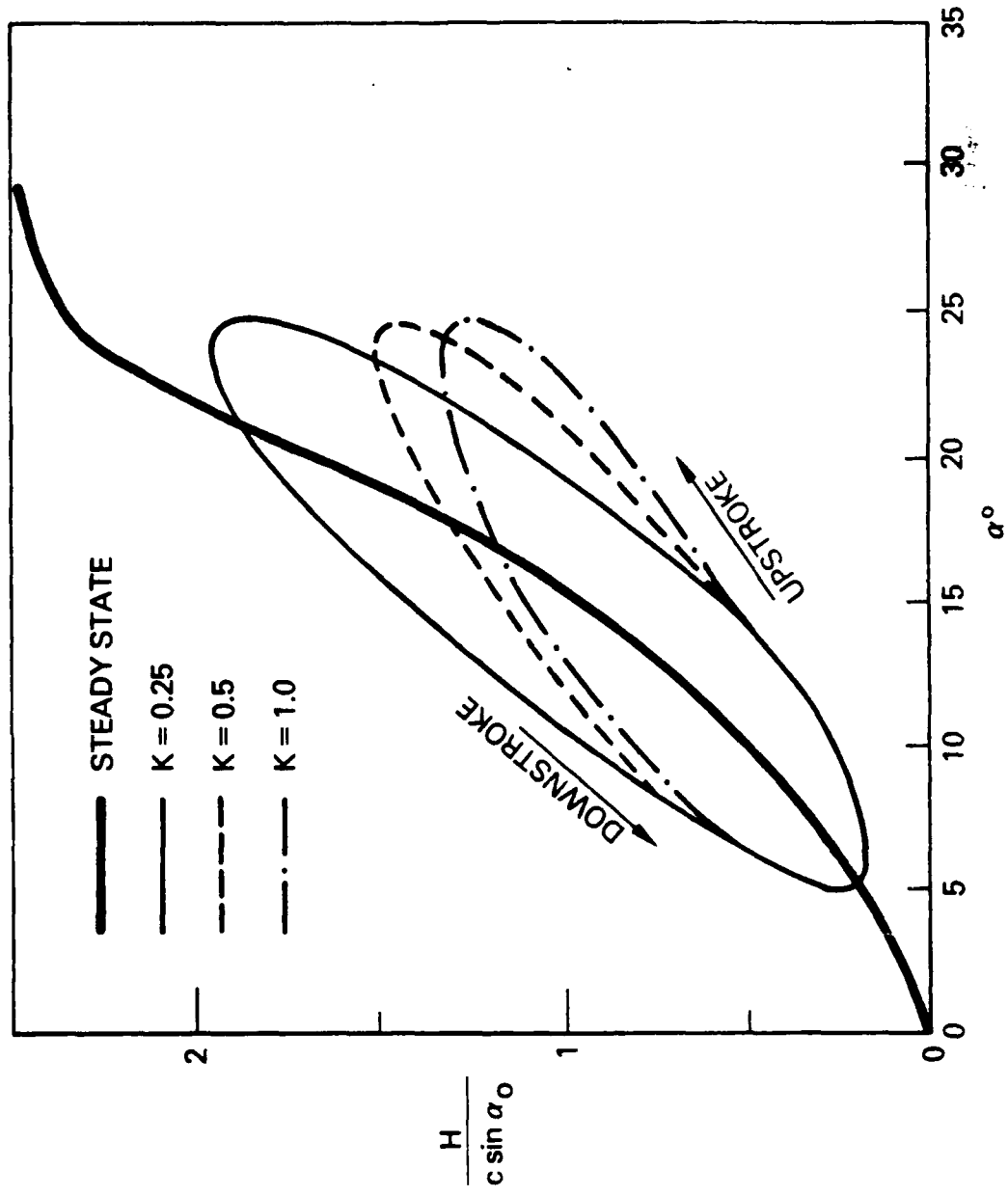
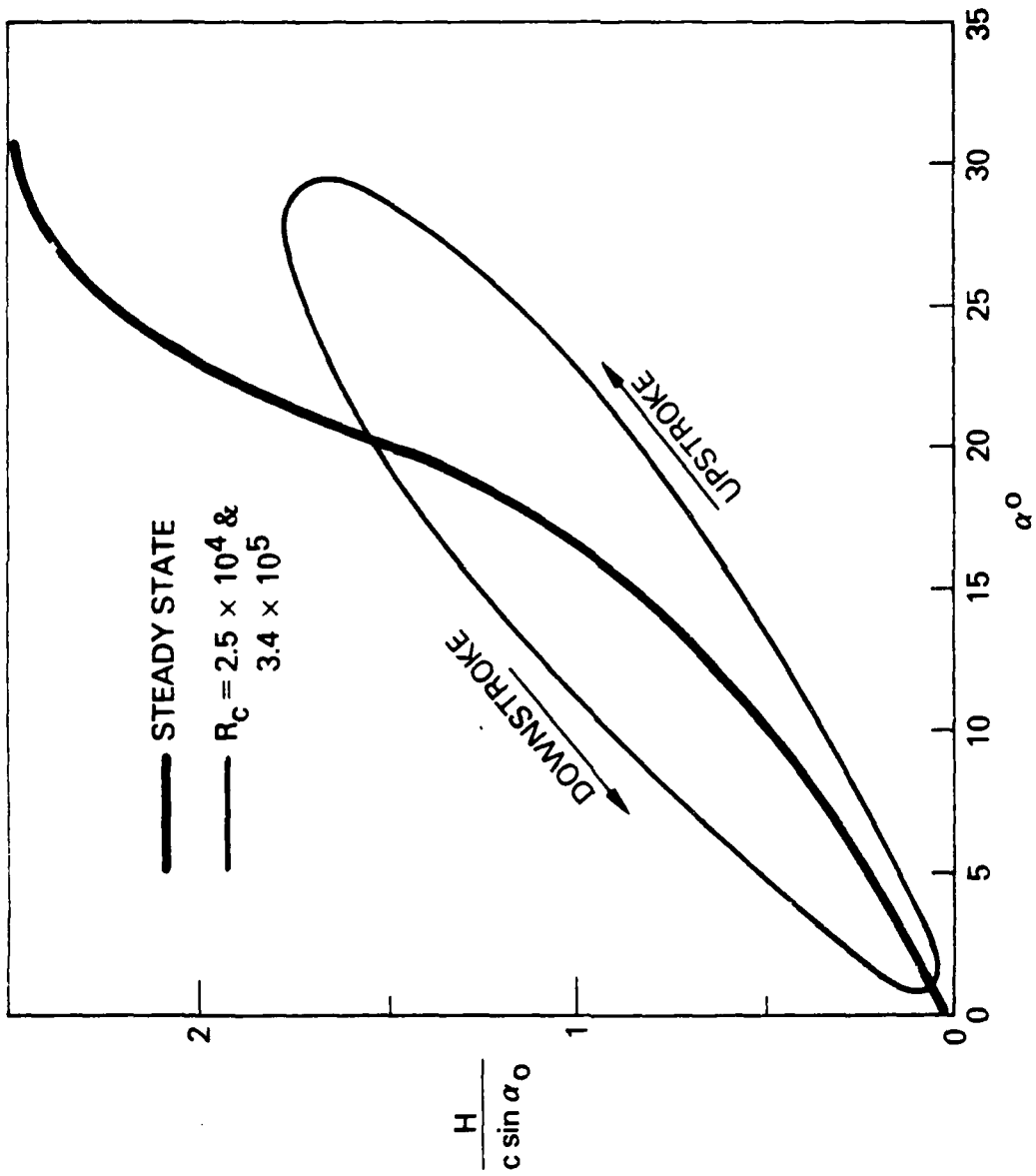


Figure 5. Side View of the Pitching Wing.  $R_C = 2.5 \times 10^4$ ,  
 $K = 0.5$ ,  $\alpha(t)^\circ = 15^\circ + 5^\circ \sin(0.4t)$ .



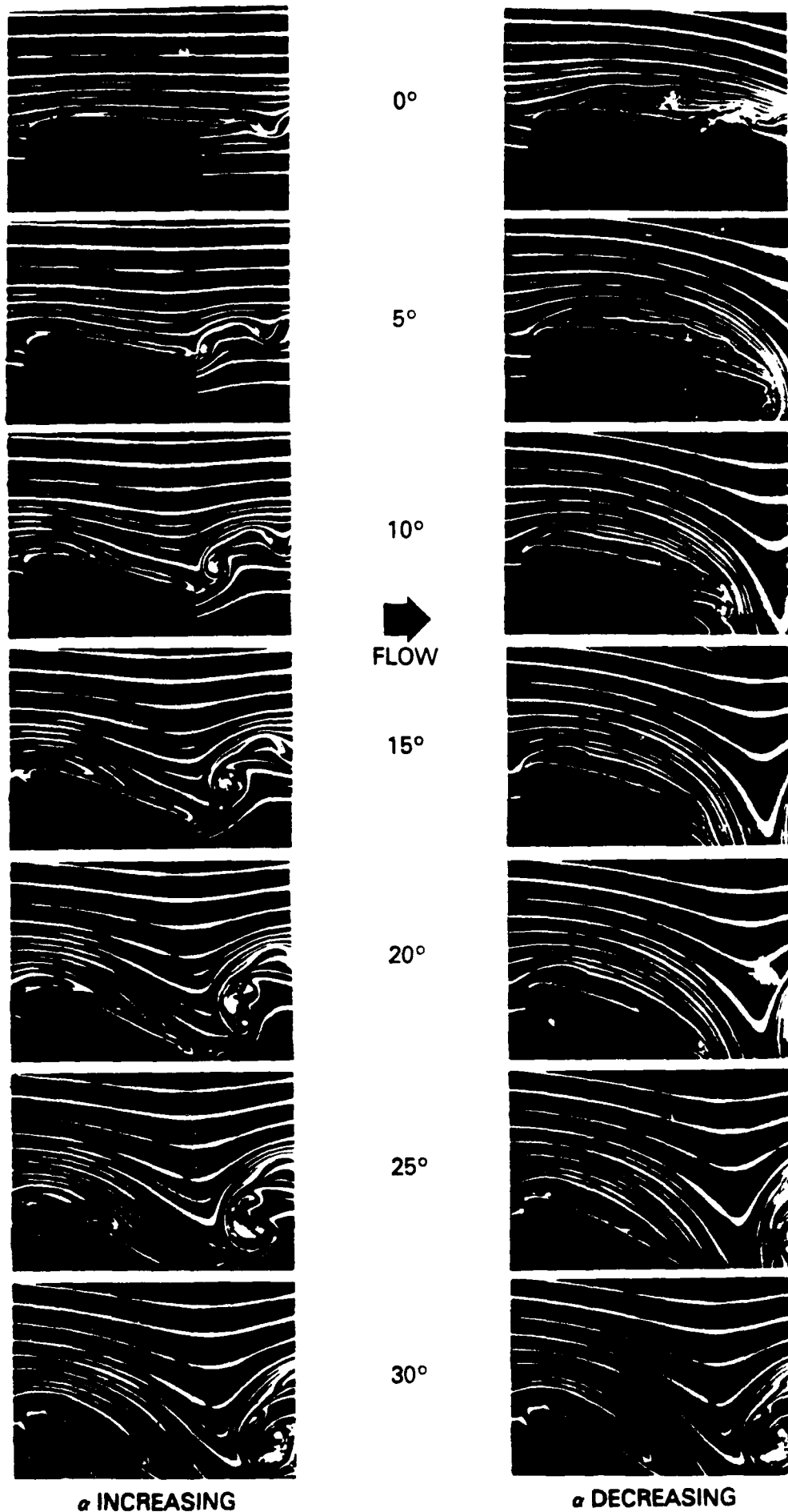
a. Effects of Reduced Frequency.  $R_c = 5.0 \times 10^4$ ,  $\alpha^\circ = 15^\circ \pm 10^\circ$ .

Figure 6. Hysteresis Loop.



b. Effects of Reynolds Number.  $K = 1.0$ ,  $\alpha^\circ = 15^\circ \pm 15^\circ$ .

Figure 6. Hysteresis Loop (Concluded).



$\alpha$  INCREASING
  $\alpha$  DECREASING

**Figure 7. Side View Using the Dye-Layer Technique.  $R_C = 2.5 \times 10^4$ ,  $K = 3.0$ ,  $\alpha(t) = 15^\circ + 15^\circ \sin(2.4t)$ .**

UNSTEADY FLOW AROUND AN OGIVE-CYLINDER

Mohamed Gad-el-Hak\*

and

Chih-Ming Ho\*\*

October 1985

Flow Research Company

21414-68th Avenue South

Kent, WA 98032

---

Presented as Paper 86-0572 at the AIAA 24th Aerospace Sciences Meeting,  
Reno, Nevada, January 6-9, 1986.

\*Senior Research Scientist. Member AIAA

\*\*Professor, Department of Aerospace Engineering, University of Southern  
California, Los Angeles, CA 90089. Member AIAA.

UNSTEADY FLOW AROUND AN OGIVE-CYLINDER

Mohamed Gad-el-Hak

and

Chih-Ming Ho

Flow Research Company

21414-68th Avenue South

Kent, WA 98032

ABSTRACT

The time-dependent flow around an ogive-cylinder undergoing large amplitude, harmonic pitching motion was investigated using flow visualization techniques. The slender body of revolution was towed in an 18-m water channel at Reynolds numbers up to  $1.2 \times 10^5$ . Fluorescent dyes were either introduced uniformly from the body's porous surface or placed as horizontal sheets in the slightly stratified tank prior to a run. The dyes were excited with a sheet of laser light projected in the desired plane to mark the flow in the separation region around the body, the flow in the wake, and the potential flow away from the body. The separation process and the geometry of the leeward vortices were studied under different reduced frequencies and Reynolds numbers. The unsteady separation phenomenon is found to be significantly different from the separation on a body in steady flight.

NOMENCLATURE

D	maximum body diameter
H	height of separation region
L	body length
f	pitching frequency
K	reduced frequency, $\pi f D / U_{\infty}$
$R_D$	Reynolds number, $U_{\infty} D / \nu$
t	time (sec)
$U_{\infty}$	towing speed
x,y,z	Cartesian coordinates fixed with the body
$\alpha(t)$	time-dependent angle between the body centerline and the towing direction
$\alpha_A(t)$	time-dependent angle between the body centerline and the relative velocity vector
$\alpha_0$	mean pitching angle
$\alpha_{00}$	amplitude of harmonic motion
$\beta$	angle between the plane of symmetry of the separation vortex and the vertical axis
$\nu$	kinematic viscosity

1. INTRODUCTION

There has been a recent interest in the concept of supermaneuverability where previously unattained regions of the maneuver envelope for a fighter aircraft are attempted, such as post-stall flight maneuver and side slipping.<sup>1,2</sup> The performance of a highly-maneuverable aircraft is critically dependent upon the accurate prediction of the flow around the wings, body and other parts of the vehicle. While the wings are of the utmost importance aerodynamically, the unsteady flow around the body must play a role in the maneuverability of

the airplane. Similarly, an understanding of the unsteady flow around a missile is essential for predicting the aerodynamic forces during maneuvering, which incidentally is not constrained by pilot limitations and could therefore operate at higher normal accelerations and higher angles of attack (beyond the linear range) than a typical aircraft.

At high angles of attack, the symmetric or asymmetric leeward separation on an axisymmetric body is exceedingly complex, and progress in forming the basis for describing and modeling how vorticity is shed from the body to the leeward wake has depended crucially upon experiment.<sup>3</sup> While much remains to be investigated, a reasonable overall understanding of the steady flow around an axisymmetric body is evolving. Unfortunately, little is known about the influence of time-dependent motions (e.g., pitching oscillations) on the time-evolution of the leeward vortex structure or the flow field in general. Nielsen,<sup>3</sup> in his broad survey of missile aerodynamics, does not even discuss time-dependent motions. This is unlike the relatively large body of past and ongoing theoretical and experimental research dealing with unsteady flows around two- and three-dimensional airfoils.<sup>4-17</sup>

To provide a 'first look' at the unsteady motion around a body of revolution, flow visualization techniques were used in the present investigation to study the time-dependent flow around an ogive-cylinder undergoing large amplitude, harmonic pitching motion. The slender body was towed in an 18-meter water channel, and the flow was visualized using fluorescent dyes and sheets of laser light. The apparatus and the visualization method are described in the next section. In Section 3, the effects of changing the Reynolds number and the reduced frequency on the unsteady separation phenomenon are categorized and elaborated. Concluding remarks are presented in the last section.

## 2. EXPERIMENTAL APPROACH

The flow over an ogive-cylinder undergoing a time-dependent pitching motion about the 0.5 station was studied. The slender body of revolution is made of polyvinyl chloride plastic, its maximum diameter is 4 cm, and has a fineness ratio of 10. The body was towed in the water channel described by Gad-el-Hak et al.<sup>18</sup> This towing tank is 18 m long, 1.2 m wide and 0.9 m deep, and the towing speed,  $U_\infty$ , was varied in the range of 5 to 300 cm/sec. This provided a Reynolds number change in the range of  $2 \times 10^3 \leq R_D \equiv U_\infty D / \nu \leq 1.2 \times 10^5$ , where  $D$  is the maximum body diameter and  $\nu$  is the kinematic viscosity.

A four-bar mechanism was used to sting-mount and to pitch the body around the desired position along its length. In the experiments reported herein, the body was pitched around  $x = 0.5 L$ , where  $x$  is the distance along the axis of symmetry measured from the nose and  $L$  is the body's length. The mean angle of attack could be set from  $0^\circ$  to  $45^\circ$ , but was set at  $15^\circ$  for the present investigation. A Boston Ratiotrol motor drove the four-bar linkages to produce approximately sinusoidal oscillations of amplitude  $\pm 5^\circ$ ,  $\pm 10^\circ$  or  $\pm 15^\circ$  about a given mean angle of attack. The reduced frequency,  $K \equiv \pi f D / U_\infty$ , where  $f$  is the pitching frequency, was varied in the range of 0.04 to 0.75, and a digital readout displayed the instantaneous angle between the body centerline and the towing direction,  $\alpha(t)$ .

The complex, unsteady, separated flow around the slender body was visualized using the dye-layer technique described by Gad-el-Hak.<sup>19</sup> Horizontal layers of fluorescent dye were placed in the weakly stratified water channel prior to towing the body, and excited using sheets of laser light projected in the desired plane. Longitudinal and transverse planes of the flow field were visualized to provide better detail and to locate more precisely the separation vortex position. The dye layers marked the flow in the separation region

around the body, the flow in the wake region, and the potential flow away from the lifting surface. For more detailed visualization of the separation vortices, fluorescent dye was continuously seeped into the flow from the entire body surface. This was accomplished by covering the body with a thin, porous cloth saturated with (dry) dye crystals. As the body moved through the tank, the dye dissolved slowly into the surrounding water and marked the leeward vortices rather well. The visualization results were recorded using 35-mm photographs and 16-mm ciné films (available upon request).

### 3. RESULTS AND DISCUSSION

The flow over an ogive-cylinder undergoing a time-dependent pitching motion about the 0.5 station was studied. The slender body was towed in an 18-meter water channel and fluorescent dye visualization techniques were used to investigate the unsteady separation process and the geometry of the leeward vortices, and to provide a global physical picture of the time-dependent flow field. For a particular run conditions, few selected side and end views of the flow will be depicted in here as still photographs. However, a visual image of the complex flow field can be more readily constructed by viewing the ciné films in as many longitudinal and transverse planes as possible. Also, the first (starting) oscillation cycle is different from the second or subsequent cycles, hence the first cycle will not be shown in any of the figures presented here.

#### 3.1 Frontward and Rearward Vortices

The separation pattern for a pitching slender body is quite different from that for a body in steady flight. At constant angle of attack, the boundary layer fluid separates along lines on the lee side due to the forward motion of

the body.<sup>20</sup> Vortices are formed by the rolling up of the resulting sheets of vorticity. These vortices are symmetrical at low angles of attack, becoming asymmetric at moderate to large attack angles.<sup>21</sup> For a pitching missile, separation may also be triggered by the harmonic motion. The reduced frequency  $K \equiv \pi f D / U_\infty$ , determines the relative importance of the harmonic and forward motions. Let the angle between the missile axis and the towing direction be expressed as:

$$\alpha(t) = \alpha_o + \alpha_{oo} \sin(2\pi ft),$$

where  $\alpha_o$  and  $\alpha_{oo}$  are the mean and amplitude of the harmonic motion,  $f$  is the pitching frequency and  $t$  is time. It can be shown by considering the relative velocity vector and after some algebra that the aerodynamic angle of attack<sup>†</sup> at the nose,  $\alpha_A$ , is given by:

$$\alpha_A(t) = \alpha(t) - \arctan \left\{ \frac{\pm \pi f L \cos \alpha \sqrt{\phi^2(t)}}{U_\infty \pm \pi f L \sin \alpha \sqrt{\phi^2(t)}} \right\},$$

where  $\phi^2(t) \equiv (2\alpha \alpha_o - \alpha^2 + \alpha_{oo}^2 - \alpha_o^2)$ , and the sign change reflects whether  $\alpha$  is increasing (upstroke) or decreasing (downstroke). As an example, for  $f = 0.16$  Hz and  $U_\infty = 10$  cm/sec ( $K = 0.2$ ), the above equation for the aerodynamic angle of attack yields a value of  $\alpha_A \approx -6^\circ$  when  $\alpha = 5^\circ$  and increasing, and a value of  $\alpha_A \approx 32^\circ$  for  $\alpha = 20^\circ$  during the downstroke. This effect is more pronounced for larger pitching frequency or smaller towing speed. Similar expressions could easily be derived for other positions along the body, where the relative velocity vector is different for each location. Of course,  $\alpha_A(t) = \alpha(t)$  at the pivot point,  $x/L = 0.5$ .

---

<sup>†</sup>Angle between the missile axis and the relative velocity vector.

The above effects are best illustrated using side views of the flow field. In Figure 1, horizontal dye layers were excited using a vertical sheet of laser light parallel to the towing direction and at  $z = 1$  cm off the body centerline. The flow is from left to right and the slender body underwent the pitching motion  $\alpha(t)^\circ = 15 + 15 \sin(t)$ . The Reynolds number based on diameter was  $R_D \equiv U_\infty D/\nu = 4 \times 10^3$ , and the reduced frequency was  $K \equiv \pi f D/U_\infty = 0.2$ . The photographs in the figure show a typical oscillation cycle for both the upward and downward motions of the body at  $\alpha = 0^\circ, 5^\circ, 10^\circ, 15^\circ, 20^\circ, 25^\circ$  and  $30^\circ$ . It is clear that two distinct separation regions evolve in the unsteady case. We term these the "Frontward and Rearward Separations." The former occurs mainly in the nose region during the downstroke and the latter evolves during the upstroke and starts near the tail of the body. The rearward separation is closest to the tail at about  $\alpha = 5^\circ$  during the upstroke (the downstream half of the body is moving downward). The pitching motion causes a high velocity gradient to exist on either side of the body, creating two shear layers. The unstable shear layers roll-up into a pair of counter-rotating vortices, and the light sheet intersects one of the two structures. The rearward separation front propagates upstream at a speed of about  $0.2 U_\infty$  then slows down to a very low speed,  $0.05 U_\infty$ , in the second half of the upstroke, reaching  $x = 0.4 L$  at the maximum angle of attack  $\alpha = 30^\circ$ . At the beginning of the downstroke, a thin layer of fluid keeps propagating upstream. At  $\alpha = 25^\circ$ , the reverse flow reaches the nose region of the body and the resulting intense shear produced by the thin reverse flow seems to trigger the frontward separation region in the form of a second pair of counter-rotating vortices, that continues to grow as the angle of attack decreases to  $10^\circ$ , then decays for the rest of the downstroke. The primary separation front starts propagating downstream as the attack angle decreases,

initially at a speed of about  $0.05 U_{\infty}$ , increasing to about  $0.15 U_{\infty}$  at  $\alpha = 10^\circ$ . Similar unsteady separation processes have been observed for two-dimensional airfoils undergoing large amplitude pitching motion, where a primary trailing edge separation seems to trigger a secondary leading edge separation.<sup>22</sup>

As will become more obvious later in this paper when the end views are presented, the large separation region shown in Figure 1 near the tail of the body at attack angles exceeding  $15^\circ$ , represents the cumulative signature of several different flow phenomena on the dye marker. These are the rearward vortex originating in that region, the frontward vortex starting at the nose and convecting downstream, and finally the turning of the frontward vortex into the longitudinal plane of the photographs. The signature of the frontward and rearward vortices can be distinguished by viewing the first and second oscillation cycles. During the first upstroke, the frontward vortices are not as yet formed and only the rearward vortex pair is observed. Some information regarding the geometry of the two vortex pairs can then be obtained from the visualization results. At the reduced frequency of  $K = 0.2$ , the rearward separation vortices achieve their maximum height at the attack angle of  $\alpha = 20^\circ$  during the downstroke, while the frontward vortex pair are largest at  $\alpha = 10^\circ$  during the upstroke motion. In the streamwise direction, the heights of both the frontward and rearward vortices grow almost linearly with distance along the body, indicating a nearly conical shape for the two vortex pairs at each phase of the pitching motion.

The position of the separation front could be readily measured from the ciné films at each phase of the cycle. A typical example is shown in Figure 2 for the rearward separation front occurring on the pitching missile at the same run conditions depicted in Figure 1. The distance from the nose,  $x$ , is

nondimensionalized using the body length  $L$ . Note that in Figure 2 the ordinate represents a missile pointing upward (tail at the origin).

### 3.2 Effects of Reduced Frequency

There are two time scales in the unsteady flow generated by a pitching body; the period of the oscillating motion and the time for the separation front to propagate from the tail towards the nose of the body. The dimensionless frequency  $K$  is the ratio of a pitching velocity scale to the flow speed or, alternatively, the ratio of a convection time scale to a pitching period. At low reduced frequencies, the separation vortices convect at a faster rate relative to an oscillation period and the flow has more time to adjust to angle of attack variations. Conversely, when the reduced frequency is large, the period of oscillation is short and the vortices seem to convect at a slower rate. Two reduced frequencies,  $K = 0.2$  and  $0.4$ , are depicted in the end views in Figures 3 and 4. The dye layers were excited with a vertical sheet of laser light perpendicular to the towing direction at  $x/L = 0.75$ .<sup>†</sup> For both runs, the body underwent the pitching motion  $\alpha(t)^\circ = 15^\circ \pm 15^\circ$  and the Reynolds number was  $R_D = 4 \times 10^3$ . At the lower reduced frequency,  $K = 0.2$ , the frontward vortices from one cycle convects to the position  $x = 30$  cm at the beginning of the following cycle ( $\alpha = 0^\circ$ ). On the other hand, for the higher reduced frequency,  $K = 0.4$ , the arrival time is delayed to the end of the upstroke of the following cycle ( $\alpha = 30^\circ$ ). The photographs show clearly the

---

<sup>†</sup>This is the position of the light sheet when the body is at zero angle of attack. As the missile pitches, the vertical sheet of laser intersects positions along the body progressively towards its tail. For example, at  $\alpha = 30^\circ$  the light sheet marks the station  $x/L = 0.79$ , as compared to  $x/L = 0.75$  at  $\alpha = 0^\circ$ .

evolution of the rearward counter-rotating vortices and their interaction with the frontward separation region. Strong downward motion in the dye layers above the body is more readily observed at the higher reduced frequency (Figure 4). Note that changes in the dye pattern in the plane of visualization result from both longitudinal and transverse flow motions.

### 3.3 Streamwise Evolution of the Separation Vortices

Both the frontward and rearward vortex pairs undergo a growth-decay cycle as the angle of attack changes, much the same as the growth-decay cycle observed for the leading edge vortices on a pitching delta wing.<sup>16,17</sup> End views using transverse sheets of light at different streamwise positions were used to study the evolution of the separation vortices. The laser light excited fluorescent dye that was seeped continuously from the porous body surface. Three such views are presented in Figures 5, 6 and 7, for  $x = 20, 30$  and  $40$  cm, respectively. In all three runs the Reynolds number was  $R_D = 4 \times 10^3$ , the missile underwent the harmonic pitching motion  $\alpha(t)^\circ = 15 + 15 \sin(t)$ , and the reduced frequency was  $K = 0.2$ . It is interesting to compare Figures 3 and 6, which represent identical run conditions but different visualization methods. The dye layers placed in the tank prior to towing the model mark the flow (Figure 3) quite differently from the dye seeping continuously from the body surface (Figure 6). This is due to the well known fact that flow visualization with dye depicts the integrated history of the marker's motion rather than its local (instantaneous) behavior.<sup>23</sup> Consequently, the observed results are strong function of the method of introducing the dye into the flow field.

The mutual induction between the vortices within a pair produces a strong downward motion. As shown in Figure 7 for  $x = 40$  cm ( $x/L = 1$ ), the rearward

vortices do not follow the motion of the body. During one pitching cycle, the tail of the missile moves downward then upward as the angle of attack changes from  $0^\circ$  to  $30^\circ$  and back to  $0^\circ$ . The rearward vortices continue to move downward, however, and are actually below the body at  $\alpha = 5^\circ$  during the downstroke.

From the end views, the size variation of the two vortex pairs during an oscillation period could be determined. The vortices clearly undergo a hysteresis loop. For example, at  $x/L = 1$  (Figure 7) the frontward vortex pair has their maximum height at  $\alpha = 10^\circ$  during the upstroke, while the rearward vortices reach a maximum height at  $\alpha = 20^\circ$  during the downstroke. It also appears from the transverse cuts of the separation regions that both the frontward and rearward vortex pairs are symmetric.

### 3.4 Geometry of the Vortex Pairs

The streamwise growth of the frontward vortices is obtained from the transverse views at different streamwise locations. The results for a reduced frequency of  $K = 0.2$  and Reynolds number of  $R_D = 4 \times 10^3$  are shown in Figure 8. In here,  $H$  is the vortex height as sketched in the insert in the figure, and the broken line represents data for the attack angle of  $\alpha = 0^\circ$ , while the solid line maps the vortex growth at  $\alpha = 10^\circ$  during the upstroke. The linear behavior is striking and may indicate that such vortex pair is prone to theoretical modeling.

At any particular angle of attack, the flow patterns were very different during the upward and downward motions, indicating the existence of a hysteresis loop. The hysteresis in the vortex pair growth is seen in Figure 9 which depicts the variation of the separation region height,  $H$ , as the angle of attack changes. The evolution for both the frontward and rearward vortices at  $x/L = 1.0$ ,  $K = 0.2$  and  $R_D = 4 \times 10^3$  is shown in the figure. For comparison,

the height of the steady state vortex pair is also plotted for two Reynolds numbers,  $R_D = 4 \times 10^3$  and  $4 \times 10^4$ . At the same Reynolds number and at the attack angle of  $\alpha = 30^\circ$ , the separation region in the steady case is about three times larger than that for the pitching body.

An interesting quantity that further characterizes the separation vortices is the angle between the plane of symmetry of the vortex and the vertical axis,  $\beta$ , which indicates the relative location of the vortices along the sides of the body. This angle changes as the angle of attack varies and increases along the body length. Near the nose of the missile, the frontward vortices are located near the top (small  $\beta$ ). At further downstream positions, the vortices gradually shift towards the sides of the body and  $\beta$  increases. As seen in Figures 6 and 7 for  $x/L = 0.75$  and  $1.0$ , the angle  $\beta$  for the frontward vortices decreases during the upstroke as the tail moves downward and the phase angle changes from  $\alpha = 0^\circ$  to  $30^\circ$ . As the tail moves upward during the downstroke and the angle of attack changes from  $\alpha = 30^\circ$  to  $0^\circ$ , the angle  $\beta$  for the rearward vortices increases, reaching values as high as  $135^\circ$ .

The variation of  $\beta$  with  $x/L$  for the frontward vortex pair is shown in Figure 10. Here,  $\alpha = 15^\circ$  during the upstroke, the Reynolds number is  $R_D = 4 \times 10^3$  and the reduced frequency is  $K = 0.2$ . At  $x/L = 0.25$ ,  $\beta = 25^\circ$  and increases to about  $75^\circ$  at the tail of the body. The angle  $\beta$  generally increased as the reduced frequency increased. At lower  $K$ , both vortex pairs are generally located near the top surface. However, at large reduced frequency the oscillating motion of the body is significant especially near its nose and tail, and extreme values of  $\beta$  are achieved.

### 3.5 Reynolds Number and Oscillation Amplitude Effects

The Reynolds number affects the geometry of the separation vortices over a missile moving at constant angle of attack. The steady state values for the vortex height  $H$  at different attack angles were plotted in Figure 9 for two Reynolds numbers  $R_D = 4 \times 10^3$  and  $4 \times 10^4$ . Reynolds number effects are more pronounced at high angles of attack. At  $\alpha = 30^\circ$ , the vortex height for the higher Reynolds number is about half that at the lower speed. At the low Reynolds number, the boundary layer in the attached region was transitional and intermittent regions of turbulence could be observed from the dye visualizations. At Reynolds number of  $R_D = 4 \times 10^4$ , the boundary layer flow was turbulent and the dye marking the separation vortices was observed to be well mixed.

For the unsteady case Reynolds number effects are not as pronounced. Figure 11 shows the rearward vortex height variation with angle of attack for two Reynolds numbers  $R_D = 8 \times 10^3$  and  $4 \times 10^4$ . The reduced frequency for both runs is  $K = 0.04$  and  $H$  is measured at  $x/L = 0.75$ . At this low reduced frequency, the flow is similar to the steady flow case, although a hysteresis loop still exists. Also, the frontward vortex pair stays near the top of the body and the angle  $\beta$  does not vary significantly with the angle of attack.

At higher reduced frequencies, the unsteady effects dominate the flow and are mainly responsible for the variations of the aerodynamic properties. Existing studies on two-dimensional, unsteady airfoils have shown that Reynolds number is not a primary control parameter.<sup>8</sup> In the present investigation at a reduced frequency of  $K = 0.2$ , there was no measurable difference in the measured values of  $H$  when the Reynolds number is increased over one order of magnitude. In fact, the reduced frequency becomes the primary control parameter. As shown in Figures 9 and 11, the hysteresis loop is quite different when the reduced frequency changes from  $K = 0.04$  (Figure 11) to  $K = 0.2$  (Figure 9).

Adler & Luttgies,<sup>14</sup> have concluded that subtle changes in pitching parameters induce significant effects in the resulting flow field around a three-dimensional rectangular wing. To investigate these effects for the pitching slender body, the sinusoidal oscillation amplitude was varied in the range of  $5^\circ$  to  $15^\circ$  about a given mean angle of attack. Figure 12 shows an end view of the slender body undergoing the pitching motion  $\alpha(t)^\circ = 15 + 10 \sin(t)$ . The Reynolds number based on diameter was  $R_D = 4 \times 10^3$ , and the reduced frequency was  $K = 0.2$ . Dye seeped continuously from the porous body surface and was excited using a vertical sheet of laser light perpendicular to the flow and located at  $x/L = 0.75$ . The photographs in Figure 12 show a typical oscillation cycle for both the upward and downward motions of the body at  $\alpha = 5^\circ, 10^\circ, 15^\circ, 20^\circ$  and  $25^\circ$ . The reduced frequency, Reynolds number, mean angle of attack and visualization station for the run depicted in Figure 12 are the same as those for the run shown in Figure 6. Only the oscillation amplitude changed from  $\pm 15^\circ$  in Figure 6 to  $\pm 10^\circ$  in Figure 9. The effect on the leeward vortices is dramatic. Their size, circulation and degree of symmetry change as the oscillation amplitude is reduced by 30 percent.

The angle  $\beta$  between the plane of symmetry of either the frontward or the rearward vortex pair and the vertical axis increased monotonically as the oscillation amplitude increased in the range of  $\pm 5^\circ$  to  $\pm 15^\circ$ . This could be explained by considering the shear generated by the harmonic motion of the body. Larger amplitude oscillation results in a separation shear layer that is thinner and vorticity that is more concentrated. The vortex roll-up is then more pronounced and  $\beta$  is larger.

#### 4. CONCLUSIONS

The complex flow patterns on a pitching slender body were visualized by using fluorescent dye techniques. An ogive-cylinder was towed in an 18-meter water channel and underwent large amplitude, harmonic pitching motion about the 0.5 station. It is found that the unsteady separation phenomenon is significantly different from the separation around a body in steady flight. Two separation vortex pairs were identified as the slender body underwent a complete pitching cycle. We term these the "Frontward and Rearward Separation Vortices". During the upstroke, the unsteady separation starts near the tail of the body and propagates upstream as the angle of attack increases. During the downstroke, the separated zone moves downstream and a secondary separation is triggered by the primary one near the nose of the body. Both separation regions are in the form of counter-rotating vortex pairs that undergo a growth-decay cycle.

The size, circulation and degree of symmetry of the leeward vortices change dramatically with subtle changes in the pitching parameters. On the other hand, at moderate to large reduced frequencies, the Reynolds number effects are negligible. The unsteady effects dominate viscous effects and are mainly responsible for the variations of the aerodynamic properties.

The present investigation provided a first look at the unsteady motion around a body of revolution undergoing a pitching motion. Other modes of unsteadiness should also be studied, for example plunging or time-dependent ambient velocity. References 6 and 15 indicate that the mode of the unsteady motion can significantly affect the hysteresis loops and the aerodynamic properties of a lifting surface. The results of the visualization experiments should be used to design fast-response probe experiments to measure the velocity field and to correlate the visualization events with the unsteady forces and moments experienced by the slender body.

ACKNOWLEDGEMENT

This work is supported by the U.S. Air Force Office of Scientific Research, under Contract No. F49620-85-C-0028, and monitored by Dr. J. D. Wilson. The authors would like to acknowledge the valuable help of Messrs. Morton Cooper and Randy Srnsky.

REFERENCES

1. Herbst, W. B., "Dynamics of Air Combat," J. Aircraft 20, pp. 594-598, 1983.
2. Herbst, W. B., "Supermaneuverability," in Unsteady Separated Flows, eds. M. S. Francis & M. W. Luttges, Univ. Colorado, pp. 1-9, 1983.
3. Nielsen, J. N., "Missile Aerodynamics - Past, Present, Future," AIAA Paper No. 79-1819, 1979.
4. McCroskey, W. J., Carr, L. W., and McAlister, K. W., "Dynamic Stall Experiments on Oscillating Airfoils," AIAA J. 14, pp. 57-63, 1976.
5. Nayfeh, A. H., Mook, D. T., and Yen, A., "The Aerodynamics of Small Harmonic Oscillations Around Large Angles of Attack," AIAA Paper No. 79-1520, 1979.
6. Carta, F., "A Comparison of the Pitching and the Plunging Response of an Oscillating Airfoil," NASA CR-3132, 1979.
7. Konstadinopoulos, P., Mook, D. T., and Nayfeh, A. H., "A Numerical Method for General Unsteady Aerodynamics," AIAA Paper No. 81-1877, 1981.
8. McCroskey, W. J., "Unsteady Airfoils," Ann. Rev. Fluid Mech. 14, pp. 285-311, 1982.
9. McCroskey, W. J., and Pucci, S. L., "Viscous-Inviscid Interaction on Oscillating Airfoils in Subsonic Flow," AIAA J. 20, pp. 167-174, 1982.
10. Robinson, M. C., and Luttges, M. W., "Unsteady Flow Separation and Attachment Induced by Pitching Airfoils," AIAA Paper No. 83-0131, 1983.
11. Konstadinopoulos, P., Mook, D. T. and Nayfeh, A. H., "Numerical Simulation of the Subsonic Wing-Rock Phenomenon," AIAA Paper No. 83-2115, 1983.
12. Walker, J. M., and Helin, H. E., "An Experimental Investigation of an Airfoil Undergoing Large Amplitude Pitching Motions," AIAA Paper No. 85-0039, 1985.

13. Helin, H. E., and Walker, J. M., "Interrelated Effects of Pitch Rate and Pivot on Airfoil Dynamic Stall," AIAA Paper No. 85-0130, 1985.
14. Adler, J. N., and Luttgies, M. W., "Three-Dimensionality in Unsteady Flow About a Wing," AIAA Paper No. 85-0132, 1985.
15. Chen, S.-H., and Ho, C.-M., "Unsteady Aerodynamics of a Plunging Airfoil," Bul. Am. Phys. Soc. 30, 1985.
16. Gad-el-Hak, M., and Ho, C.-M., "The Pitching Delta Wing," AIAA J., in press, 1985.
17. Gad-el-Hak, M. and Ho, C.-M., "Unsteady Vortical Flow Around Three-Dimensional Lifting Surfaces," AIAA J., in press, 1985.
18. Gad-el-Hak, M., Blackwelder, R. F., and Riley, J. J., "On the Growth of Turbulent Regions in Laminar Boundary Layers," J. Fluid Mech. 110, pp. 73-95, 1981.
19. Gad-el-Hak, M., "The Use of the Dye-Layer Technique for Unsteady Flow Visualization," J. Fluids Eng., in press, 1985.
20. Nielsen, J. J., "Nonlinearities in Missile Aerodynamics," AIAA Paper No. 78-0020, 1978.
21. Cooper, M., Gapcynski, J. P., and Hasel, L. E., "A Pressure Distribution Investigation of a Finess-Ratio-12.2 Parabolic Body of Revolution (NACA RM-10) at  $M = 1.59$  and Angles of Attack to  $36^\circ$ . NACA RM L52G14a, Oct. 1952.
22. McAlister, K. W., and Carr, L. W., "Water Tunnel Visualizations of Dynamic Stall," in Nonsteady Fluid Dynamics, eds. D. E. Crow & J. A. Miller, ASME, pp. 103-110, 1978.
23. Gad-el-Hak, M., Blackwelder, R. F., and Riley, J.J., "Visualization Techniques for Studying Transitional and Turbulent Flows," in Flow Visualization 3, ed. W. J. Yang, Hemisphere, pp. 568-575, 1983.

FIGURE CAPTIONS

- Figure 1. Side View of the Slender Body Undergoing a Pitching Motion.  
 $R_D = 4 \times 10^3$ ;  $K = 0.2$ ;  $\alpha(t)^\circ = 15^\circ + 15^\circ \sin(t)$ .  
Vertical Sheet of Laser is Parallel to the Flow at  $z = 1.0$  cm.
- Figure 2. Propagation of the Rearward Separation Front.  
 $R_D = 4 \times 10^3$ ;  $K = 0.2$ .
- Figure 3. End View Using the Dye-Layer Technique.  
 $R_D = 4 \times 10^3$ ;  $K = 0.2$ ;  $\alpha(t)^\circ = 15^\circ + 15^\circ \sin(t)$ .  
Vertical Sheet of Laser at  $x = 30$  cm.
- Figure 4. End View Using the Dye-Layer Technique.  
 $R_D = 4 \times 10^3$ ;  $K = 0.4$ ;  $\alpha(t)^\circ = 15^\circ + 15^\circ \sin(2t)$ .  
Vertical Sheet of Laser at  $x = 30$  cm.
- Figure 5. End View of the Slender Body Undergoing a Pitching Motion.  
 $R_D = 4 \times 10^3$ ;  $K = 0.2$ . Vertical Sheet of Laser at  $x = 20$  cm.
- Figure 6. End View of the Slender Body Undergoing a Pitching Motion.  
 $R_D = 4 \times 10^3$ ;  $K = 0.2$ . Vertical Sheet of Laser at  $x = 30$  cm.
- Figure 7. End View of the Slender Body Undergoing a Pitching Motion.  
 $R_D = 4 \times 10^3$ ;  $K = 0.2$ . Vertical Sheet of Laser at  $x = 40$  cm.

Figure 8. Streamwise Growth of the Frontward Vortices.

$$R_D = 4 \times 10^3; K = 0.2.$$

Figure 9. Evolution of Frontward and Rearward Vortices.

$$R_D = 4 \times 10^3; K = 0.2; x/L = 1.0.$$

Figure 10. Streamwise Variation of  $\beta$ .  $R_D = 4 \times 10^3; K = 0.2;$

$$\alpha = 15^\circ \text{ (Upstroke).}$$

Figure 11. Effects of Reynolds Number on the Hysteresis Loop.

$$K = 0.04; x/L = 0.75.$$

Figure 12. Effects of Oscillation Amplitude.

$$R_D = 4 \times 10^3; K = 0.2; \alpha(t)^\circ = 15^\circ + 10^\circ \sin(t).$$

Sheet of Laser is Perpendicular to the Flow at  $x = 30 \text{ cm}$ .



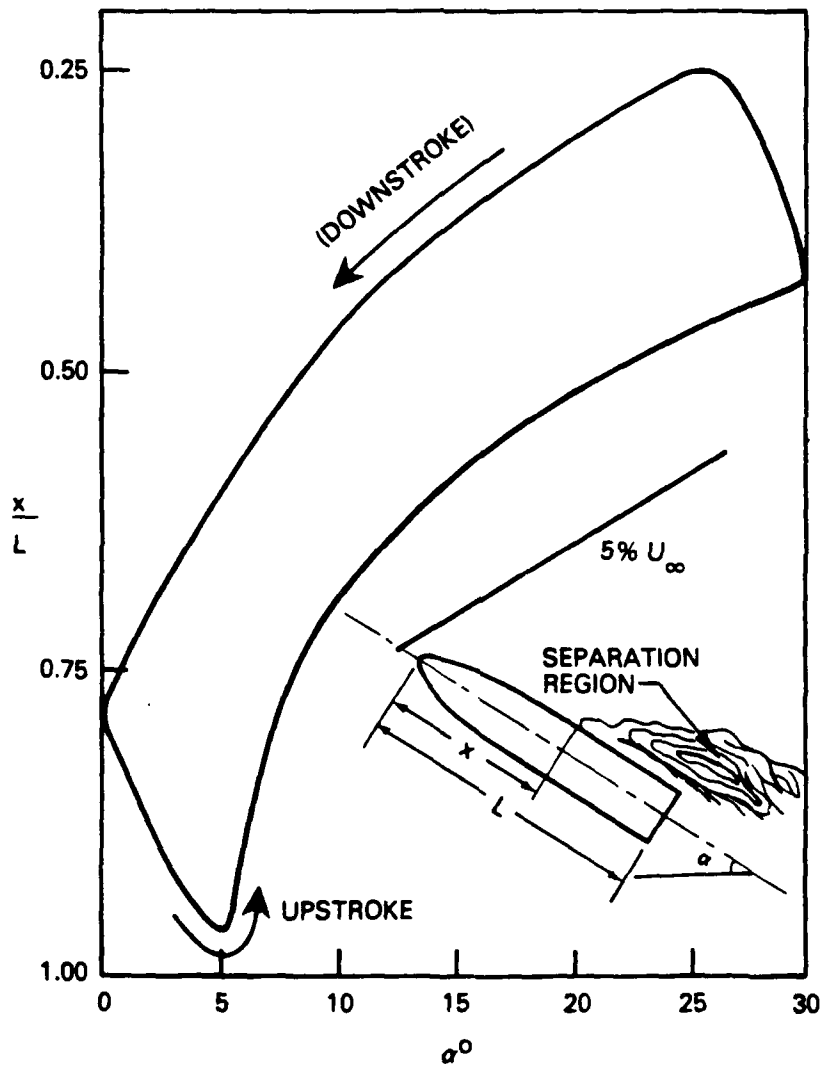


Figure 2. Propagation of the Rearward Separation Front.  
 $R_D = 4 \times 10^3$ ;  $K = 0.2$



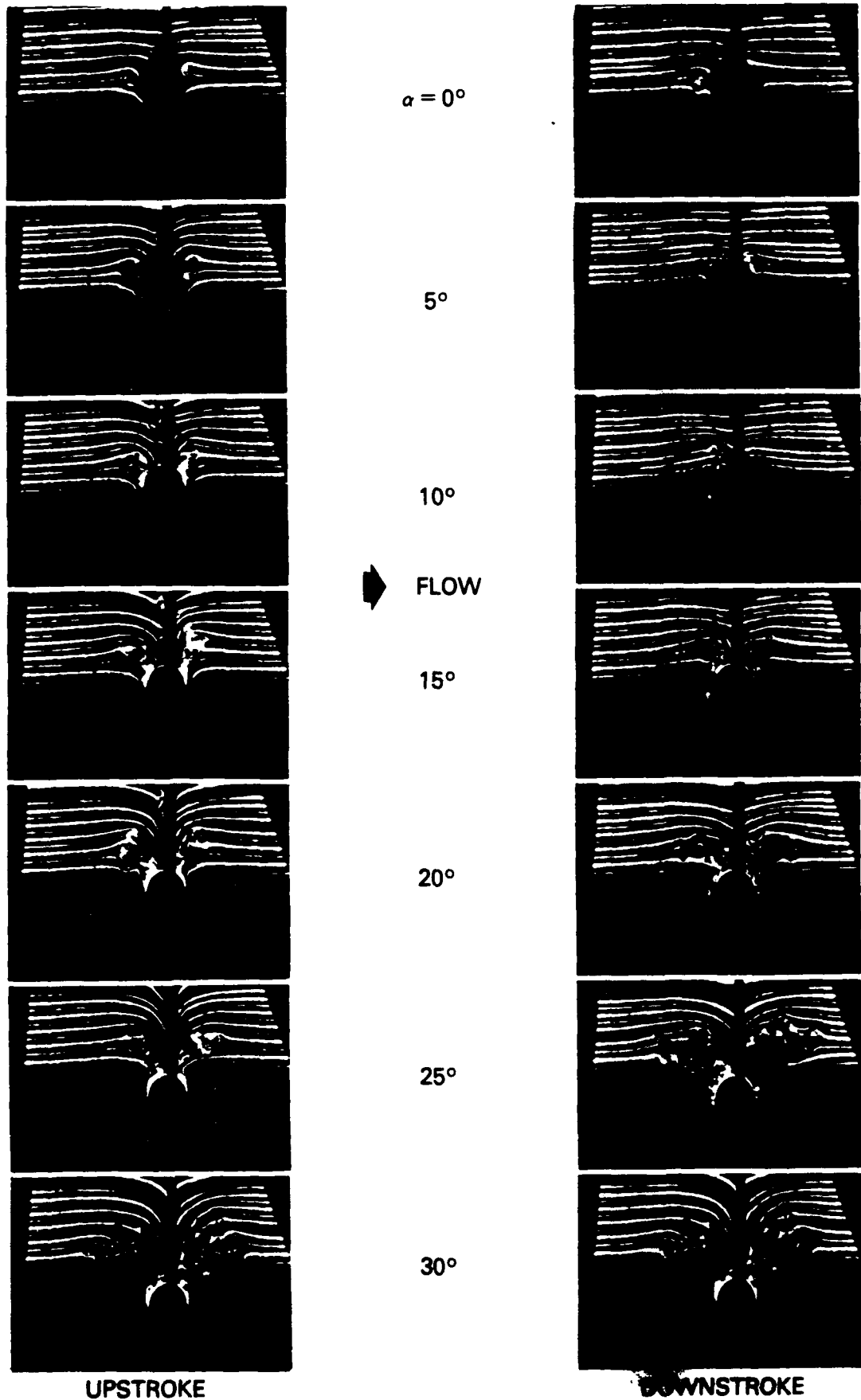
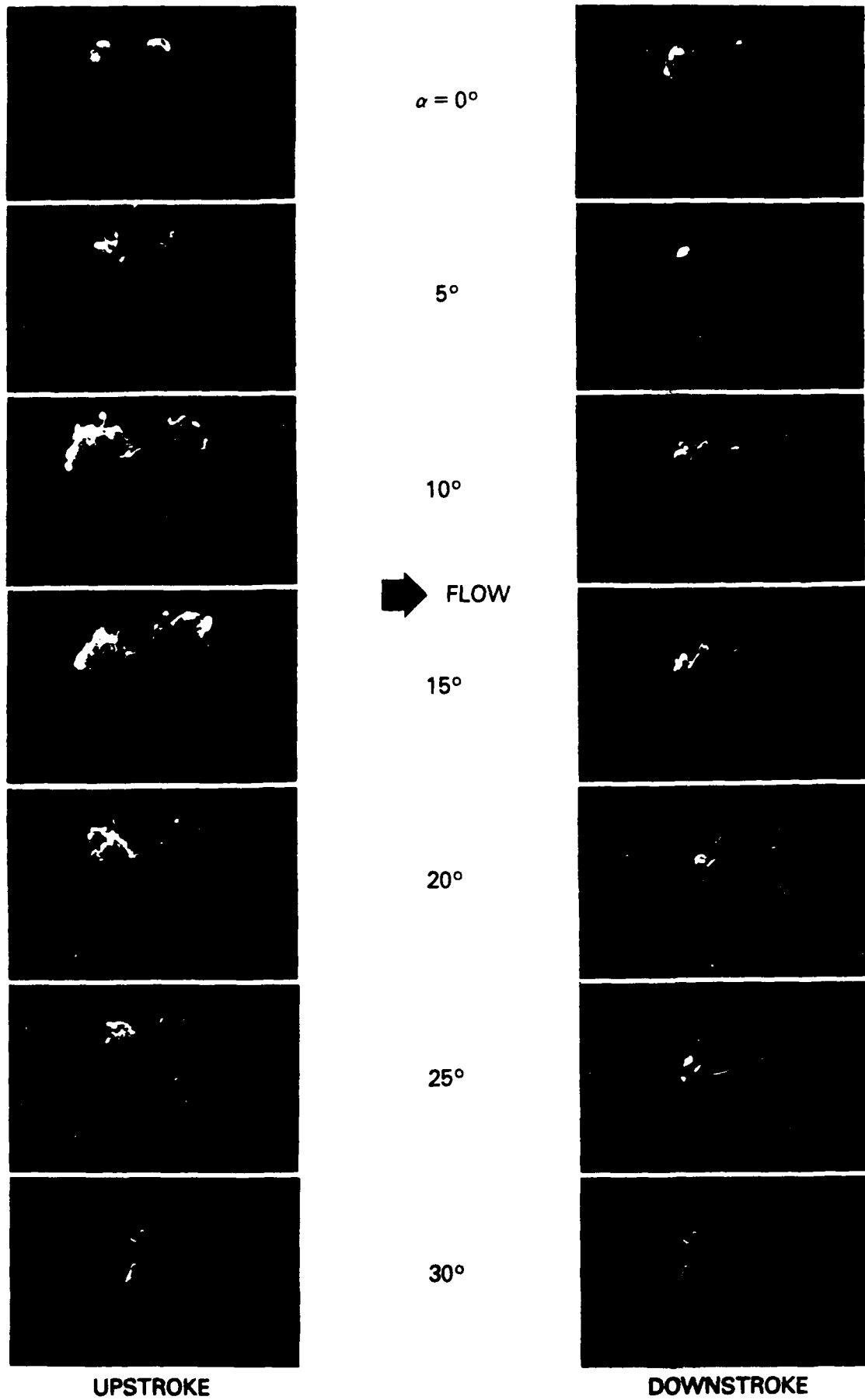
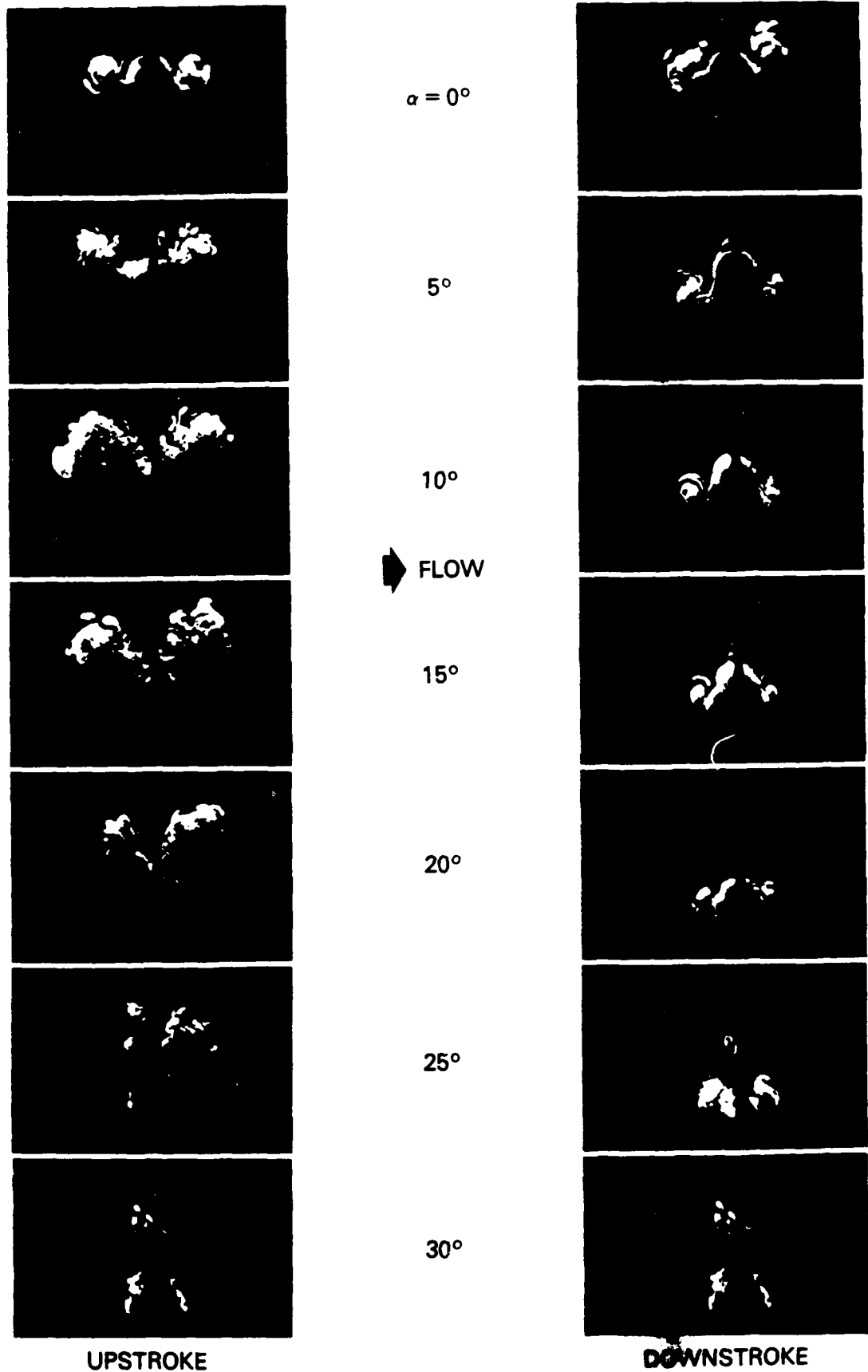


Figure 4. End View Using the Dye-Layer Technique.  $R_D = 4 \times 10^3$ ;  $K = 0.4$ ;  $\alpha(t) = 15^\circ + 15^\circ \sin(2t)$ . Vertical Sheet of Laser at  $x = 30$  cm.





**Figure 6. End View of the Slender Body Undergoing a Pitching Motion.  $R_D = 4 \times 10^3$ ;  $K = 0.2$ . Sheet of Laser at  $x = 30$  cm.**



**Figure 7. End View of the Slender Body Undergoing a Pitching Motion.  $R_D = 4 \times 10^3$ ;  $K = 0.2$ . Sheet of Laser at  $x = 40$  cm.**

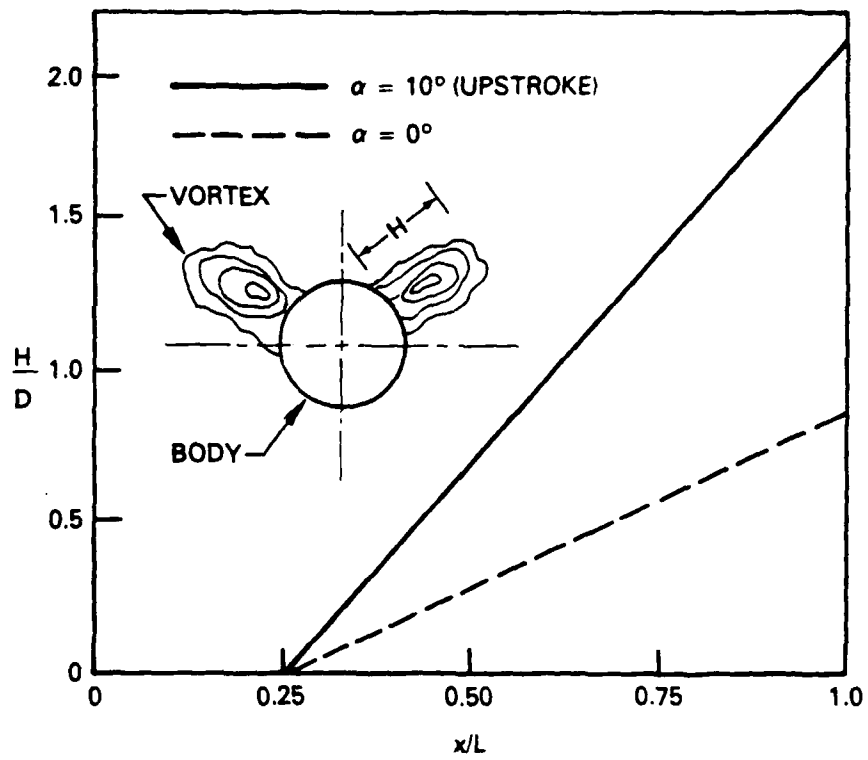


Figure 8. Streamwise Growth of the Frontward Vortices.  
 $R_D = 4 \times 10^3$ ;  $K = 0.2$

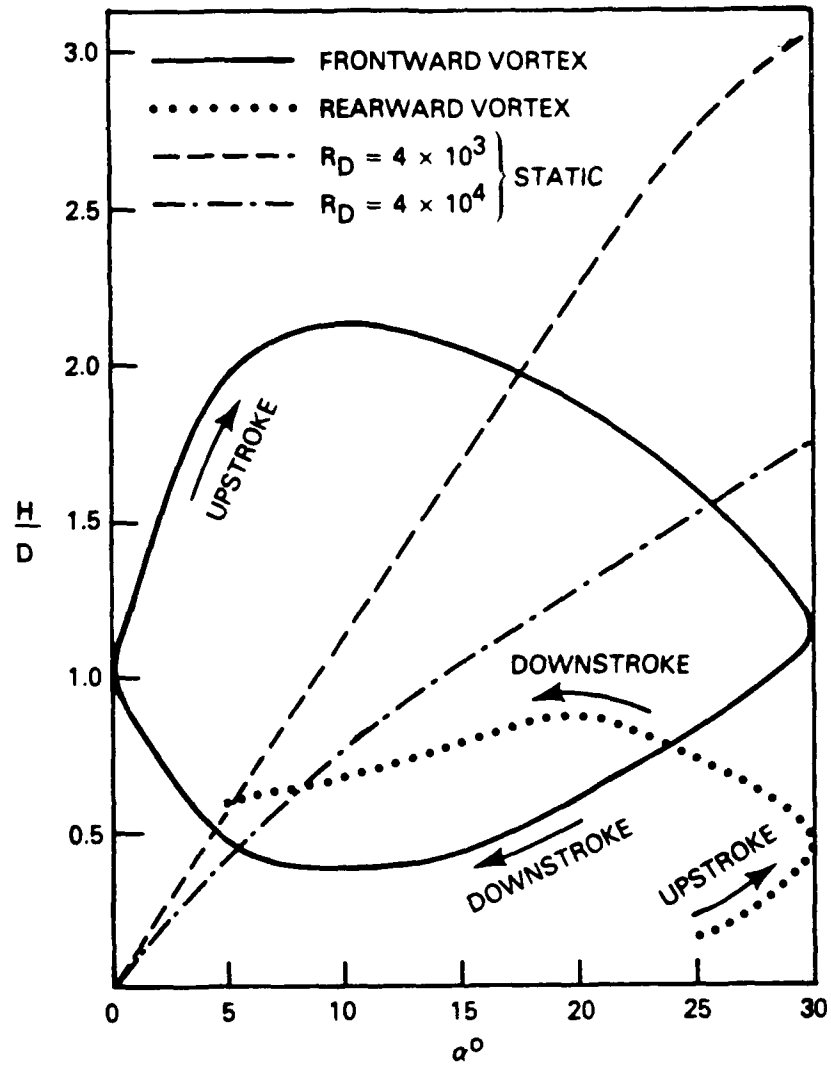


Figure 9. Evolution of Frontward and Rearward Vortices.  
 $R_D = 4 \times 10^3$ ;  $K = 0.2$ ;  $x/L = 1.0$

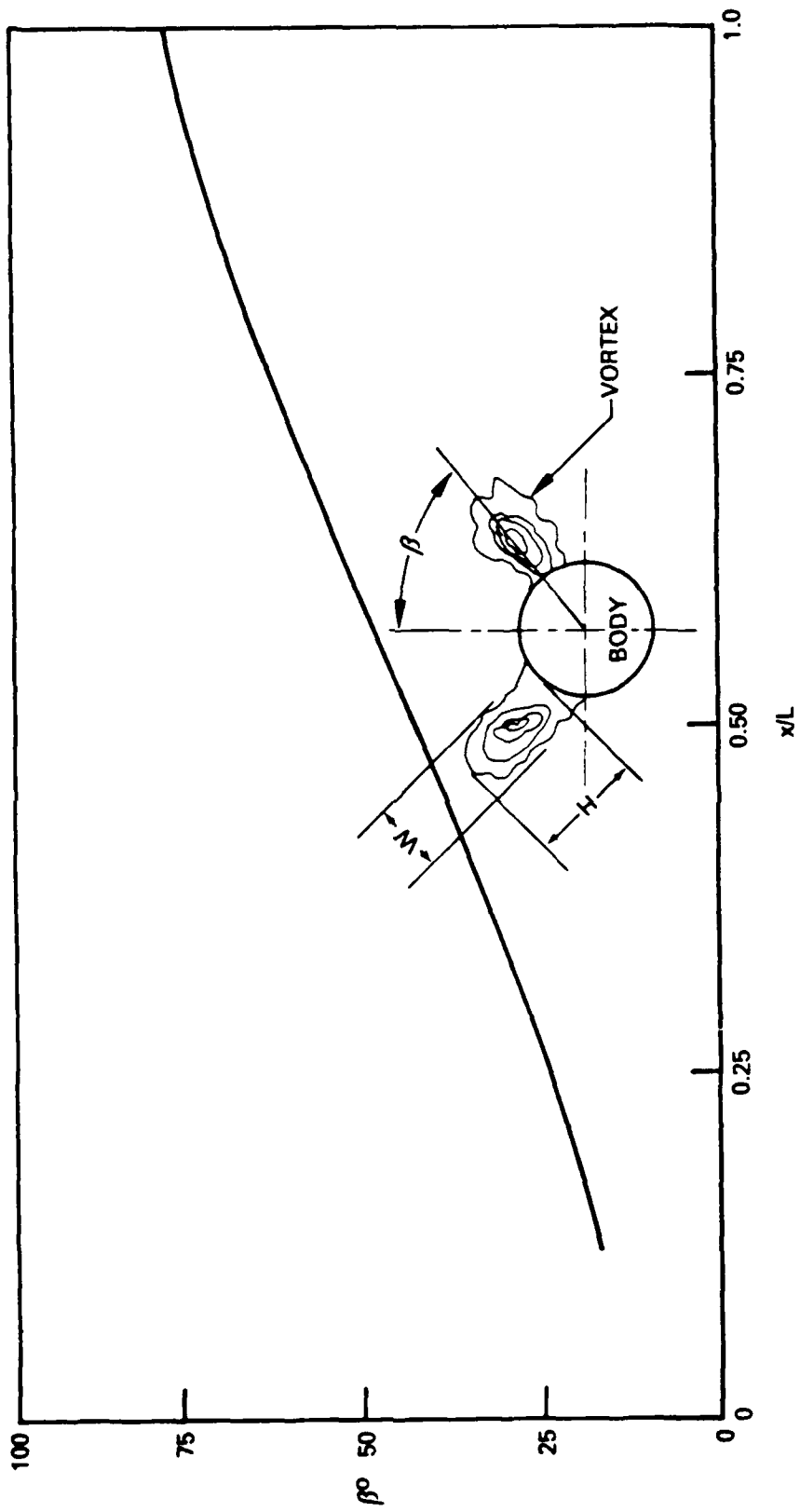


Figure 10. Streamwise Variation of  $\beta$ .  $RD = 4 \times 10^3$ ;  $K = 0.2$ ;  
 $\alpha = 15^\circ$  (Upstroke).

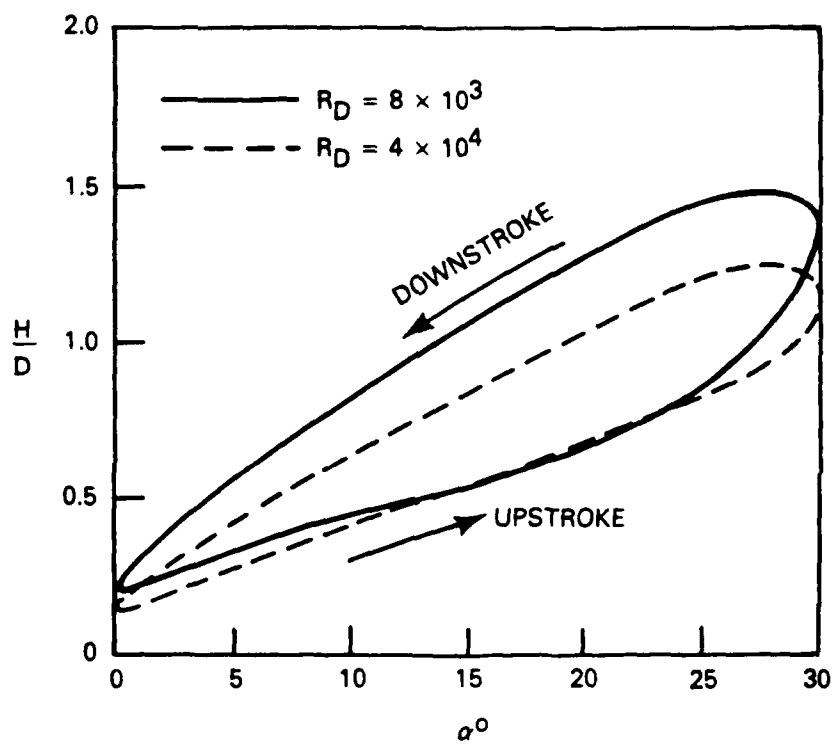


Figure 11. Effects of Reynolds Number on the Hysteresis Loop.  
 $K = 0.04$ ;  $x/L = 0.75$

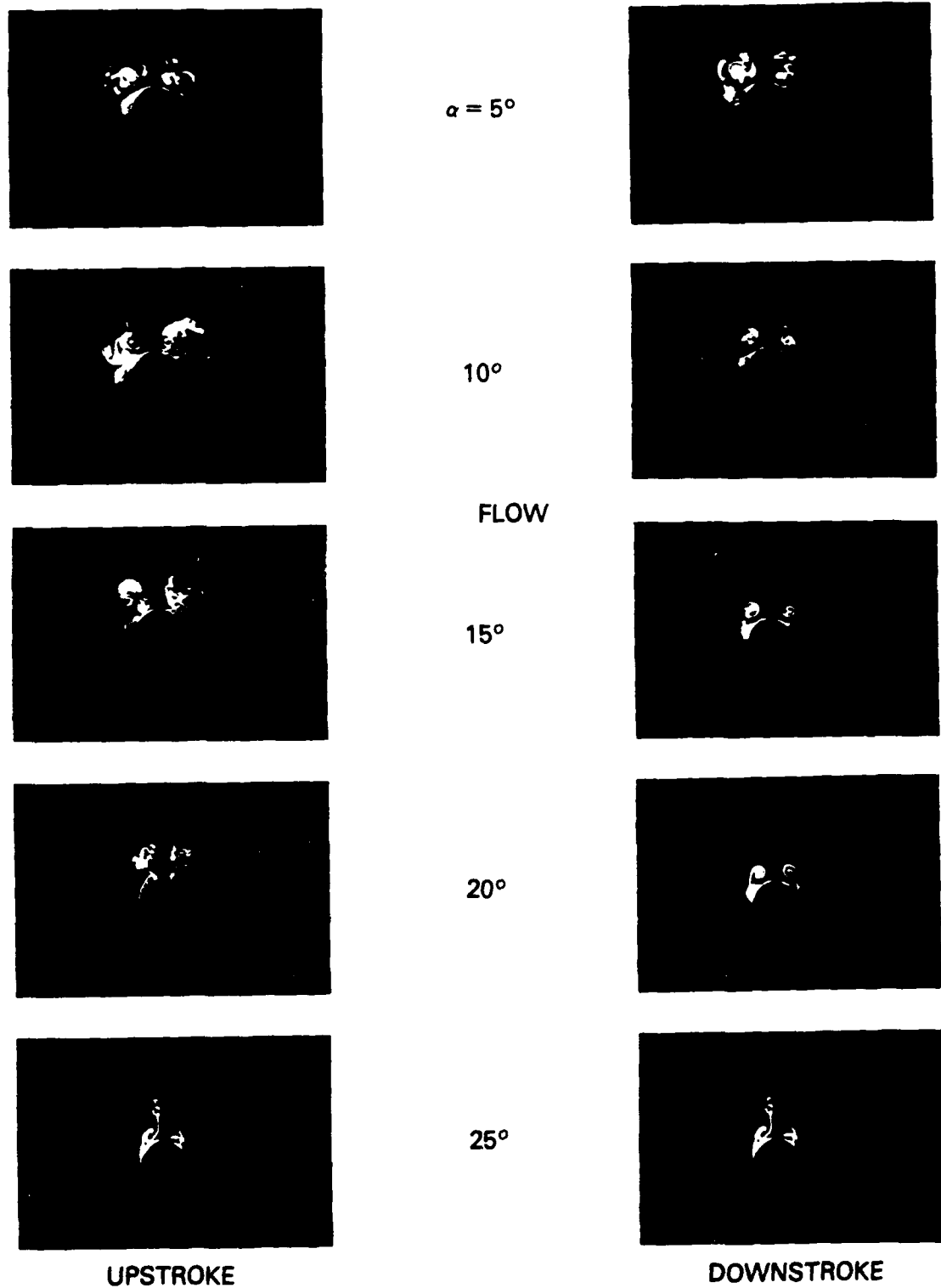


Figure 12. Effects of Oscillation Amplitude.  $Re = 10^3$ ;  $K = 0.2$ ;  $\alpha(t) = 15^\circ + 10^\circ \sin(t)$ . Sheet of Laser is Perpendicular to the Flow at  $x = 30$  cm.

Appendix V: Unsteady Flow Around an Ogive-Cylinder